Tables of contents


Chapter 1 : Introduction ---- 4

Chapter 2 : Design of the first test series---- 10

*2.1. Geometry*---- 11

*2.2. Dead load* ---- 12

*2.3. Preliminary assessment of the walls* ---- 13

2.3.1. Mechanical and geometrical characteristics---- 13

2.3.2. Strength verification and acceleration assessment---- 13

*2.4. Building aspects (beams of support)*---- 16

*2.5. Set up of the walls* ---- 16

*2.6. Origin of axis and axis convention*---- 17

*2.7. Instrumentation of the walls*---- 18

*2.8. Characteristics of instrumental devices*---- 21

*2.9. Calibration of instrumental devices*---- 22

*2.10. Excitation waveforms*---- 23

*2.11. Security and safety*---- 24

Chapter 3 : Processing of the results of the first test series ---- 25

*3.1. Sequences of the tests* ---- 26

*3.2. Acceleration really experimented on the table*---- 29

*3.3. Measurements during the static loading*---- 30

3.3.1. Young Modulus of masonry ---- 30

3.3.2. Young Modulus of acoustic insulation devices ---- 32

3.3.3. Comparison with the EC 6 ---- 33

*3.3.3.1. Young Modulus of masonry* ---- 33

*3.3.3.2. Young Modulus of acoustic insulation devices* ---- 33

*3.4. White Noise tests*---- 34

3.4.1. Post-processing of the laboratory---- 34

*3.4.2.* Own post-processing---- 37

3.4.3. Comparison with the preliminary assessment ----48

*3.5. Seismic tests* ---------- 50
3.5.1. Assessment of the compressive length ---------- 50
*3.5.1.1. Determination of useful parameters* ---------- 50
*3.5.1.2. Calculation of the compressive length* ---------- 54
*3.5.1.3. Amplitude of the rocking motion* ---------- 59
3.5.2. Horizontal relative displacements between the wall and the support beam- 61
3.5.3. Rocking of the mass ---------- 64
3.5.4. Horizontal shear ---------- 67
*3.5.4.1. Horizontal shear in the wall* ---------- 67
3.5.4.1.1. Horizontal shear in the long walls ---------- 68
3.5.4.1.2. Horizontal shear in the short walls ---------- 69
*3.5.4.2. Horizontal shear in the acoustic insulation devices* ---------- 71
3.5.4.2.1. Horizontal shear in the bottom SonicStrip ---------- 71
3.5.4.2.2. Horizontal shear in the top SonicStrip ---------- 73
3.5.5. Comparison with the vision system ---------- 77
*3.5.5.1. Justification of the comparison* ---------- 77
*3.5.5.2. Scaling of the time* ---------- 77
*3.5.5.3. Post-processing and comparison of the results* ---------- 78
3.5.5.3.1. Using of the vertical displacements ---------- 78
3.5.5.3.2. Using of the horizontal displacement ---------- 80
3.5.6. Comparison with the preliminary assessment - ---------- 82
*3.5.6.1. Compressive length* ---------- 82
*3.5.6.2. Rocking behaviour* ---------- 84

**Chapter 4 : Design of the second test series** ---------- 86
*4.1. Geometry of the specimens* ---------- 87
*4.2. Dead load* ---------- 88
*4.3. Preliminary assessment of the specimens* ---------- 89
4.3.1. Mechanical characteristics ---------- 89
4.3.2. Geometrical characteristics ---------- 90
4.3.3. Assessment of the acceleration ---------- 96
*4.3.3.1. Compressive length* ---------- 98
*4.3.3.2. Shear strength* ---------- 106
*4.3.3.3. Crushing of the units* ---------- 107
*4.3.3.4. Torsion strength* ---------- 107
*4.3.3.5. Designed acceleration* ---------- 109

4.3.4. Specificities of the Y-direction ---------- 112
4.3.5. Comparison with a specimen without flanges ---------- 113
4.3.6. Comparison with a simple wall ---------- 113
*4.4. Building aspects (beams of support)* ---------- 114
*4.5. Origin of axis and axis convention* ---------- 115
*4.6. Instrumentation of the specimens* ---------- 115
4.6.1. Characteristics of instrumental devices ---------- 115
4.6.2. Positions of instrumental devices ---------- 115

**Chapter 5 : Results of the second test series** ---------- 117
*5.1. Introduction* ---------- 118
*5.2. Set up of the specimens* ---------- 118
*5.3. Sequences of the tests* ---------- 119
*5.4. Acceleration really experimented on the table* ---------- 122
*5.5. Observations and comments of the tests-* ---------- 123
5.5.1. Specimen with T-shaped walls ---------- 123
5.5.1.1. *Position of the slab* ---------- 123
5.5.1.2. *Phenomena observed* ---------- 124
5.5.2. Specimen with L-shaped walls ---------- 126
5.5.2.1. *Position of the slab* ---------- 126
5.5.2.2. *Phenomena observed* ---------- 127
5.5.2.2.1. First loading case ---------- 127
5.5.2.2.2. Second loading case ---------- 127

**Chapter 6 : Conclusions &prospects** ---------- 129

**Chapter 7 : Bibliography** ---------- 132

**Annexes**

# Chapter 1 : Introduction

Historically, masonry is a traditional material used for several types of buildings, like private dwellings, town halls, churches, etc. This construction follows good practice methods, which include many rules and construction techniques. In this field, the contribution of civil engineers is limited, usually leaving the task of designing these buildings to architects.
However, the intervention of civil Engineers is increasingly necessary today. Indeed, the masonry is more and more used at the limit of the material capacity, for example under more important compression level than in the past (e.g. apartment buildings or lightweight concrete blocks houses, with a traditional masonry structural layout. Moreover, ecological and economical considerations require a more efficient use of this material.
All the considerations are contained in the "*Eurocode 6 : Design of masonry structures*", where verification methodologies and rules are proposed.

Regardless of this, the consideration of seismic action on buildings requires understanding the behaviour of masonry structures under these specific horizontal actions. The seismic behaviour of that type of structures is extensively described by $Miha\ Tomaževič$ in the book entitled "*Earthquake-Resistant Design of Masonry Buildings*" (Tomazevic, 1999). In his book, $Miha\ Tomaževič$ recalls the methodology used in standards to simulate earthquakes and their actions, the State of Art in the late 1990's and some hints to repair the damages caused by earthquakes or to prevent earthquake damages in existing buildings.

In the last years, several researches and Master's Theses have been carried out in that field. Some of the theses were written by students of the University of Liège and concern the subject of the seismic behaviour of masonry structures. Reading these theses was useful to understand and become familiar with concepts and aspects related to masonry.
The first one, written by Benjamin Cerfontaine, has the aim to develop a user-friendly software. The software can check the resistance of a masonry building to an earthquake following rules in accordance with the Eurocode 8 standards. Moreover, this software is also valid to verify the building according to the Eurocode 6. (Cerfontaine, 2010)
The second one, written by Sophie Grigoletto, deals with the rocking. The objective of her work was the study of the seismic behaviour of structures with a discontinuous behaviour. The interesting part concerns the study of the dynamic behaviour of a rigid body. Thanks to it, we understand the behaviour of the type of structures and a numerical method was developed to solve the equations governing their behaviour. (Grigoletto, 2006)

In that general context, some laboratory tests have been performed. Among them, we can first talk about the quasi-static cyclic tests on different types of masonry spandrels (K.Beyer, A.Abo-El-Ezz & A.Dazio, 2010). The tests were carried out to investigate the influence of spandrels on the global behaviour of unreinforced masonry walls under seismic action.

Other static-cyclic tests were performed at the University of Liège on typical Belgian clay masonry in collaboration with the company Wienerberger. These are summarized here after.
A first test series was made in collaboration between University of Liège and Wienerberger in 2010. Its announced goal was "to characterize the performances of bearing walls made of Belgian type of clay blocks in context of low to moderate seismic hazard". Two aspects were examined in more details :

- the influence of the presence of regular shape and size door opening on the walls behaviour and the effects of different reinforcements and configurations of the concrete lintel ;
- the influence of the presence of acoustic devices at the wall top and bottom. The acoustic devices are designed to fulfil the acoustic performance prescribed for apartments in Belgium.

The test series comprises 8 walls, divided into two sets of 4 walls. The dimensions of the 8 specimens were the same. Details of the configurations and of the differences between the specimens are summarized in Table 1 and can also be found in the testing report "*Cyclic shear behaviour of clay masonry walls – Part 1 : walls including acoustic devices or with a door opening*" (Hervé Degee & Laurentiu Lascar, 2011). The instrumentation layouts are also available in this report.

**Table 1 – Description of the specimens**

| Test | Description |
|---|---|
| A1 | Full wall without any specific elements |
| A2 | Full wall with continuous SonicStrips (10mm thick) at the bottom and top of the wall |
| A3 | Wall with a door opening and a regular lintel (support 150 mm on each side of the opening). The specimen is unsymmetrical |
| A4 | Same as A3 with vertical confining elements |
| B1 | Full wall with discontinuous SonicStrips (10mm thick) at the bottom and top of the wall |
| B2 | Full wall with polyurethane SonicStrips. |
| B3 | Wall with a door opening and a long lintel (support 450 mm on each side of the opening). The specimen is unsymmetrical |
| B4 | Same as A3 with Murfor placed in every two horizontal mortar layer |

The tests were static cyclic. The test procedure had 2 phases. The first one was to compress the wall up to a chosen level of compressive stress. The second one was to cyclically apply an imposed horizontal displacement, which increases every 3 cycles.

The results of this test program are in the following Table 2, taken from the above mentioned report.

**Table 2 - Results taken from the report of "*Cyclic shear behaviour of clay masonry walls – Part 1 walls including acoustic devices or with a door opening*".**

| Test | Ultimate load + (kN) | Ultimate load - (kN) | Ultimate drift + (mm/%) | Ultimate drift - (mm/%) | Ductility + | Ductility - | Collapse mechanism |
|---|---|---|---|---|---|---|---|
| A1 | 133.0 | 137.1 | 7.5 / 0.27 | 8.4 / 0.30 | 1.8 | 1.7 | Diagonal cracking. Maximum drift corresponds to crushing of the toe |
| A2 | 73.8 | 74.3 | 23.5 / 0.84 | 22.2 / 0.79 | 3.1 | 2.9 | Vertical cracking on the superior 2/3rd of the wall (already initiated during the pre-compression stage on the first 2 layers of blocks) followed diagonal cracking at the A2 bottom of the wall. Final drift corresponds to crushing of the toe |
| B1 | 76.1 | 69.7 | 12.5 / 0.45 | 12.1 / 0.43 | 1.4 | 1.6 | Sub-vertical cracking starting from the top of the wall. Final drift corresponds to the sub-vertical cracking reaching the bottom of the wall. |
| B2 | 68.1 | 63.9 | 22.3 / 0.79 | 22.0 / 0.79 | 2.1 | 2.1 | 2 networks of the vertical cracking. Final drift corresponds to vertical cracking reaching the bottom of the wall. |
| A3 | 76.1 | 73.8 | 8.8 / 0.32 | 7.6 / 0.27 | 1.7 | 1.1 | Crushing of the block at the lintel support |
| A4 | 100.8 | 76.3 | 8.4 / 0.30 | 7.4 / 0.26 | 1.8 | 2.6 | Development of a full network of diagonal cracking – Collapse by internal crushing of the block in the intersection on the diagonals |
| B3 | 82.0 | 76.6 | 5.3 / 0.19 | 6.1 / 0.22 | 1.7 | 1.8 | Diagonal cracking starting from the blocks support of the lintel |
| B4 | 76.9 | 71.2 | 7.2 / 0.26 | 8.0 / 0.29 | 2.3 | 2.6 | Crushing of the blocks at the lintel support (structure remains however stable thank to the Murfor) – Collapse by internal crushing of the blocks in the middle of the wall. |

The collapse mechanism happens by cracking and/or crushing of the units. Detailed results are available in the report of the testing program. The collapse mechanism of the test A1 is illustrated in Figure 1.

**Figure 1 – Collapse mechanisms (left : A1 – right : B1)**

The second test series aimed at "*characterizing the performances of the connection material used at the vertical intersection of two prefabricated masonry walls* (Figure 2) *to replace the traditional binding of the masonry"*.

**Figure 2 – T-shaped wall**

Once again, the investigations were focused on two aspects :

- the influence of the level of compressive stress and the imposed horizontal displacement on the behaviour of the connecting ;
- the behaviour of T-shaped masonry shear walls in precast masonry panels.

In this case, 3 walls having the same dimensions and detailing were tested. The difference between each test was the level of compressive stress. The T-shaped walls consisted of a main wall with given dimensions. Details of the configurations and instrumentation layouts can be found in the testing

report "*Cyclic shear behaviour of clay masonry walls – Part 2 : Cyclic shear test on prefabricated clay masonry walls with T-shaped*" (Hervé Degee & Larentiu Lascar, 2011).
The testing program also consisted in static cyclic tests. The testing procedure was the same as the one described for the first testing program.
For this program, the authors concluded about the maximum joint displacement and its behaviour. Two other conclusions about the shear cracking pattern and the use of Eurocode 6-1 procedures are very interesting. The first one shows that the pattern is the same as the one observed for traditional masonry systems. The second one proves that the values, given by the Eurocode 6-1 procedures for assessing the global resistance of a shear wall, are accurate for moderate compression level and conservative for high compression level.

Besides the static cyclic tests, a huge project was performed from the tenth of June 2004 to the tenth of June 2008, called "*ESECMaSE*" for "*Enhanced Safety and Efficient Construction of the Masonry Structures in Europe*". The project was divided in 11 work packages and in three phases. The third phase of this project (10/06/06 – 10/06/08) contained several types of tests, including shaking table tests. The aim of the shaking table tests was the study of masonry buildings under seismic loading and the identification of behaviour factors for these buildings (Stuerz, 2009). Especially, the work package 7 (D 7.2.c) reports the results of pseudo-dynamic and shaking table tests on the earthquake resistance of masonry materials.

Now, experimental tests on the behaviour of load-bearing masonry subjected to earthquake actions are carried out within the European research project SERIES. This Master's Thesis concerns the two phases of the SERIES project TA5 .

The purpose of the first phase is to elaborate a better understanding of the seismic behaviour of masonry walls in dynamic conditions and to investigate the consequences of the use of rubber elements (SonicStrips) aiming at improving the acoustic performance of buildings.

Although that study of the first phase is necessary and useful, the buildings are more complicated than a single wall and many other phenomena have to be examined. Indeed, when we look at a traditional building, we can see that the walls are connected together and they usually form T- or L-shaped walls (Figure 3). We sometimes make a hole in a wall to create an opening, such as a door or a window (Figure 4). The connection of, at least, two walls and the opening have consequences on the wall behaviour.

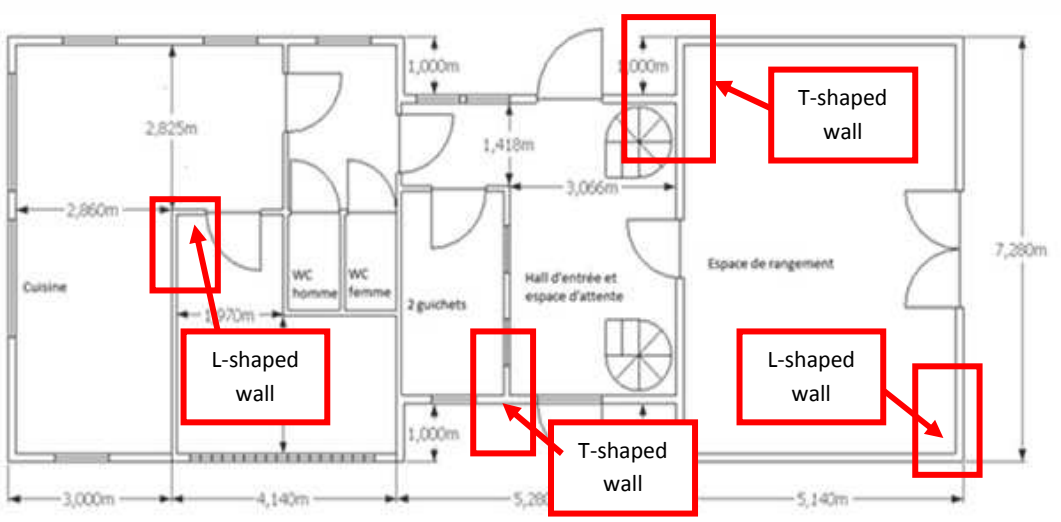


Figure 3 - Building plans[1]

Figure 4 - Door opening

The second phase has a double purpose. The first one is to characterize the effects due to the presence of a opening. The second one is the study of the influence of the wall shape on the seismic behaviour and the comparison of this kind of walls with simple ones. The second test series consists of two specimens. The specimens have two walls with an opening between them and linked together by a lintel.

[1] Plans from the course "Projet Intégré de Génie Civil" of University of Liège (de Acetis, Marcocci, Mordant, Pagna ; 2011)

# Chapter 2 :
# Design of the first test series

## 2.1. Geometry

As already said, the first phase has to purposes. The first one is to elaborate a better understanding of the seismic behaviour of masonry walls in dynamic conditions. The second one is to investigate the consequences of the use of rubber elements (SonicStrips) aiming at improving the acoustic performance of buildings.
Four walls are tested in order to complete this purpose. Two of them have an aspect ratio close to 1, the others have one close to 0.4. These dimensions are chosen to study the behaviour of walls which failure mode is different. The strength of the wall with aspect ratio close to 1 seems to be limited by shear, while the bending limits the strength of the walls with aspect ratio close to 0.4. Exact dimensions are the following :

- Length x Height x Width = *2.1m x 1.8m x 0.14m*
- Length x Height x Width = *0.72m x 1.8m x 0.14m*

Two walls (one of each aspect ratio) are built with acoustic insulation devices at the bottom and the top. The other two are built without any device of this type. This choice will allow the study of the influence of the devices, used to improve the acoustic performances, on the dynamic seismic behaviour.

As a summary, the tests include four different walls which behaviour can be compared according to the wall dimensions or to the presence of devices improving the acoustic performance. The four configurations are illustrated in Figure 5 to Figure 7.


Figure 5 – Start of the wall construction


Figure 6 – Top (left side) and bottom (right side) view of walls with aspect ratio close to 0.4

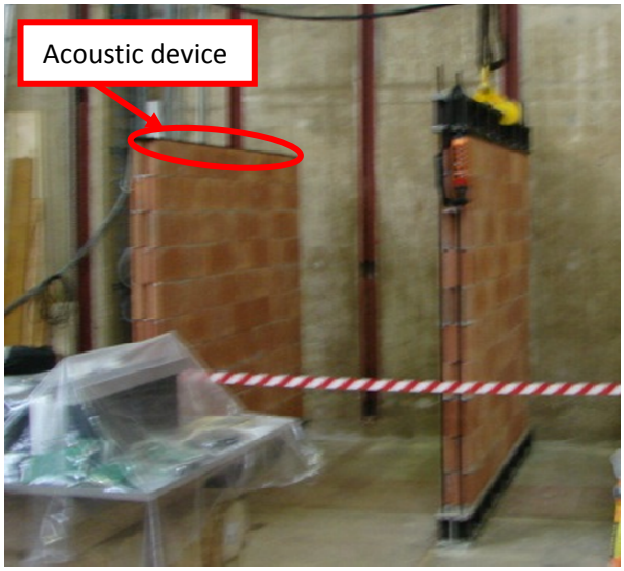


Figure 7 – View of the walls with aspect ratio close to 1, and with acoustic devices (left side) or without (right side)

## 2.2. Dead load

To emulate the structural floor load, a mass is placed on the top of the wall. To respect the capacities of the shaking table of the laboratory, this mass is of 5 tons at most (Figure 8).

Figure 8 – View of the dead load

Even if the mass value is limited by the table capacities, a minimum compression level is compulsory in order to model realistic conditions of load-bearing masonry . With a 5 tons dead load, the compressive stress is about 0.5 MPa for the 0.72m long wall and about 0.15 MPa for the 2.1m long wall. These values are in the usual boundaries of the compression level in masonry.
Therefore, this 5 tons dead load is placed on wall for the tests.

## 2.3. Preliminary assessment of the walls

### 2.3.1. Mechanical and geometrical characteristics

The units used to realize the walls are "*Zonnebeke POROTHERM"*. The walls are built in thin bed masonry with "*PORO+mortar*". Vertical joints are empty and horizontal ones are glued. The block size is :

$$(Length\ x\ Width\ x\ Height) = (300.0\ mm\ x\ 138.0\ mm\ x\ 188.0\ mm)$$

Mechanical characteristics of the units and masonry are the following ones :

- Normalised compressive strength of units (EN 772-1 Annex A)

$$f_b = 13.0\ N/mm^2$$

- Measured characteristic masonry compressive strength (EN 1052-1)

$$f_k = 5.6N/mm^2$$

- Characteristic compressive strength (EN 1996-1-1)

$$f_k = 4.2N/mm^2$$

- Characteristic compressive strength (NBN-EN 1996-1-1)

$$f_k = 3.9N/mm^2$$

No specific characterization has been carried out for shear behaviour. Usual standard values are considered for further assessment :

- Initial shear strength (NBN-EN 1996-1-1)

$$f_{vk0} = 0.3N/mm^2$$

- Characteristic shear strength (NBN-EN 1996-1-1)

$$f_{vk} = 0.5f_{vk0} + 0.4\sigma_d \leq 0.045f_b\ (= 0.585N/mm^2)$$

Regarding acoustic insulation devices, characteristics of the SonicStrip can be found in Annex A.

The geometrical characteristics needed are the inertia and the shear area. In case of simple rectangular walls, these characteristics are easy to determine.

### 2.3.2. Strength verification and acceleration assessment

A preliminary calculation is carried out to assess the value of the acceleration that can be sustained by the wall. The calculation model consists in verifying of the shear stress, the crushing of the units and the rocking. It is based on the concept of compressive length and the verification is made as follows.

The first step consists in doing a first guess of the horizontal shear $V$ and in calculating the compressive length. The horizontal shear represents the inertial effect of the seismic action and it is applied where the mass is located (wall top). Therefore, the horizontal shear involves a bending moment at the wall base. In addition to the compressive stress, the wall is also stressed by a horizontal shear and a bending moment. The value of the bending moment $M$ at the wall base is given by :

$$M = V.H$$

Where $H\ [m]$ is the wall height

It's is assumed that all forces ($N, V\ and\ M$) are applied at the gravity centre of the section.

Once the stresses are known, the couple (bending moment $M$, compressive stress $N$) applied at the gravity centre is replaced by an equivalent compressive stress $N'$applied at a given distance of the gravity centre. This distance is called "eccentricity $e$" and is such as :

$$N' = N \qquad e = \frac{M}{N}$$

The compressive length can then be deduced from the equilibrium equations for materials without tensile strength, where Navier's equations are not valid (Figure 9).

$$L_c = \begin{cases} 0 & if\ e \geq L/2 \\ \left[3.\left(\frac{L}{2} - e\right)\right] & if\ e < L/2\ \wedge\ e > L/6 \\ L & if\ e \leq L/6 \end{cases}$$

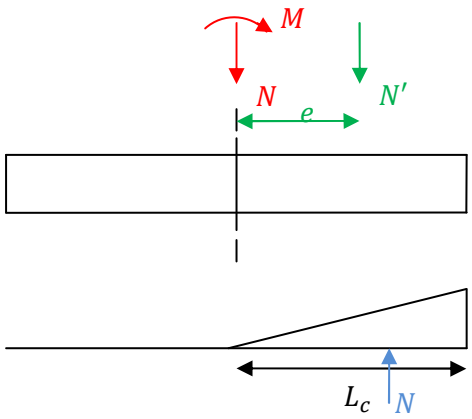


Figure 9 – Sketch for the equilibrium equations

These equations assume a linear distribution of the compressive stresses.

The second step is the verification of the wall resistance. Firstly, several values are calculated thanks to the knowledge of the geometry of the wall, of the compressive load and length, of the mechanical properties of materials and of the characteristic initial shear strength of masonry under zero compressive stress $f_{vk0}$:

- compressive stress in masonry, $\sigma$;

$$\sigma = \frac{N}{t.Lc}$$

- characteristic compressive strength of masonry, $f_k$;

$$f_k = 0.5\ f_b^{0.8}$$

- short term secant modulus of elasticity of masonry, $E$;

$$E = 1000\ f_k$$

- shear modulus of masonry, $G$;

$$G = 0.5\ E$$

- characteristic shear strength of masonry, $f_{vk}$;

$$f_{vk} = \min\left(\frac{f_{vk0}}{2} + 0.4\sigma; 0.045 f_b\right)$$

- the design value of shear resistance

$$V_{Rd} = t.L_c.f_{vk}$$

Then, the verification is made. The overturning is verified as long as the compressive length is positive. The crushing of the units is all right if the compressive stress in masonry is smaller than the characteristic compressive strength. Meanwhile, the shear strength of the wall is checked if the design value of shear resistance is greater than the horizontal shear. In other words, if the following relation is verified :

$$\frac{V - V_{Rd}}{V_{Rd}} < 0$$

The first guess of the horizontal shear must fulfil all the criteria of the verification.

Finally, an iterative calculus is done by increasing the value of the horizontal shear. The increase is applied until one of the verifications is no more checked. The maximum value of the horizontal is the last one which fulfils the criteria.

The third and last step is the calculation of the acceleration. For this, the maximum value of the horizontal shear is divided by the mass applied to the wall top and by a factor 2.5. This factor comes from the elastic response spectra of the Eurocode 8. Masonry walls are stiff structures, their period is a priori on the constant spectral acceleration branch. Therefore, the factor must be applied.

$$Mass = N/10 \qquad a_g = \frac{1}{2.5}.\frac{V_{Rd}}{Mass}$$

The formulae above are valid because the structure can be considered as a single-degree freedom structure. The data and the results are summarized in Table 3.

Table 3 - Data and results of design method[2]

| Tested wall | Length [m] | Compressive load [kg] | Compression Level [MPa] | $V_{Sd}$ [N] | $a_g$ [m/s²] | Stiffness $K$ [N/m] | Period $T$ [s] |
|---|---|---|---|---|---|---|---|
| **Long wall** | 2.10 | 5000 | 0.2 | 26200 | 2.0 | $58{,}69.10^6$ | 0.058 |
| **Long wall** | 2.10 | 8000 | 0.3 | 39400 | 2.0 | $58{,}69.10^6$ | 0.073 |
| **Short wall** | 0.72 | 5000 | 0.5 | 9000 | 0.7 | $3{,}92.10^6$ | 0.224 |
| **Short wall** | 0.72 | 8000 | 0.8 | 13500 | 0.7 | $3{,}92.10^6$ | 0.284 |

The preliminary assessment method is also useful to estimate the natural period,$T$ of the system. For this, the stiffness, $K$, of the system is calculated. Then, knowing the mass, the period can be found. The results are also given in Table 3.

$$K = \frac{1}{\frac{H^3}{3E.\frac{L^3.t}{12}} + \frac{H}{G.\frac{5}{6}.L.t}} \qquad T = 2.\pi\sqrt{\frac{Mass}{K}}$$

The used method is based on formulas coming from different references books as (Eurocode6, 2004) or (Tomazevic, 1999). The value of short term secant modulus of elasticity must catch our attention. In the stiffness calculus, it is taken as $500f_k$ to take the cracking into account (Eurocode 8, 2004).

[2] Design method and results done by H. Degee

## 2.4. Building aspects (beams of support)

Each wall is built and tested between two HEM 160 profiles. The beams are used as wall mounting and for transporting the wall, as explained later. The HEM 160 profiles are stiffened every 300mm to prevent excessive deformations that could cause cracks in walls.

Figure 10 – HEM 160 profile

Figure 10 shows the presence of pieces of expanded metal panels. The panels are added to improve the roughness of the face of the beam flange in contact with the masonry wall. The shear resistance of the beam-wall interface is also improved.

## 2.5. Set up of the walls

As can be seen in Figure 7, the walls are not built on the shaking table for many reasons. Among them, the main ones are the fact that the table would be obstructed for weeks and the wish to prevent any damage of the table. Indeed, the laboratory has other activities and this kind of facilities are very expensive. Considering this, the walls have to be erected somewhere else and, once the walls are ready to be tested, they are transported on the shaking table.

Two solutions are possible to transport the walls. The first one, abandoned because of the difficulties of flatness, is to move the wall by grabbing it by the lower beam and to ensure that it will not switch. The second solution is to take the wall from the top beam. Here, the problem is the low tensile strength of the masonry wall. To avoid this problem, the idea is to connect directly the top and the bottom beams by steel bars (Figure 11) and put them in tension with the intention of pre-compressing the wall. In this way, the wall is in decompression and not in tension.

Figure 11 – View of the steel bars

Deducing the value of the tension to put in each bar is quite easy. First of all, we calculate the weight of the wall and the steel beams

$$Weight = [(Length\ x\ Heigth\ x\ Width)\ x\ \rho + 2\ x\ W_{beam}]\ x\ g$$

where $\rho\ [kg/m^3]$ is the density and $g\ [m/s^2]$ is gravity

Then, the weight is divided by the number of steel bars to get the strain $S$ required in one bar.

We have to know how to apply each bar with the desired strain. This depends on the technology we use, namely bars strained with bolts. In this case, there is a relationship between strain and applied torque (Jaspart, 2010):

$$M_t = K\ x\ S\ x\ d$$

where $K[-]$ is usually taken to 0.2, $S[N]$ is the strain ans $d\ [m]$ is bolt diameter.

This formula is normally used to determine the clamping force in a high-strength bolt, but our application is similar. Thanks to it, the value of the torque $M_t$ can be deduced and can be applied with a torque wrench.

## 2.6. Origin of axis and axis convention

The origin and axis convention must be chosen for two reasons. The first one to be sure of the position of every instrumental device placed on the wall. The second one is the wish to avoid the risk of confusion between two devices. In the Engineering Research Centre of Bristol University, the axis origin is the centre of the shaking table. For the axis convention, the next one is applicable :

- X-axis is positive from the near to the far end of the table ;
- Y- axis is positive from left to right ;
- Z-axis is positive upward

The reference for notions of “near”, “far end”, “left” and “right” of the shaking table is the control mezzanine located as shown in Figure 12. In this one, the notions are identified.

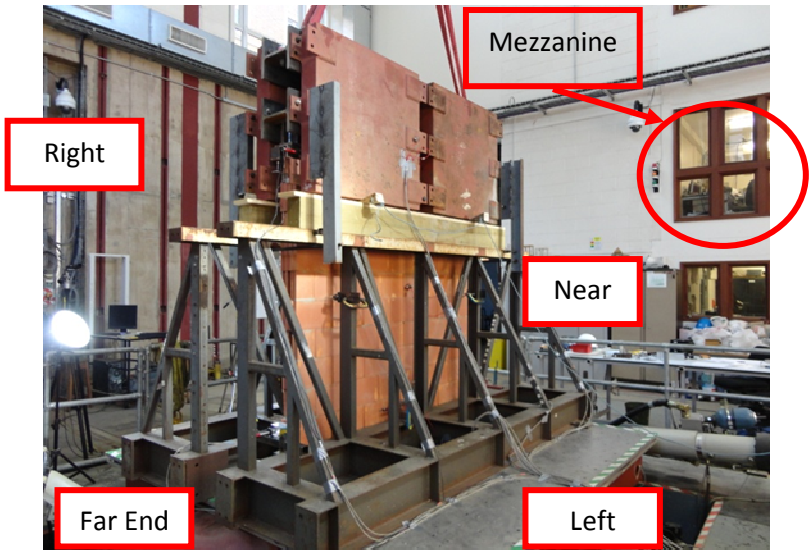


Figure 12 – View of the control mezzanine

## 2.7. ***Instrumentation of the walls***

Phenomena observed in earthquakes are very fast and not so apparent. These ones have to be recorded in order to collect, describe and interpret data. Recording the tests is done with two types of measurement : acceleration and displacement.
All the whole details of the equipment are not given in this work, but the interested reader can refer to the following document "*TA5/TMS – Seismic Behaviour of L- and T-shaped Unreinforced Masonry Shear Walls Including Acoustic Insulation Devices*", available at the "*Earthquake Engineering Centre*" of the University à Bristol (Department of Civil Engineering).

Something more interesting for an Engineer is knowing where the devices are placed on the wall and what they measure. The instrumentation layouts are illustrated in Figure 13 to Figure 16. These layouts are those used during the tests. The legend for each instrumentation layout can be found in Figure 17

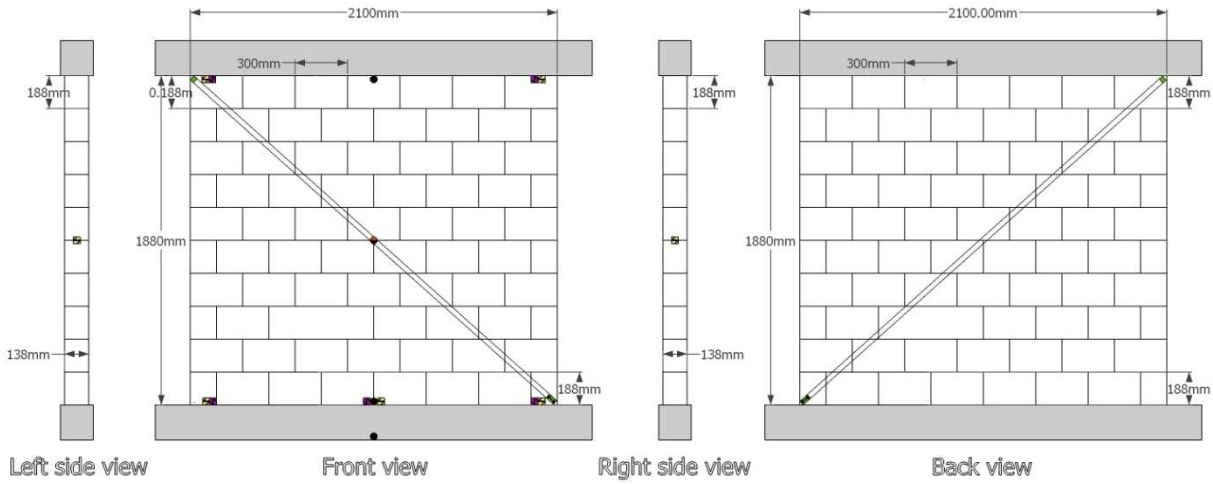


Figure 13 – Instrumentation layout for Specimen 1

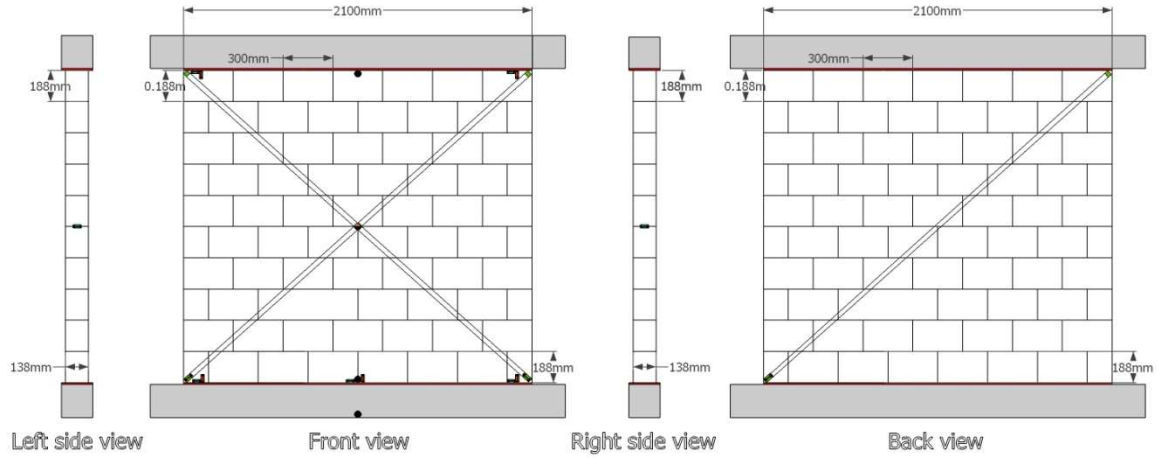


Figure 14 – Instrumentation layout for Specimen 2

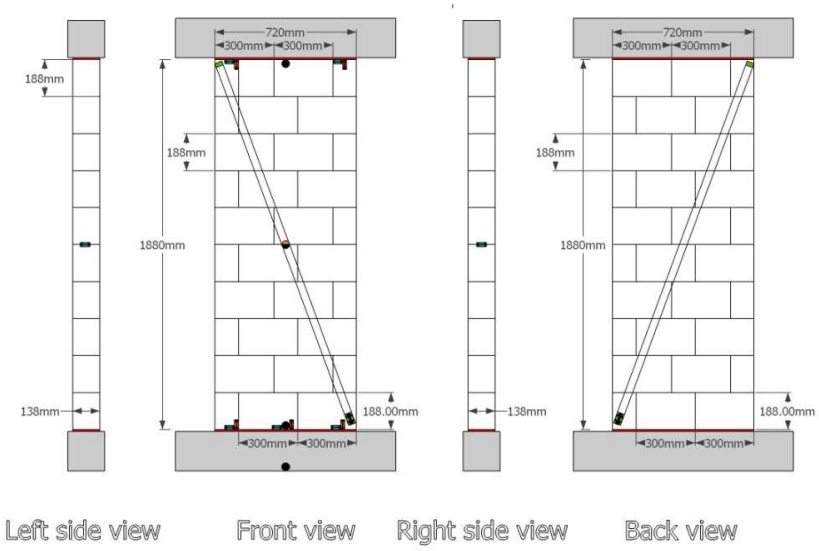


Figure 15 – Instrumentation layout for Specimen 3

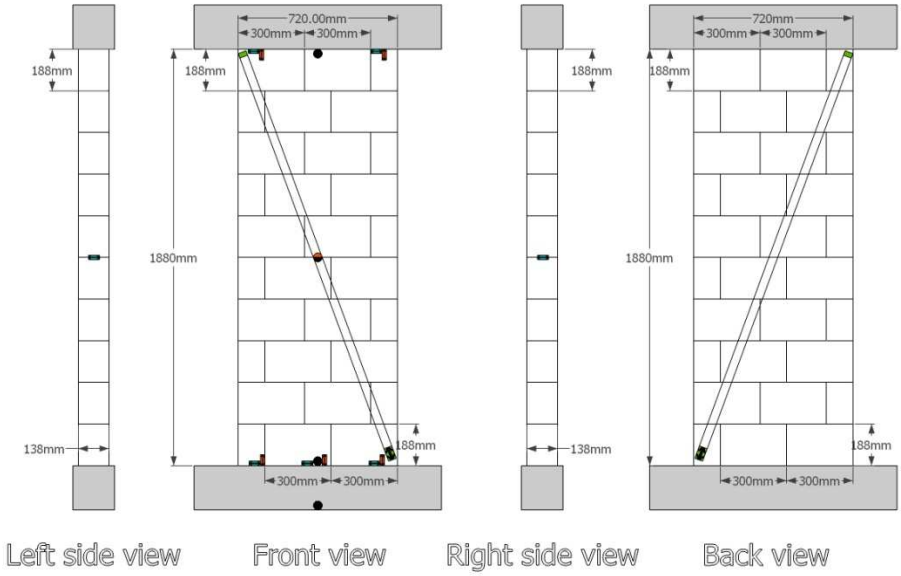


Figure 16 – Instrumentation layout for Specimen 4

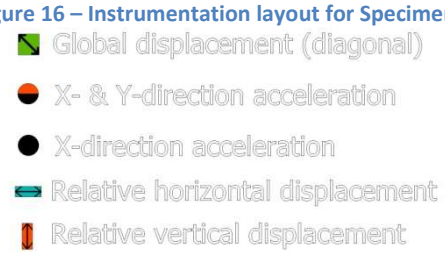


Figure 17 – Legend for Instrumentation layout

Every tested wall has the same instrumentation. The reasons are not only technical and practical, but also due to the desire to make easier the post-processing and the comparisons between each configuration.

In addition, some devices are directly attached to the table, namely one X-direction accelerometer, and on the mass, namely one X-direction accelerometer and eight sensors for the global displacement in X- and Z-directions. The table is also fitted out with 10 sensors to control its 6 liberty degrees.

Finally, a total of 31 devices are present on the table, the wall and the mass. In Table 4, we can see the position and the type of measurement of the devices for the long walls. In this table, different pieces of information are given, among which:

- the first column is the place where each device is fixed ;
- the second one is used to link the device to the data ;
- the third one gives the name of the device, which characteristics are detailed later ;
- the fourth one holds the coordinates according to the origin and the axis conventions ;
- the fifth column describes the measurement ;
- the sixth gives the calibration factors.

A last column is present to give some more useful information, such as the reference of relative displacement, etc.

Table 4 – Information for instrumentation devices (long walls)

| Basis | No chan. | Type of Device | Position | Measurement | Calibration factor | Note [3] |
|---|---|---|---|---|---|---|
| On table | 1 | SETRA 141A | (-1.30 ; 0.00 ; 0.00) | X-acceleration | 1 | |
| | 2 | SETRA 141A | (-1.10 ; -0.05 ; 0.05) | - X-acceleration | 1 | |
| On wall | 3 | SETRA 141A | ( 0.00 ; 0.07 ; 0.20) | X-acceleration | 1 | |
| | 4 | SETRA 141A | ( 0.00 ; 0.07 ; 1.20) | X-acceleration | 1 | |
| | 5 | SETRA 141A | ( 0.00 ; 0.07 ; 1.20) | Y-acceleration | 1 | |
| | 6 | SETRA 141A | ( 0.00 ; 0.07 ; 2.00) | X-acceleration | 1 | |
| On mass | 7 | SETRA 141A | ( 0.10 ; 0.07 ; 2.10) | X-acceleration | 1 | |
| On wall | 8 | LVDT | (-1.10 ; -0.01 ; 0.25) | Z-displacement | 2.178 | R.T. |
| | 9 | LVDT | (-1.10 ; -0.07 ; 1.90) | - Z-displacement | 2.1654 | R.M. |
| | 10 | LVDT | ( 1.10 ; 0.02 ; 0.25) | Z-displacement | 1.4673 | R.T. |
| | 11 | LVDT | ( 1.10 ; -0.06 ; 1.90) | - Z-displacement | 1.4831 | R.M. |
| | 12 | LVDT | ( 0.15 ; 0.07 ; 0.25) | Z-displacement | 1.369 | R.T. |
| | 13 | LVDT | (-0.80 ; 0.07 ; 1.15) | - Y-displacement | 1.3835 | R.T. |
| | 14 | LVDT | ( 0.80 ; 0.07 ; 1.15) | - Y-displacement | 2.1728 | R.T. |
| | 15 | LVDT | (-1.10 ; 0.03 ; 0.30) | X-displacement | 2.8562 | R.T. |
| | 16 | LVDT | ( 0.00 ; 0.07 ; 0.35) | - X-displacement | 5.4193 | R.T. |
| | 17 | LVDT | ( 1.10 ; -0.03 ; 0.35) | - X-displacement | 5.5649 | R.T. |
| | 18 | LVDT | (-0.95 ; 0.07 ; 1.90) | X-displacement | 10.7215 | R.M. |
| | 19 | LVDT | ( 1.00 ; 0.07 ; 2.00) | - X-displacement | 2.735 | R.M. |
| | 20 | Celesco | ( 0.95 ; -0.07 ; 0.30) | Diag. displac. | 21.338 | |
| | 21 | Celesco | ( 0.95 ; 0.07 ; 0.30) | Diag. displac. | 21.546 | |
| Table sensors | 22 | Instron | / | X-displacement | 10 | |
| | 23 | Instron | / | Y-displacement | 10 | |
| | 24 | Instron | / | Z-displacement | 10 | |
| | 25 | Instron | / | $\rho$-angle | 0.1 | |
| | 26 | Instron | / | $\emptyset$-angle | 0.1 | |
| | 27 | Instron | / | X-acceleration | 1 | |
| | 28 | Instron | / | Y-acceleration | 1 | |
| | 29 | Instron | / | Z-acceleration | 1 | |
| | 30 | Instron | / | $\rho$-acceleration | 1 | |
| | 31 | Instron | / | $\emptyset$-acceleration | 1 | |

[3] R.M. means that the measurement is relative to the mass
R.T. means that the measurement is relative to the table

For the short walls, the instrumentation is the same, but the positions of LVDT change for the x-coordinate.
A remark has to be made about the recording. At the beginning of every test, the data origin is equal to the last measurement of the previous test. We have to keep this fact in mind when we will interpret the results of the tests.

The instrumentation layout also includes a vision system data. It consists of the data processed from a Imetrum Video-Gauge Vision System (VS). Eight targets are placed on the frame and the mass (Figure 18) and their horizontal and vertical displacements are recorded. Their coordinates are given in the Table 5.

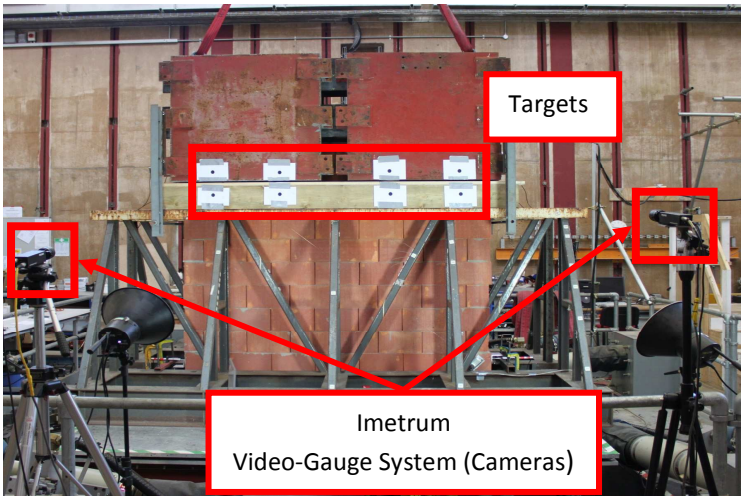


Figure 18 - View of the targets for the Imetrum Video-Gauge Vision System (VS).

Table 5 - Position of the targets for the Imetrum Video-Gauge Vision System (VS).

| Location | Coordinates (x [m],z [m]) | | | |
|---|---|---|---|---|
| | Left | Middle left | Middle right | Right |
| **On the mass** | ( -0.9 ; 2) | ( -0.4 ; 2) | ( 0.4 ; 2) | ( 0.9 ; 2) |
| **On the frame** | ( -0.9 ; 1.8) | ( -0.4 ; 1.8) | ( 0.4 ; 1.8) | ( 0.9 ; 1.8) |

## 2.8. Characteristics of instrumental devices[4]

- Acceleration measurement

SETRA type 141A accelerometers are used. The accelerometers generally have a calibrated range of +/-8g that is traceable to national standards.

- Displacement measurement

Displacements of the test specimen relative to the ES will be monitored using either Celesco draw wire displacement transducers or Linear Variable Differential Transformers (LVDT), whichever is most convenient. These are deployed within specified chains of electronic equipment that comprise also of an amplifier and a filter. Each displacement transducer chain that will is during testing is recorded (as a row) within the Test Instrumentation Record.

[4] Description from the report "*Test Method Statement – TA5/TMS – Seismic Behaviour of L- and T-shaped Unreinforced Masonry Shear Walls Including Acoustic Insulation Devices*".

## 2.9. Calibration of instrumental devices

The first step, before any test, is to calibrate the instrumental devices. This operation is done to be sure that the relation between the magnitude we want to measure and the measured value is correct. Indeed, the “LVDT”, “Celesco”, “SETRA” or “Instron” devices are electrical ones and give data in Volts, whereas they measure displacements or accelerations. The calibration gives the relation to convert the electrical signal in meters or in meters by second square.

To explain how calibrating one device, an example with the LVDT one is taken. First, we push the pointer step by step and keep it pushed during a few seconds. Each step increases the depth by a random, but steady value. This action is recorded to obtain a graph like the one shown in Figure 19.

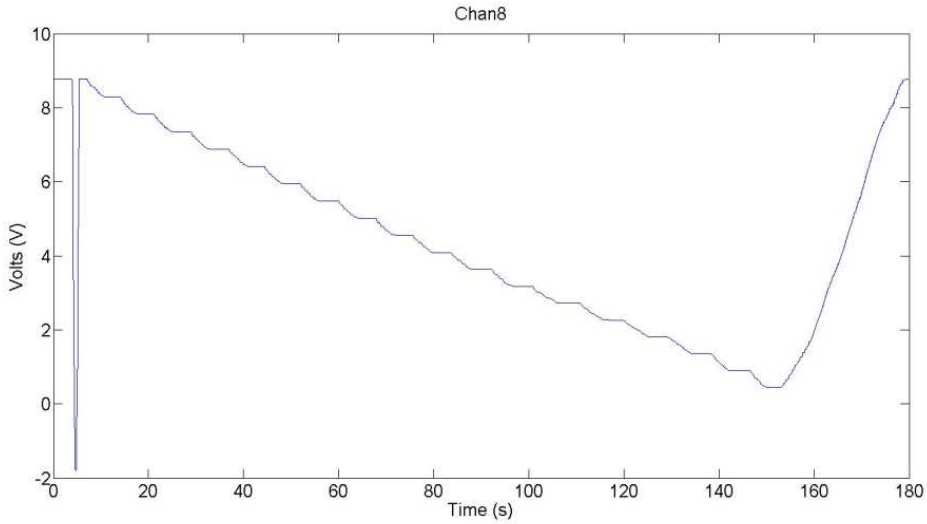


Figure 19 – Calibration : example with channel 8

Then, a program, developed by the laboratory, fit in a straight from the graph to connect the electrical signal to the measured magnitude, as illustrated in Figure 20.

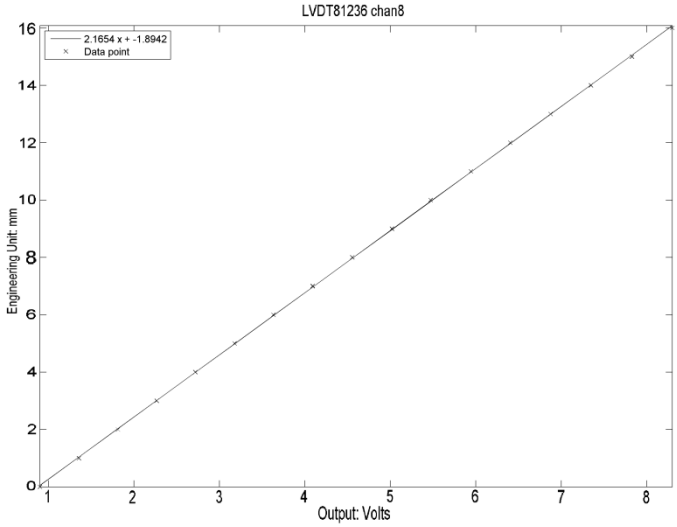


Figure 20 – Interpolation of the example

Finally, the calibration factor is given by the slope of the straight. The factors for all instrumentation devices are given in Table 4. The meaning of the factor value is the next. Let’s take for example the channel 8, the calibration factor means that a variation of 1 Volt is equivalent to a displacement of 2.178 mm.

## 2.10. Excitation waveforms

To simulate an earthquake, the test specimens can be excited with different types of waveform. All walls are designed according to Eurocode 6 and 8, hence the waveform used must be such as its effects are similar to those of an earthquake back in the Eurocode 8.The excitation waveform used for the tests is given in Figure 21.

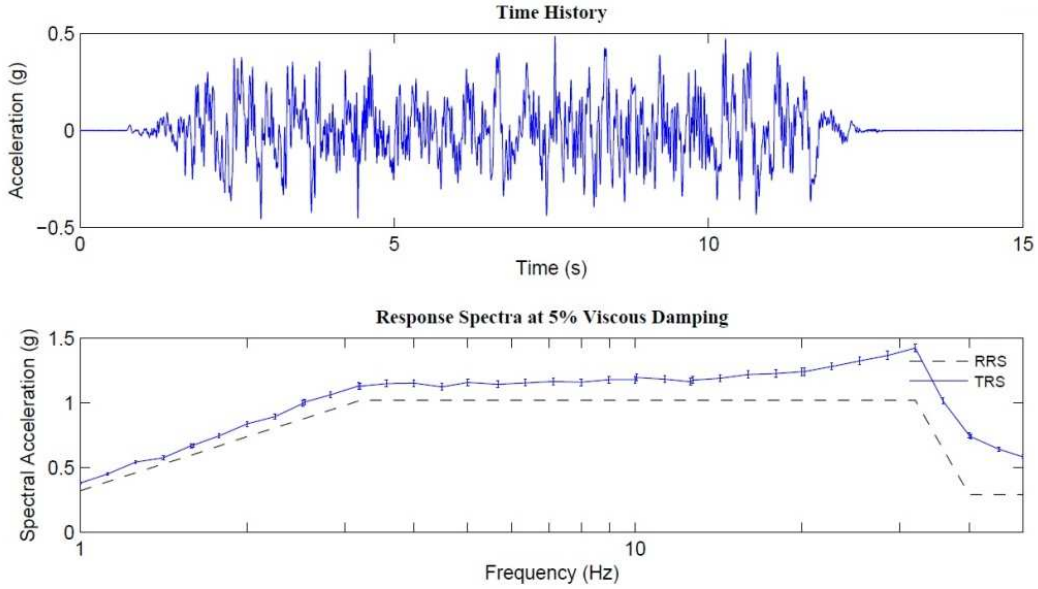


Figure 21 – Characteristics of waveform used

Figure 21 shows two graphs. In the one at the top, we observe the time history of acceleration sent to the table. The time history can be divided in different part. At the beginning, the acceleration is zero. Between the first second and the third second, it increases and the maximum is reached after 3 seconds. The maximum level rests for 8 seconds. Between second 11 and second 13, the acceleration decreases and comes back to zero after 13 seconds.

In the graph at the bottom of Figure 21, there are two Spectral acceleration, a first curve called RSS and another called TRS. The RRS curve is the theoretical spectral acceleration we want and the TRS is the one which is really sent to the table. The maximum acceleration is 0.485g and the minimum is -0.455g.

## 2.11. Security and safety

To end this chapter, some words about the security and the safety during the preparation and the tests are necessary. Besides the wearing of safety helmet and shoes, some devices are provided to prevent the risk of accidents, injuries and damages.

The main one is the presence of steel structures (side frames) on each side of the wall. On these structures, a timber beam is fixed by screws to reduce the vertical space in case of fall of the mass placed on the wall. The mass has rollers bearing on side frames to avoid unwanted out-of-plane motions. The mass is also hung from the crane throughout the duration of the tests and its uprising is avoided by steel bars. This devices' scheme is given in Figure 22[5] .

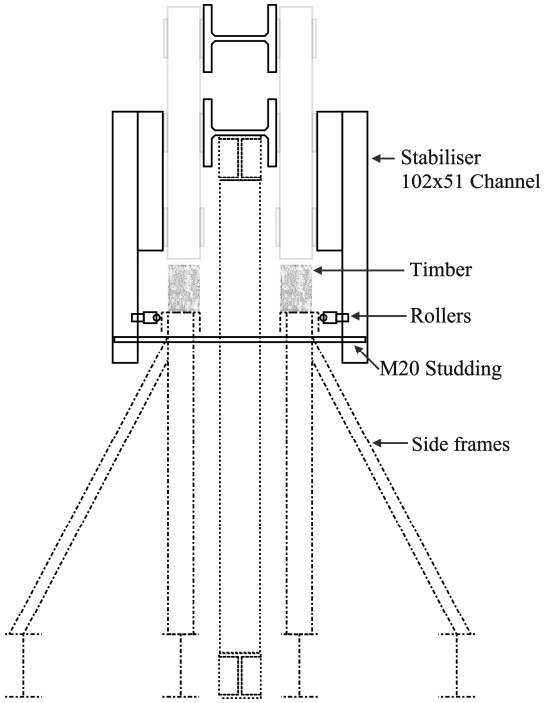


Figure 22 – Safety equipment

During the tests, nobody can stay in the laboratory, except the staff and nobody can go on the shaking table.

[5] Drawing from the report "*Test Method Statement – TA5/TMS – Seismic Behaviour of L- and T-shaped Unreinforced Masonry Shear Walls Including Acoustic Insulation Devices*".

# Chapter 3 :
# Processing of the results of the first test series

## *3.1. Sequences of the tests*

Once the excitation waveform is chosen and the instrumentation is controlled and works, we can begin to test the specimens.
The first measurements are taken during the static loading. The data provided during the loading allow the assessment of Young Modulus of masonry or the SonicStrip device.

Then, the wall is subjected to seismic action. The seismic action is characterized by an acceleration. The first value of the acceleration is not the one we have calculated in the preliminary assessment because the aim of the project is to develop a better understanding of the seismic behaviour of tested masonry walls. Therefore, the acceleration sent to the table is increased step by step. Its increment depends on the phenomena observed during testing. The stopping criteria are such as, on one hand, we have enough data to fill in our objectives and, on the other hand, no damages are done to the table.

In order to have some characteristics of each wall, like its natural frequencies and its damping, each seismic test is followed by a low level "Noise test". This kind of tests is longer than the seismic ones because a stationary configuration is required. This need is due to the assumptions made in the Signal Theory.

For the tests sequences themselves, the idea is to facilitate comparisons between :

- the behaviour of walls of different size ;
- the behaviour of walls of the same size, but one of them owns acoustic insulation devices.

However, we have no interest to directly test the walls with the design acceleration and the acceleration increment must depend on what we observe. It follows some differences between the tests sequences of long walls and short walls.

First, we give the sequence for long walls in Table 6. The ones for short walls in Table 7 and Table 8 are given. To remind, the design acceleration is :

- For long walls : $a_g = 0.2g$
- For short walls : $a_g = 0.07g$

NB : In Table 6, Table 7 and Table 8, the test acceleration which is the nearest of the design acceleration, is highlight in yellow.
In these tables, we observe that test is repeated twice. This repetition is done to be able to compare and to notice how the wall behaviour evolves under a repeated seismic action.

Table 6 – Earthquake Simulator test log for long walls

| Test No. | Type of test | % | PGA [g] | Level [mm/V] | Acq rate [Hz] |
|---|---|---|---|---|---|
| 1 | Static load (SL1) | / | / | / | / |
| 2 | Noise (N1) | / | / | 1.5 | 512 |
| 3 | Noise (N2) | / | / | 2.5 | 512 |
| 4 | Noise (N3) | / | / | 1.5 | 512 |
| 5 | Seismic (S1) | 10 | ~0.05 | / | 512 |
| 6 | Noise (N4) | / | | 1.5 | 512 |
| 7 | Seismic (S2) | 20 | ~0.1 | / | 512 |
| 8 | Noise (N5) | / | | 1.5 | 512 |
| 9 | Seismic (S3) | 20 | ~0.1 | / | 512 |
| 10 | Noise (N6) | / | | 1.5 | 512 |
| 11 | Seismic (S4) | 40 | ~0.2 | / | 512 |
| 12 | Noise (N7) | / | | 1.5 | 512 |
| 13 | Seismic (S5) | 60 | ~0.3 | / | 512 |
| 14 | Noise (N8) | / | | 1.5 | 512 |
| 15 | Seismic (S6) | 80 | ~0.4 | / | 512 |
| 16 | Noise (N9) | / | | 1.5 | 512 |
| 17 | Seismic (S7) | 100 | ~0.5 | / | 512 |
| 18 | Noise (N10) | / | | 1.5 | 512 |
| 19 | Seismic (S8) | 120 | ~0.6 | / | 512 |
| 20 | Noise (N11) | / | | 1.5 | 512 |
| 21 | Seismic (S9) | 140 | ~0.7 | / | 512 |
| 22 | Noise (N12) | / | | 1.5 | 512 |

As we can see in Table 6, the tests are stopped while the acceleration is about 0.7g, 0,679g precisely. This value is about three times higher than the one achieved by the design. Furthermore, the wall can resist to a bigger acceleration. Actually, we didn't increase the value of the acceleration anymore because the behaviour of the long wall without SonicStrip devices became dangerous and the team preferred to stop increasing the acceleration before any damages occur to the table.

Table 7 – Earthquake Simulator test log for short wall with "SonicStrip"

| Test No. | Type of test | % | PGA [g] | Level [mm/V] | Acq rate [Hz] |
|---|---|---|---|---|---|
| 1 | Static load (SL 1) | / | / | / | / |
| 2 | Static load (SL 2) | / | / | / | / |
| 3 | Noise (N1) | / | / | 1.5 | 512 |
| 4 | Noise (N2) | / | / | 3.0 | 512 |
| 5 | Noise (N3) | / | / | 1.5 | 512 |
| 6 | Seismic (S1) | 10 | ~0.05 | / | 512 |
| 7 | Noise (N4) | / | / | 2.0 | 512 |
| 8 | Seismic (S2) | 15 | ~0.075 | / | 512 |
| 9 | Noise (N5) | / | / | 2.5 | 512 |
| 10 | Seismic (S3) | 15 | ~0.075 | / | 512 |
| 11 | Noise (N6) | / | / | 2.5 | 512 |
| 12 | Seismic (S4) | 20 | ~0.1 | / | 512 |
| 13 | Noise (N7) | / | / | 2.5 | 512 |
| 14 | Seismic (S5) | 30 | ~0.15 | / | 512 |
| 15 | Noise (N8) | / | / | 2.5 | 512 |
| 16 | Seismic (S6) | 30 | $\sim 0.15g$ | / | 512 |
| 17 | Noise (N9) | / | / | 2.5 | 512 |
| 18 | Seismic (S7) | 40 | $\sim 0.2g$ | / | 512 |
| 19 | Noise (N10) | / | / | 2.5 | 512 |

Table 8 – Earthquake Simulator test log for short wall without "SonicStrip"

| Test No. | Type of test | % | PGA [g] | Level [mm/V] | Acq rate [Hz] |
|---|---|---|---|---|---|
| 1 | Static load (SL1) | / | / | / | / |
| 2 | Static load (SL2) | / | / | / | / |
| 3 | Static load (SL3) | / | / | / | / |
| 4 | Noise (N1) | / | / | 1.5 | 512 |
| 5 | Noise (N2) | / | / | 1.5 | 512 |
| 6 | Seismic (S1) | 10 | $\sim 0.05$ | / | 512 |
| 7 | Noise (N3) | / | / | 2.5 | 512 |
| 8 | Seismic (S2) | 15 | $\sim 0.075$ | / | 512 |
| 9 | Noise (N4) | / | / | 2.5 | 512 |
| 10 | Seismic (S3) | 15 | $\sim 0.075$ | / | 512 |
| 11 | Noise (N5) | / | / | 2.5 | 512 |
| 12 | Seismic (S4) | 20 | $\sim 0.1$ | / | 512 |
| 13 | Noise (N6) | / | / | 2.5 | 512 |
| 14 | Seismic (S5) | 30 | $\sim 0.15$ | / | 512 |
| 15 | Noise (N7) | / | / | 2.5 | 512 |
| 16 | Seismic (S6) | 30 | $\sim 0.15$ | / | 512 |
| 17 | Noise (N8) | / | / | 2.5 | 512 |
| 18 | Seismic (S7) | 40 | $\sim 0.2$ | / | 512 |
| 19 | Noise (N9) | / | / | 2.5 | 512 |
| 20 | Seismic (S8) | 40 | $\sim 0.g$ | / | 512 |
| 21 | Noise (N10) | / | / | 2.5 | 512 |
| 22 | Seismic (S9) | 50 | $\sim 0.2g$ | / | 512 |
| 23 | Noise (N11) | / | / | 2.5 | 512 |

In Table 7 and Table 8, the maximum acceleration is about $0.25g$. That is between 3 and 4 times more than we predict during the design. Depending on which wall is tested, we can see that the sequences are different because problems were encountered during testing :

- During the loading phase, it took several times to put the mass on the wall. Indeed, in the first try, we see that the wall seems to be hinged due to the presence of SonicStrip devices at wall bottom and top. The solution was to attach the stabilizers and rollers before the mass was in place and to guide the mass with them.
- As in the tests sequence for long walls, a test is repeated at the same level, named 15% here. Nevertheless, we also have to repeat the tests at 30% for each short wall and at 40% only for the short wall without SonicStrip devices. The repetition was done because the safety equipment disturbs the test (steels bars collide side frames) and, so, the measurements were distorted.

For short walls, the tests were stopped because the rollers of mass stabilizers were likely to come out of their position. Thus, the mass could lead to the wall collapsing and damaging the shaking table.

All the tests results are given under a clear and precise naming :

- TA5_120327 is the folder with the results of long wall without SonicStrip ;
- TA5_120330 is the folder with the results of long wall with SonicStrip ;
- TA5_120403 is the folder with the results of short wall with SonicStrip ;
- TA5_120404 is the folder with the results of short wall without SonicStrip.

Each folder contains files with the Noise tests (N“X”), the Seismic tests (S“X”) and the Static Load tests (SL“X”) where “X” is a number in accordance with Table 6, Table 7 or Table 8.

## 3.2. Acceleration really experimented on the table

In Table 6, Table 7 and Table 8, the values of the PGA are those which are theoretical sent to the table. Because of the weight of the specimens, the real PGA are a bit lower than the theoretical values.

The values of the acceleration experimented on the table are the values that must be considered for the exploitation of the results. These values are thus given in Table 9. They are obtained thanks to the maximum value of the channel 1, which is linked to the accelerometer directly placed on the table). In the table, the highlighted lines correspond to the seismic test giving acceleration closest to the value of design.

Table 9 – Earthquake Simulator test log for short wall with “SonicStrip”

| Test | Theoretical PGA [g] | | | | Real PGA [g] | | | |
|---|---|---|---|---|---|---|---|---|
| | Wall 1 | Wall 2 | Wall 3 | Wall 4 | Wall 1 | Wall 2 | Wall 3 | Wall 4 |
| S1 | 0.0485 | 0.0485 | 0.0485 | 0.0485 | 0.0393 | 0.0426 | 0.0417 | 0.0413 |
| S2 | 0.0970 | 0.0970 | 0.07275 | 0.07275 | 0.0777 | 0.0901 | 0.0604 | 0.0654 |
| S3 | 0.0970 | 0.0970 | 0.07275 | 0.07275 | 0.0777 | 0.0877 | 0.0607 | 0.0635 |
| S4 | 0.1940 | 0.1940 | 0.0970 | 0.0970 | 0.1583 | 0.1871 | 0.0803 | 0.0867 |
| S5 | 0.2910 | 0.2910 | 0.1455 | 0.1455 | 0.2387 | 0.2784 | 0.1235 | 0.1356 |
| S6 | 0.3880 | 0.3880 | 0.1455 | 0.1455 | 0.323 | 0.3556 | 0.1278 | 0.1331 |
| S7 | 0.4850 | 0.4850 | 0.1940 | 0.1940 | 0.4496 | 0.4567 | 0.1709 | 0.1784 |
| S8 | 0.5820 | 0.5820 | / | 0.1940 | 0.5716 | 0.5692 | / | 0.1869 |
| S9 | 0.6790 | 0.6790 | / | 0.2425 | 0.6878 | 0.6392 | / | 0.2336 |

NB : Wall 1 : long wall without SonicStrip devices;
Wall 2 : long wall with SonicStrip devices;
Wall 3 : short wall with SonicStrip devices;
Wall 4 : short wall without SonicStrip devices.

## 3.3. Measurements during the static loading

The idea of the measurements done during the static loading is to take advantage of the presence of the sensors on the wall. Thanks to them, an order of magnitude of the elastic modulus of the masonry and of the SonicStrip devices is achieved.
We want to emphasize on the fact that the goal of that measurement is not to determinate the value of the elastic modulus, but only to give an idea of the magnitude.

Considering the instrumentation layouts used (Table 4), the channels 20 and 21 are the only ones useful to assess the elastic modulus of masonry wall. The channels 8 to 12 come in handy to determinate the elastic modulus of acoustic insulation devices. Other captors are useless for static loading, except for the captors of channels 14 and 15 which give the out-of-plan displacement of the wall. Thus, these two last can show if any out-of-plan displacement or buckling appears.
From the vertical displacement, we calculate the value of Young Modulus, $E\ [MPa]$, with the formula coming from the mechanics of materials :

$$E = \frac{N.H}{A\delta_v}$$

where $N\ [N]$ is the weight of the mass ;
$H\ [mm]$ is the height of the wall or the thickness of acoustic insulation device ;
$A[mm^2]$ is the surface where the mass is applied ;
$\delta_v\ [mm]$ is the measured or deduce vertical displacement.

### 3.3.1. Young Modulus of masonry

If the calculation for the SonicStrip devices is straight because the captors corresponding to the channels 8 to 12 measure vertical displacements, the approach isn't so easy for the determination of the Young Modulus of the masonry wall. Indeed, the channels 20 and 21 record a diagonal displacement. Therefore, we have first to deduce a vertical displacement from the diagonal one. Once we have the vertical displacement, the same calculation is done, regardless of whether we are interested by the masonry or the acoustic insulation.

The vertical displacement is s obtained by projecting the diagonal displacement $\delta_d$, as illustrated in Figure 23 and Figure 24. In the first figure, the diagonal displacement is measured by a wired between two points, A and B.

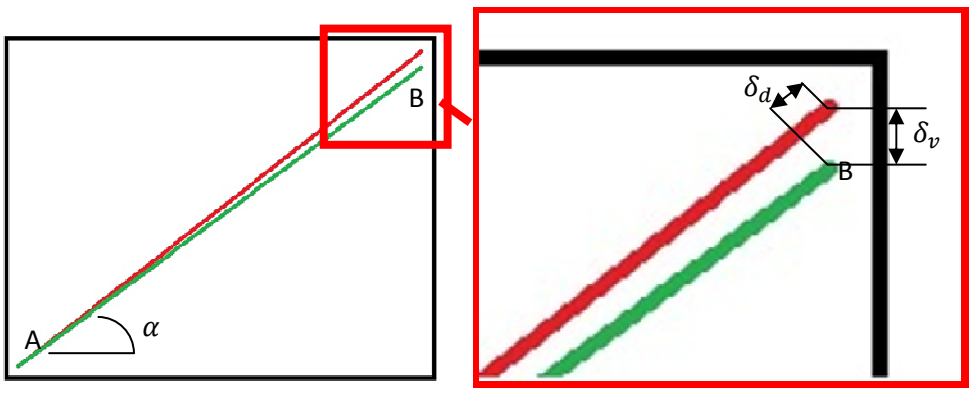


Figure 23 – View of diagonal and vertical displacements

In Figure 24, the vertical displacement is obtained by using the next relation :

$$\delta_v = \delta_d / \sin \alpha$$

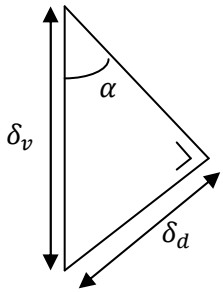


Figure 24 – Projection of diagonal displacement

Once the vertical displacement for both devices is known, we do the mean and take it to assess the value of the Young Modulus, according to the formula written above.
This procedure makes two assumptions. It is supposed that the point A stays where it is before the loading and the horizontal displacement is supposed negligible.

In this way, different values of the Young Modulus of masonry walls are obtained. These ones are shown in Table 10. Two values are given because two devices measure the diagonal displacement : the device linked to channel 20, called “back”, and the one linked to channel 21, called “front”.

Table 10 - Young Modulus for masonry

| | Type of measurement [Units] | Long wall without SonicStrip Static load 1 | Long wall with SonicStrip Static load 1 | Short wall without SonicStrip Static load 1&2 | Short wall without SonicStrip Static load 3 | Short wall with SonicStrip Static load 2 |
|---|---|---|---|---|---|---|
| “Front” side | Vertical disp. [mm] | / | −0.0401 | 0.0386 | −0.0693 | −0.4240 |
| “Back” side | Vertical disp. [mm] | −0.0475 | 0.0237 | −0.2130 | −0.0115 | −0.0833 |
| Mean on the sides | Vertical disp. [mm] | −0.0475 | −0.0082 | −0.0872 | −0.0404 | −0.2536 |
| | E [MPa] | 6 409.2 | 37 153 | 10 190 | 22 005 | 3503.2 |

The values presented in Table 10 are made to give an order of magnitude. Taking in account the procedure used to calculate these ones, with its assumptions and the use of a mean, the results can’t be accurate. In our case, the results do not seem to be workable because of the difference between the lower and upper bound.

### 3.3.2. Young Modulus of acoustic insulation devices

Calculating the Young Modulus of SonicStrip device is easier because the captors directly measure a vertical displacement. Moreover, this one is the relative displacement between the wall and the table for the bottom or the mass for the top. Thus, the crushing of acoustic insulation devices is almost directly measured.
Here, an average is done with the 2 captors at the wall top and the 3 ones at the wall bottom because we don't know if the stress is evenly distributed. The values are provided in Table 11.

Table 11 – Young Modulus for SonicStrip devices

| | Type of measurement [Units] | Long wall with SonicStrip Static load 1 | Short wall with SonicStrip Static loads 1 & 2 |
|---|---|---|---|
| Top of the wall | Near Vertical displacement [mm] | / | $-1.8459$ |
| | Far Vertical displacement [mm] | / | $-2.2777$ |
| Mean | Vertical displacement [mm] | / | $-2.0618$ |
| | Young Modulus [MPa] | / | $2.3943$ |
| Bottom of the wall | Near Vertical displacement [mm] | $-0.2850$ | $-0.6197$ |
| | Middle Vertical displacement [mm] | $0.0102$ | $-1.8520$ |
| | Far Vertical displacement [mm] | $-0.4321$ | $-0.9779$ |
| Mean | Vertical displacement [mm] | $-0.2356$ | $-1.1499$ |
| | Young Modulus [MPa] | $7.183$ | $4.2932$ |

According to the results, the Young Modulus of the acoustic insulation devices varies from 2.39 MPa to 7.183 MPa. The disparity of these values has two main sources :

- The non evenly distribution of stress
- The dispersion of the material properties guaranteed by the producer.

### 3.3.3. Comparison with the EC 6

In this section, the values given by the measurements are compared to the EC6 formulae.

#### *3.3.3.1. Young Modulus of masonry*

First, the values given by the measurements are reminded in the Table 12.

Table 12 – Young Modulus for masonry

| | Long wall without SonicStrip SL 1 | Long wall with SonicStrip SL 1 | Short wall without SonicStrip SL 1&2 | Short wall without SonicStrip SL 3 | Short wall with SonicStrip SL 2 |
|---|---|---|---|---|---|
| E [MPa] | 6 409.2 | 37 153 | 10 190 | 22 005 | 3503.2 |

As can be seen in Table 12, the calculated values are located in a huge interval, from $3503\ MPa$ to $37\ 153\ MPa$. As it was said in the chapter 3, the difference between the lower and upper bound clearly shows that the results are not reliable.

Then, the following formulae are used (Eurocode6, 2004) :

$$f_k = 0.5\ f_b^{0.8} = 3.892\ MPa \qquad E = 1000\ f_k = 3892\ MPa$$

Finally, the comparison between the calculated value and the one coming from the (Eurocode6, 2004) shows that the value of the European standard is close to the lower bound of the interval of calculated values.

#### *3.3.3.2. Young Modulus of acoustic insulation devices*

On one hand, the values given by the measurements are reminded in Table 13.

Table 13 – Young Modulus for SonicStrip devices

| | Long wall with SonicStrip Static load 1 | Short wall with SonicStrip Static loads 1 & 2 |
|---|---|---|
| Top E [MPa] | / | 2.3943 |
| Bottom E [MPa] | 7.183 | 4.2932 |

On the other hand, these calculated values are compared to the ones (from 3.00 to 12.00 MPa) guaranteed by the producer Annexe A. As the calculated values are in the interval, the conclusion is that the assessment method of the producer is valid.

## 3.4. White Noise tests

The white noise tests are performed according to the next procedure. (Dietz, 2012)
"A random (white noise) excitation with frequency content between 1Hz and 100Hz and at level of about 0.1g RMS is generated using an Advantest R9211C Spectrum Analyser. The random signal is used to drive the Earthquake Simulator (ES) in a single direction.
The 'input' and 'response' channels of the Spectrum Analyser are connected to appropriate instrumentation (e.g. ES Y acceleration and inclusion-head Y acceleration, respectively). The Spectrum Analyser acquires 32 segments of time data, convert to the frequency domain and average results to produce a transfer function. Natural frequency and damping values are determined for all coherent resonances using curve-fitting algorithm running on the Spectrum Analyser. Visual inspections will be made after each test to ensure no damage has occurred."

### 3.4.1. Post-processing of the laboratory

The working of the Spectrum Analyser is described above.

The White Noise tests are carried out when the mass is put on the wall fixed on the shaking table and after each seismic test. The transfer functions and the other data are given in the folder of the results data, but it could be interesting to show one of them for each wall. For example, we illustrate the transfer functions of the White noise tests done after the acceleration level of $S3$ $(long\ walls)$ in Figure 25and $S4$ $(short\ walls)$ in Figure 26.

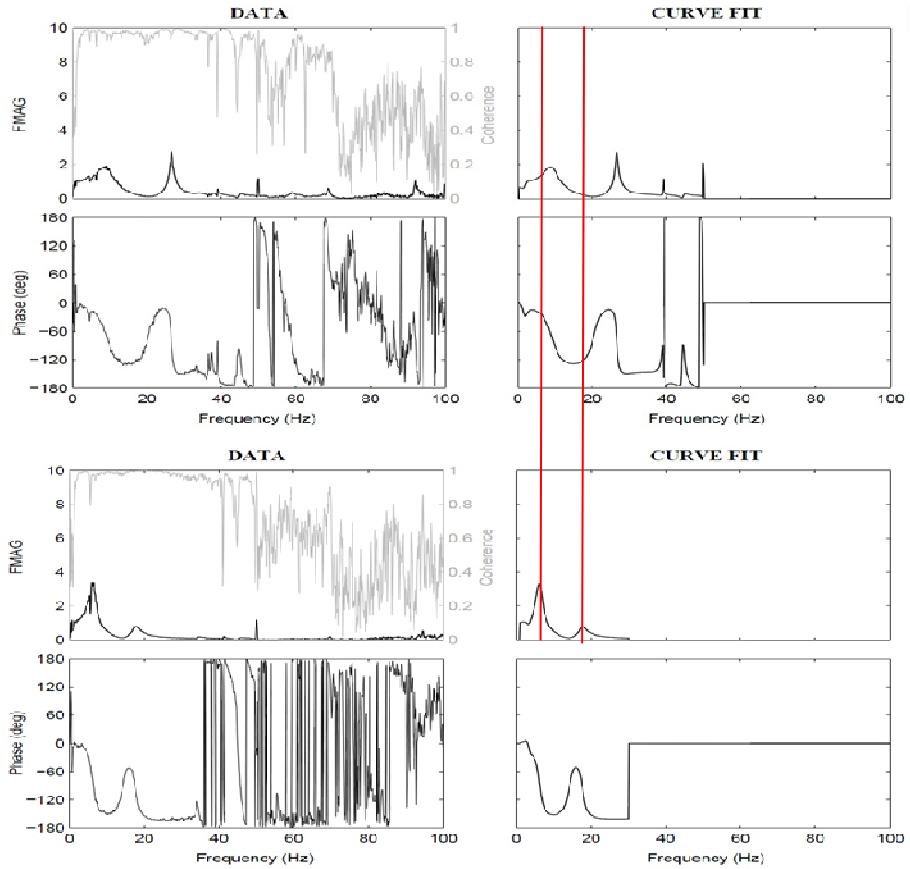


Figure 25 – Transfer Function of long walls without (above) and with (below) SonicStrip devices

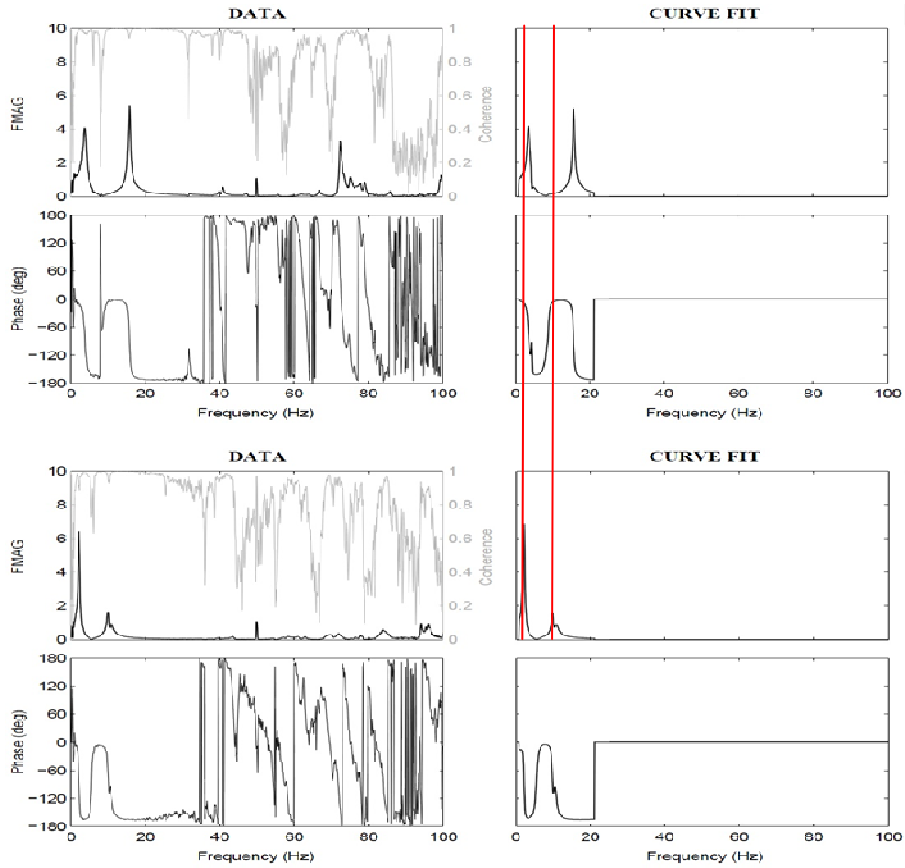


Figure 26 – Transfer Function of short walls without (above) and with (below) SonicStrip devices

In Figure 25, we see the transfer functions and the phases of the long walls without acoustic insulation devices in the four graphs above and with devices in the four graphs below. Figure 26 shows the same characteristics for short walls, with acoustic insulation for the four graphs at the top and without acoustic devices for the four graphs underneath.

In every groups of four graphs, we can find :

- Above left : the transfer function calculated with recorded data ;
- Above right : the curve fit of the transfer function ;
- Below left : the phase calculated with recorded data ;
- Below right : the curve fit of the phase.

For both figures, two red lines are drawn on the fitting curves, which cross the frequency peaks of the wall with SonicStrip devices. These peaks correspond to the Eigenmodes of the walls. In each figure, if we compare the frequencies for which the peaks occur, we observed that the peaks appear at lower frequency when the wall has acoustic insulation devices. This comparison is born out thanks to the Table 14, where we give the peaks frequency for each white noise tests. The damping are also given.

The white noise tests chosen are those which follow a seismic test.

Table 14 – Frequencies and damping of the peaks of transfer functions (Post-processing of the laboratory)

| Long wall without SonicStrip | 1st peak frequency [Hz] | 1st peak damping [%] | 2nd peak frequency [Hz] | 2nd peak damping [%] |
|---|---|---|---|---|
| N 4 | 9.23 | 8.94 | 26.94 | 1.56 |
| N 5 | 9.19 | 23.71 | 26.61 | 1.74 |
| N 6 | 9.17 | 28.46 | 26.62 | 1.82 |
| N 7 | 10.41 | 93.77 | 26.21 | 2.21 |
| N 8 | 7.67 | 82.94 | 25.97 | 2.42 |
| N 9 | 5.93 | 126.33 | 25.69 | 2.50 |
| N 10 | 6.29 | 132.20 | 25.45 | 2.50 |
| N 11 | 5.02 | 161.90 | 25.52 | 2.65 |
| N 12 | 5.26 | 95.75 | 26.11 | 2.41 |
| **Long wall with SonicStrip** | | | | |
| N 4 | 6.45 | 8.33 | 17.86 | 5.88 |
| N 5 | 6.29 | 14.30 | 17.65 | 5.78 |
| N 6 | 6.16 | 13.90 | 17.62 | 5.93 |
| N 7 | 5.91 | 28.16 | 17.30 | 6.23 |
| N 8 | 5.53 | 40.43 | 17.05 | 6.59 |
| N 9 | 4.75 | 26.29 | 16.62 | 7.18 |
| N 10 | 4.87 | 42.54 | 16.29 | 6.81 |
| N 11 | 4.68 | 36.83 | 16.08 | 7.80 |
| N 12 | 4.31 | 31.93 | 15.70 | 8.37 |
| **Short wall without SonicStrip** | | | | |
| N 3 | 3.99 | 3.86 | 15.88 | 1.30 |
| N 4 | 3.86 | 7.27 | 15.81 | 1.45 |
| N 5 | 3.77 | 14.97 | 15.81 | 1.45 |
| N 6 | 3.63 | 10.87 | 15.71 | 1.56 |
| N 7 | 3.67 | 15.06 | 15.44 | 1.91 |
| N 8 | 3.54 | 15.54 | 15.38 | 1.74 |
| N 9 | 3.50 | 17.44 | 15.00 | 2.05 |
| N 10 | 3.45 | 19.60 | 14.87 | 2.00 |
| N 11 | 3.30 | 17.84 | 14.38 | 2.32 |
| **Short wall with SonicStrip** | | | | |
| N 4 | 2.38 | 9.14 | 11.37 | 4.01 |
| N 5 | 2.30 | 6.53 | 10.83 | 3.76 |
| N 6 | 2.26 | 6.70 | 10.54 | 3.87 |
| N 7 | 2.24 | 6.52 | 10.79 | 3.99 |
| N 8 | 2.17 | 9.41 | 10.61 | 2.74 |
| N 9 | 2.21 | 8.45 | 10.49 | 4.29 |
| N 10 | 2.22 | 9.19 | 10.16 | 5.22 |

The Table 14 confirms the lower frequencies of peaks of the wall with acoustic insulation devices in comparison with the wall of the same length without these devices. It can also be seen that the value of the first peak frequency decreases after each seismic test.

The variation of the damping of the first peak is very important for the long walls (maximum between 40 and 162*%). This remarks is especially available for the long wall without SonicStrip devices (161.90%).* That means a high degradation of the wall.

The frequency of the second peak is more constant and its damping lower (max. 8.4%).

### *3.4.2.* Own post-processing

An alternative post-processing has been developed for the following reasons.
On one hand, the transfer functions of the walls present some blunt and wide peaks (Figure 25). It follows that the curve fitting is less accurate and gives approximate values of peak frequencies and damping. Thus, the results are not reliable.
On the other hand, doing our own post-processing will provide us more information. Indeed, we can not only calculate the values of the natural frequencies and the damping, but also determinate the Eigenvalues and Eigenmodes of the tested walls. These characteristics are useful to understand the behaviour of the wall.

Our own post-processing consists in using the data of the accelerometers and in calculating their Power Spectral Density (PSD) and their cross-Power Spectra Density[6]. This calculus gives us a squared matrix frequency-dependant which dimensions are the number of accelerometers considered.
Once we have the frequency-dependant cross-PSD matrix, we are able to deduce the transfer function, the natural frequencies, the damping, and the Eigenmodes of any wall after any seismic test. The natural frequencies are noticed on the figure of the transfer functions and the damping is given by the next formula :

$$\xi = \frac{\beta_2 - \beta_1}{\beta_2 + \beta_1}$$

Where $\beta_2 - \beta_1$ is the width of the mid-height peak.

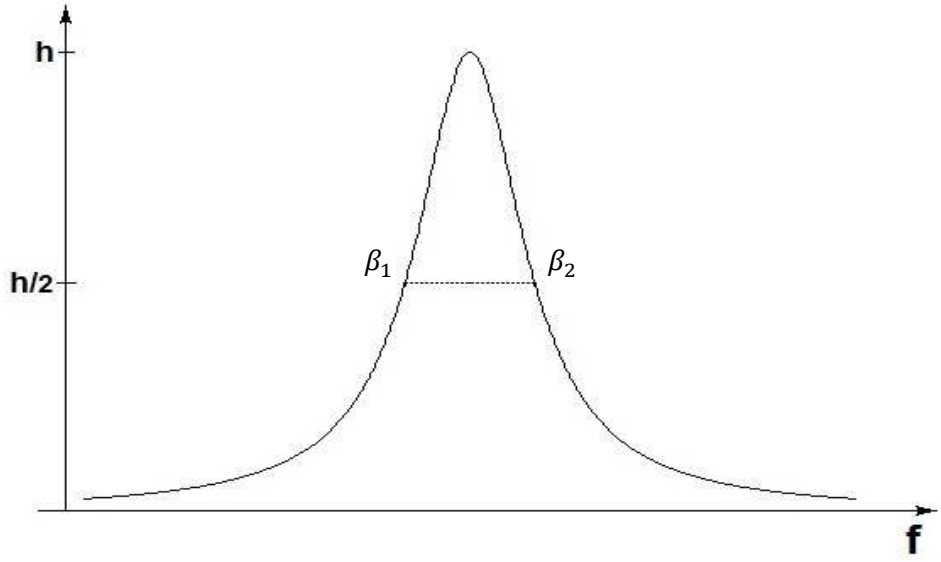


Figure 27 – Calculation of the damping

In Figure 28, Figure 29, Figure 30 and Figure 31, we draw the transfer function of each tested walls after all acceleration levels used for seismic tests. This function is obtained by the ratio between the PSD of the accelerometer placed on the bottom and the PSD of the accelerometer fixed on the mass.

[6] The calculation calls a routine develop by Vincent Denoël

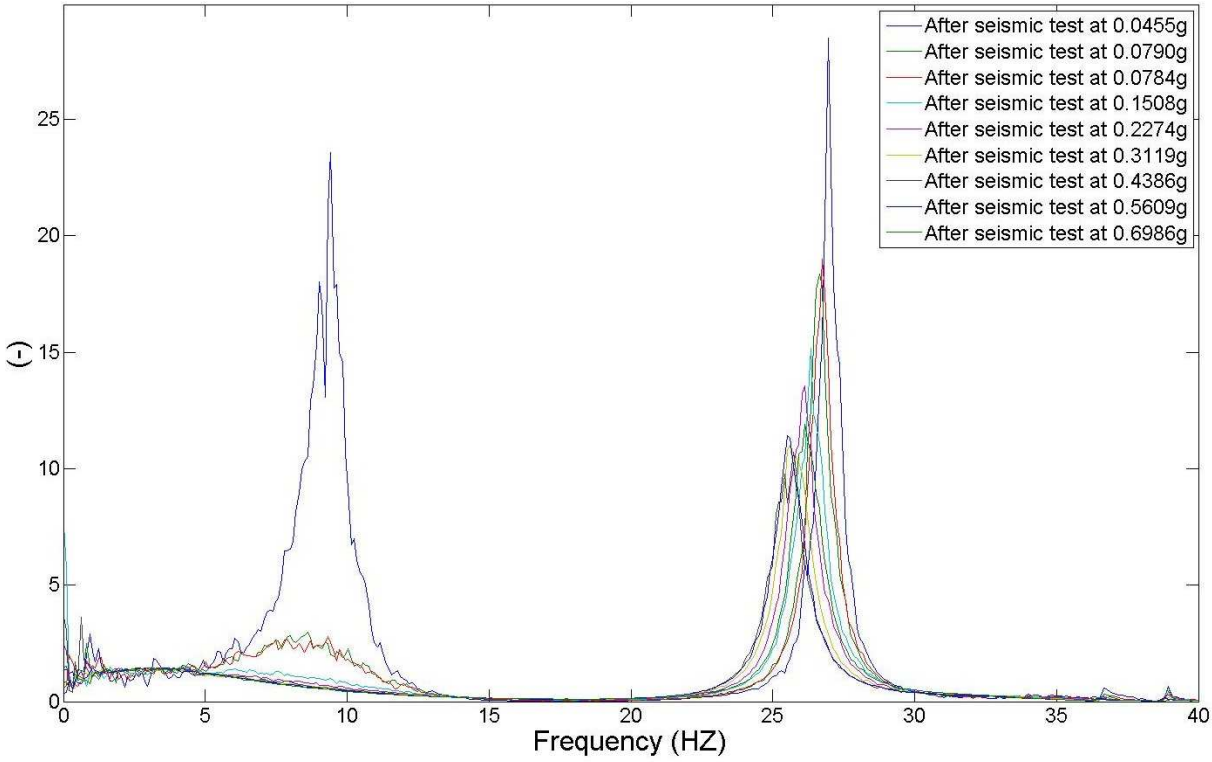


Figure 28 – Transfer functions of long wall without SonicStrip devices

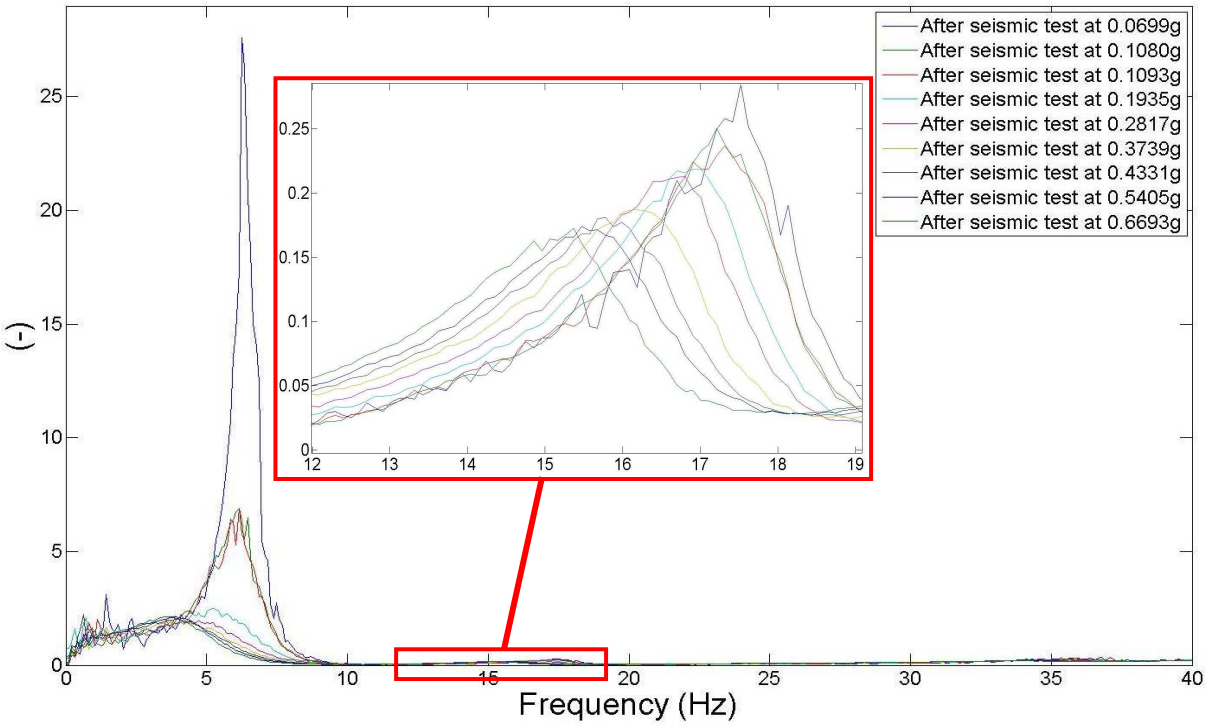


Figure 29 – Transfer functions of long wall with SonicStrip devices

For the long walls, we notice that the first peak of transfer function progressively decreases when the acceleration level of seismic tests increases. This peak also becomes larger and appears at lower frequency. The deterioration of the structure explains this phenomenon, which involves an increase of the damping. At the beginning , the value of the first peak frequency is about 9 Hz for the long wall without SonicStrip devices and about 6 Hz for the one with acoustic insulation devices.

The second peak, for its part, is nearly the same in each white noise test. Nevertheless, we observe that the peak magnitude and the appearance frequency decrease slightly when the acceleration level

of seismic tests increases. A last observation is that, after every seismic tests, the second peak frequency is about 26.5 Hz for the long wall without SonicStrip devices and about 16.5 Hz for the one with acoustic insulation devices.

In order to illustrate these comments, we put the natural frequencies (frequencies of 1st and 2nd peaks) and its damping for both walls in Table 15. They are drawn in Figure 32 (see later). It can already be said that the assessment of the frequency for the first peak is not accurate because this peak becomes quickly flat.

Table 15 – Frequencies and damping of the peaks of transfer functions (Owned post-processing – Long wall)

| Long wall without SonicStrip | 1e peak frequency [Hz] | 1e peak damping [%] | 2e peak frequency [Hz] | 2e peak damping [%] |
|---|---|---|---|---|
| N 4 | 9.43 | 6.73 | 26.95 | 1.28 |
| N 5 | 8.61 | 31.4 | 26.74 | 1.6 |
| N 6 | 9.23 | 38.69 | 26.64 | 1.68 |
| N 7 | 6.05 | / | 26.33 | 2.01 |
| N 8 | 3.40 | / | 26.13 | 1.94 |
| N 9 | 3.68 | / | 25.62 | 2.74 |
| N 10 | 3.38 | / | 25.72 | 2.76 |
| N 11 | 3.18 | / | 25.51 | 2.56 |
| N 12 | 3.18 | / | 26.13 | 2.46 |
| **Long wall with SonicStrip** | **1st peak frequency [Hz]** | **1st peak damping [%]** | **2nd peak frequency [Hz]** | **2nd peak damping [%]** |
| N 4 | 6.25 | 6.36 | 17.52 | 5.91 |
| N 5 | 6.1 | 16.78 | 17.21 | 6.86 |
| N 6 | 6.15 | 16.67 | 17.32 | 7.49 |
| N 7 | 5.23 | 50.26 | 16.91 | 8.07 |
| N 8 | 4.71 | / | 16.80 | 8.55 |
| N 9 | 4.20 | / | 16.19 | 9.63 |
| N 10 | 3.89 | / | 15.78 | 9.82 |
| N 11 | 3.89 | / | 15.47 | 10.55 |
| N 12 | 3.48 | / | 15.37 | 10.5 |

In the Table 15, some values of the damping are not calculated because of the flatness of the peak.

If the values for the long walls of Table 15 and Table 14 are compared, the following observations can be made. The values of the frequency of the 1st peak are close for the three first tests (N4, N5 and N6), but becomes different from one post-processing to the other. The relative difference between our post-processing and this of the laboratory is about 0.1% to 6% for the tests N4, N5 & N6, and about 10 to 55 % for the others. The difference is more important in the case of the long wall without SonicStrip devices because of the shapes of the peaks. Indeed, the first peak is more flat in the case of the long wall without SonicStrip devices.

Concerning the values of the frequency of the 2nd peak, the maximum relative difference between the two methods is about 4% at least.

The damping values are very close. The relative difference is at most about 0.26% for the long wall without SonicStrip devices and about 0.44% for the long wall with these devices.

In conclusion for the long walls, the deterioration of the first frequency peak and its flattening make approximate the value of the peak frequency. It results in a big variability of the value of natural frequency. Concerning the damping, it seems to be well assessed as the two post-processing give close values

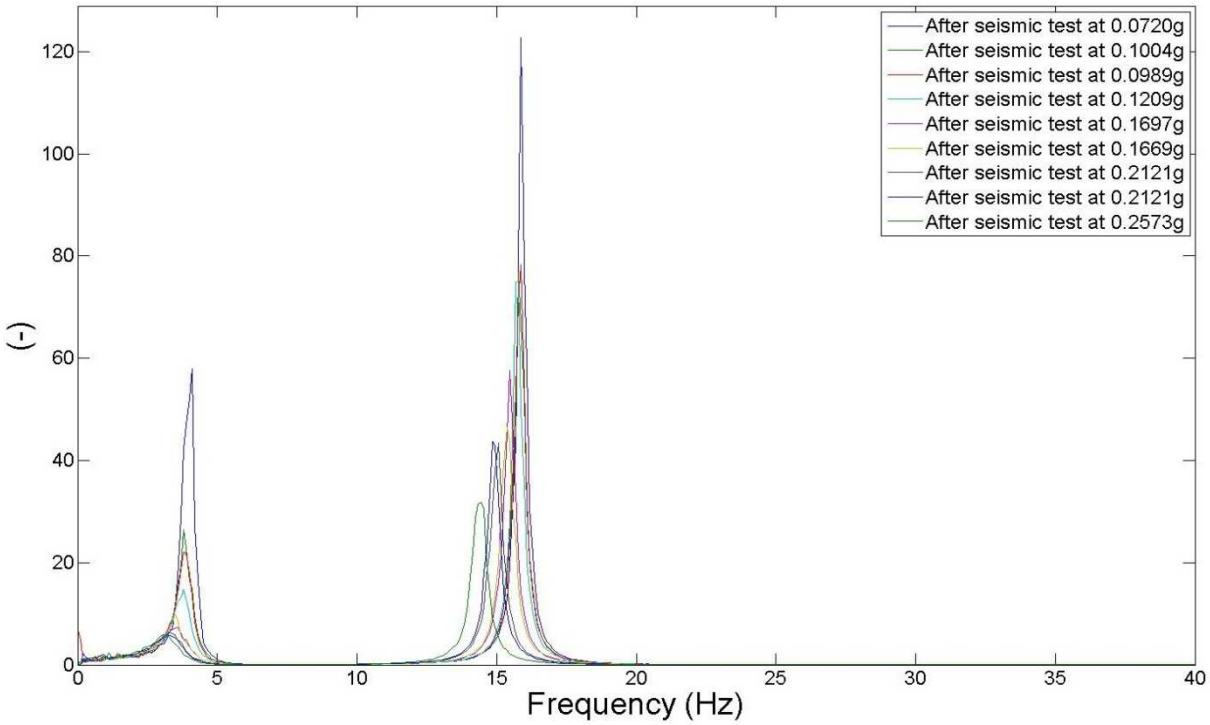


Figure 30 – Transfer functions of short wall without SonicStrip devices

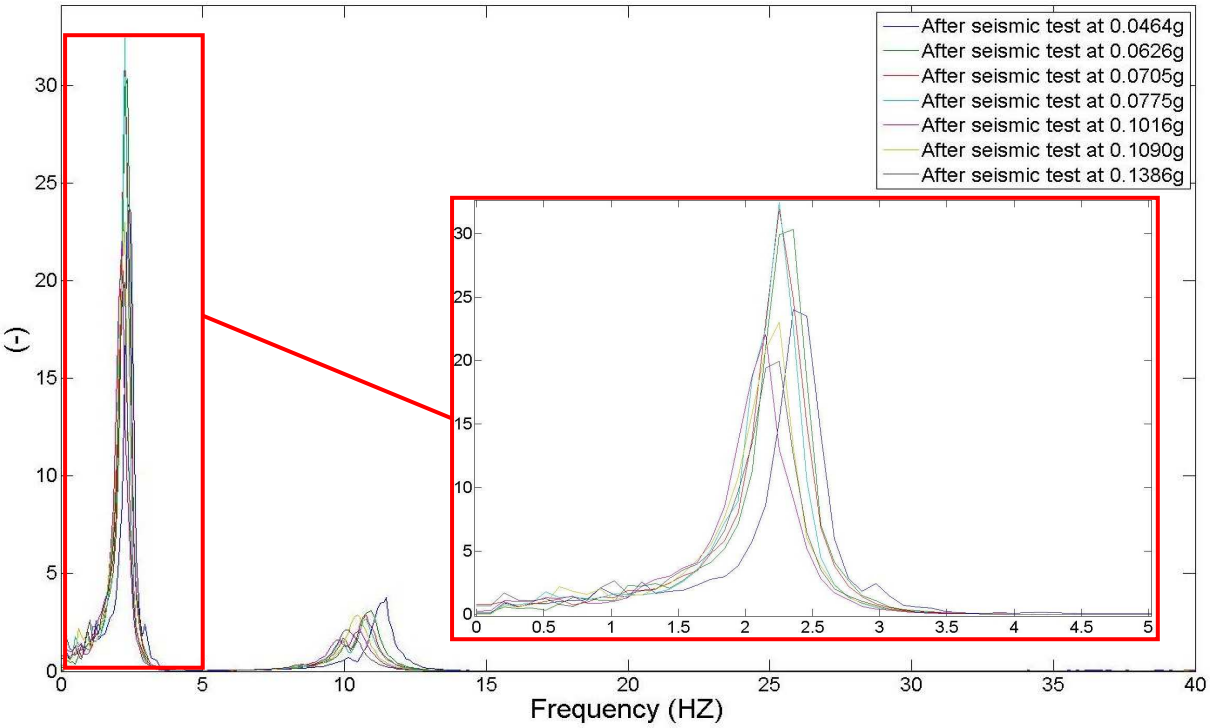


Figure 31 – Transfer functions of short wall with SonicStrip devices

For the short walls, the Figure 30 and Figure 31 show that the first peak of transfer function also decreases when the acceleration level of seismic tests increases. However, the deterioration is less important than in the case of the long walls and the peak relatively stays well definite.
The same comments can be made for the second peak of short walls than the one of long walls.

Once again, the natural frequencies (frequencies of 1st and 2nd peaks) for both short walls are put in Table 16 and drawn in Figure 33 to support the comments above. The values of damping are also given.

Table 16 – Frequencies and damping of the peaks of transfer functions (Owned post-processing – Short walls)

| Short wall without SonicStrip | 1st peak frequency [Hz] | 1st peak damping [%] | 2nd peak frequency [Hz] | 2nd peak damping [%] |
|---|---|---|---|---|
| N 3 | 4.10 | 6.43 | 15.88 | 0.98 |
| N 4 | 3.79 | 7.82 | 15.78 | 1.39 |
| N 5 | 3.79 | 8.79 | 15.88 | 1.42 |
| N 6 | 3.79 | 10.51 | 15.78 | 1.36 |
| N 7 | 3.58 | 17.94 | 15.47 | 1.55 |
| N 8 | 3.48 | 11.4 | 15.37 | 1.95 |
| N 9 | 3.28 | 20.01 | 15.06 | 1.83 |
| N 10 | 3.18 | 23.07 | 14.86 | 1.78 |
| N 11 | 3.07 | 22.75 | 14.45 | 2.23 |
| **Short wall with SonicStrip** | | | | |
| N 4 | 2.36 | 8.06 | 11.48 | 3.49 |
| N 5 | 2.36 | 8.71 | 10.96 | 4.05 |
| N 6 | 2. 24 | 8.34 | 10.76 | 3.81 |
| N 7 | 2.25 | 8.73 | 10.76 | 3.72 |
| N 8 | 2.15 | 9.78 | 10.56 | 2.56 |
| N 9 | 2.25 | 9.65 | 10.45 | 4.49 |
| N 10 | 2.25 | 10.24 | 10.04 | 3.39 |

In Table 16, the maximum difference between the values from the two post-processing is under 8% for the 1st peak and the one for the 2nd peak is about 2 %.
The damping values are also very close. The relative difference is at most about 0.41% for the short wall without SonicStrip devices and about 0.35% for the short wall with these devices.

In conclusion, there are some deteriorations of the short walls, but the peaks are still sharp after the testing program. The frequency of the peaks is also easy to find. Concerning the damping, it seems to be well assessed as the two post-processing give close values

The Figure 32 and Figure 33 summarize the natural frequencies of the four walls. The comments written previously are illustrated by these figures. A difference is particularly visible in the case of the long wall without acoustic insulation devices because the first peak of frequency of this wall is the most deteriorated after the tests.

The main conclusion of the study of the natural frequency of the walls is that the natural frequency of each peak is lower when the acoustic insulating devices are installed at the bottom and the top of the wall. If the long(short) wall without SonicStrip devices is compared with the long(short) wall with the devices, the difference between the frequencies of the same peak is about 30% for each peak.

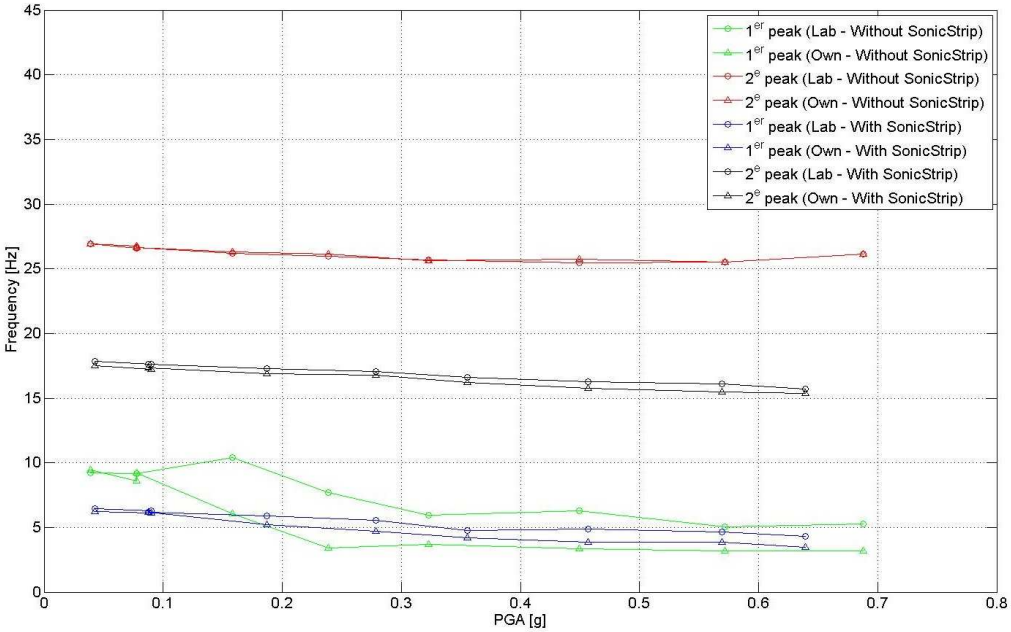


Figure 32 – Natural frequencies of the long walls according to PGA

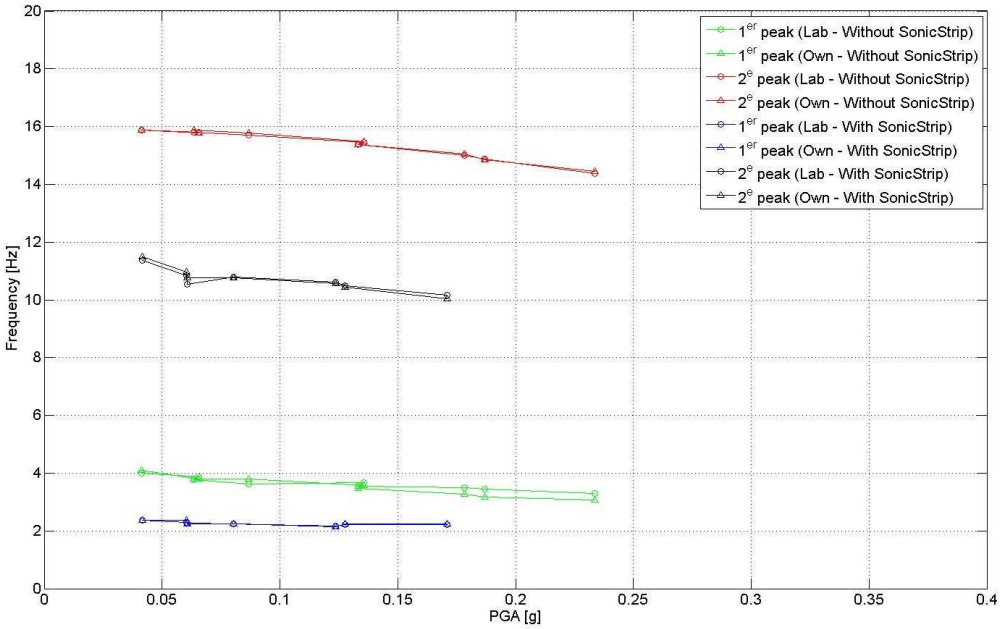


Figure 33 – Natural frequencies of the short walls according to PGA

Now we can go further than the laboratory post-processing and try to get the Eigenvalues and Eigenmodes of the tested walls.

For squared matrix frequency-dependant of cross PSD, the first step is to choose one value of frequency. As we want to find the Eigenmodes, the frequency chosen is one of the peak frequency of transfer function identified previously. Then, the eigenvalues and eigenvectors of the squared matrix are calculated. Finally, the Eigenmode relative to one natural frequency is obtained thanks to the eigenvector relative to the largest eigenvalue and we draw it to have the shape of the Eigenmode.
To remind, the size of the squared matrix is six because the instrumentation includes seven accelerometers, but only six are fixed on the structure installed on the shaking table. So, the structure is assumed as a 6 dofs structure.

As it was found during the transfer functions analysis, the walls seem to have two natural frequencies because these functions own two peaks. Therefore, we have two shapes for each wall and for each white noise tests done after the seismic ones, for a total of 18 shapes by wall. In order to compare the shapes between different tests, the elements of eigenvector relative to the largest eigenvalue are divided by the norm of the eigenvector.

Figure 34, Figure 35, Figure 36 and Figure 37 give the modal shapes of the four tested walls. The shapes are gathered together to have all shapes of the same wall for one natural frequency. For these figures, we have several graphs which represent :

- At Figure 34 top, the first modal shape of long wall without SonicStrip ;
- At Figure 34 bottom, the second modal shape of long wall without SonicStrip ;
- At Figure 35 top, the first modal shape of long wall with SonicStrip ;
- At Figure 35 bottom, the second modal shape of long wall with SonicStrip.

- At Figure 36 top, the first modal shape of short wall without SonicStrip ;
- At Figure 36 bottom, the second modal shape of short wall without SonicStrip ;
- At Figure 37 top, the first modal shape of short wall with SonicStrip;
- At Figure 37 bottom, the second modal shape of short wall with SonicStrip.

The Y-axis of these two figures gives the position of the accelerometers placed on the structure. Knowing that, we approximately know where the degrees of freedom are.

The comparison of the different graphs of Figure 34 to Figure 37 is carried out with the aim to show not only the differences between the shapes of the same Eigenmode for the different acceleration level, but also the ones between the first and the second modal shape of the same wall and those between the same modal shape of the different walls.
For that reason, the comparison is focused on three points : the alignment of the devices located on the wall, the position of the sensor at the wall bottom relative to that of the captor placed on the beam and the position of the captor at the wall top relative to this one of the sensor put on the mass.

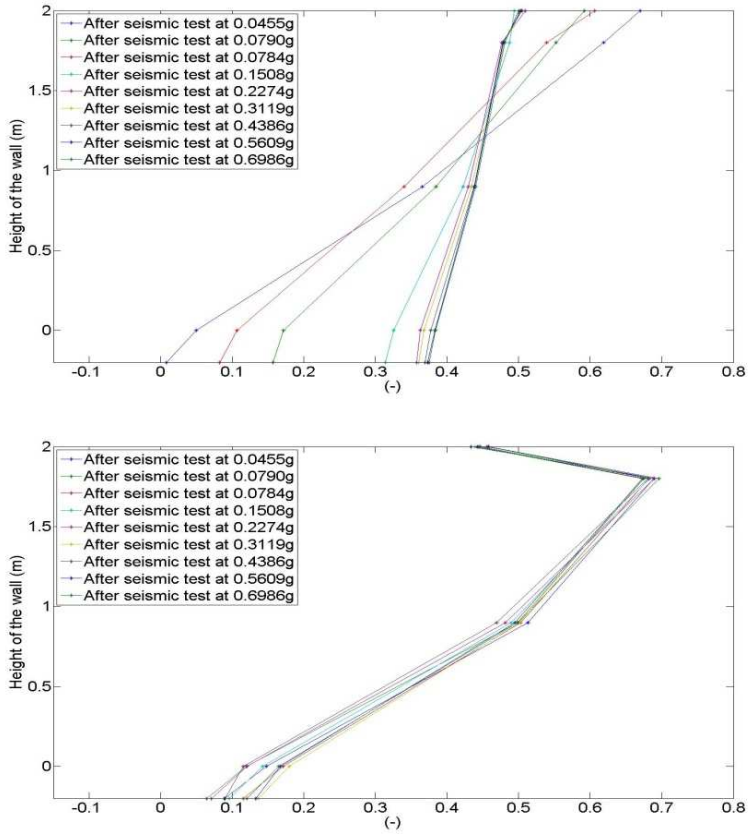


Figure 34 – 1er (above) and 2e (below) modal shapes (Long wall without SonicStrip)

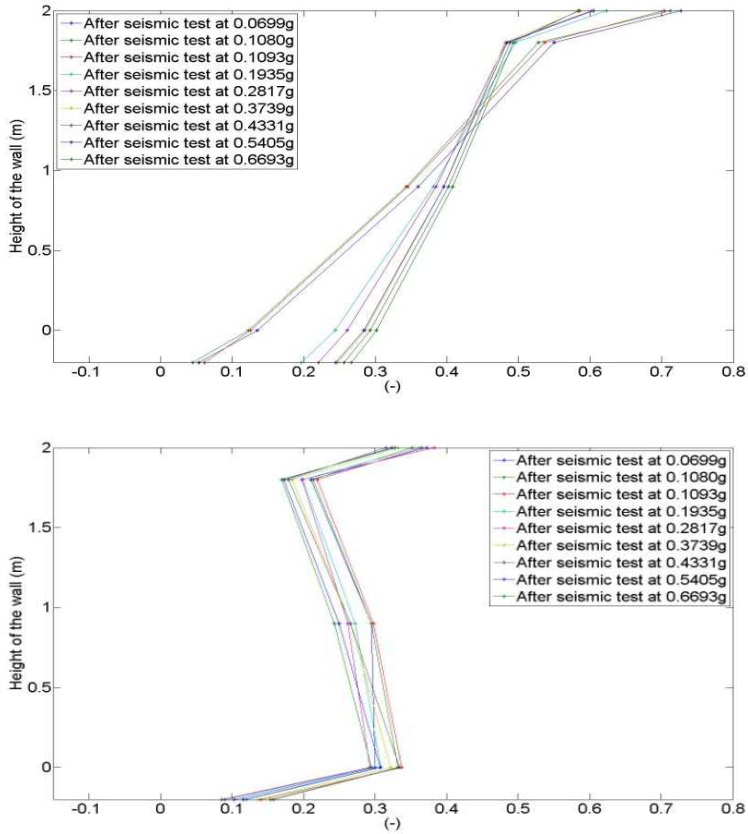


Figure 35 – 1er (above) and 2e (below) modal shapes (Long wall with SonicStrip)

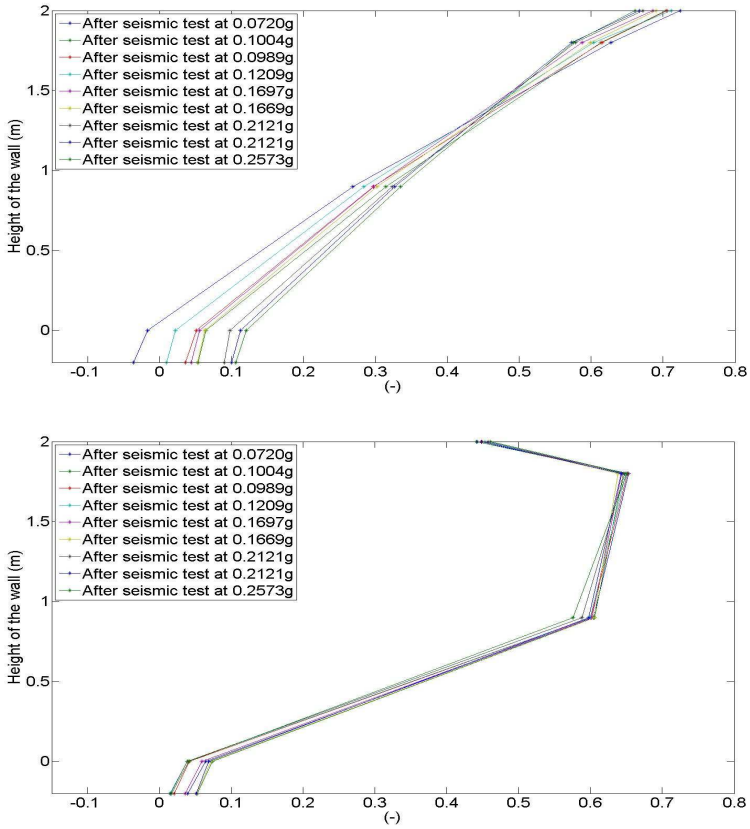


Figure 36 – 1er (above) and 2e (below) modal shapes (Short wall without SonicStrip)

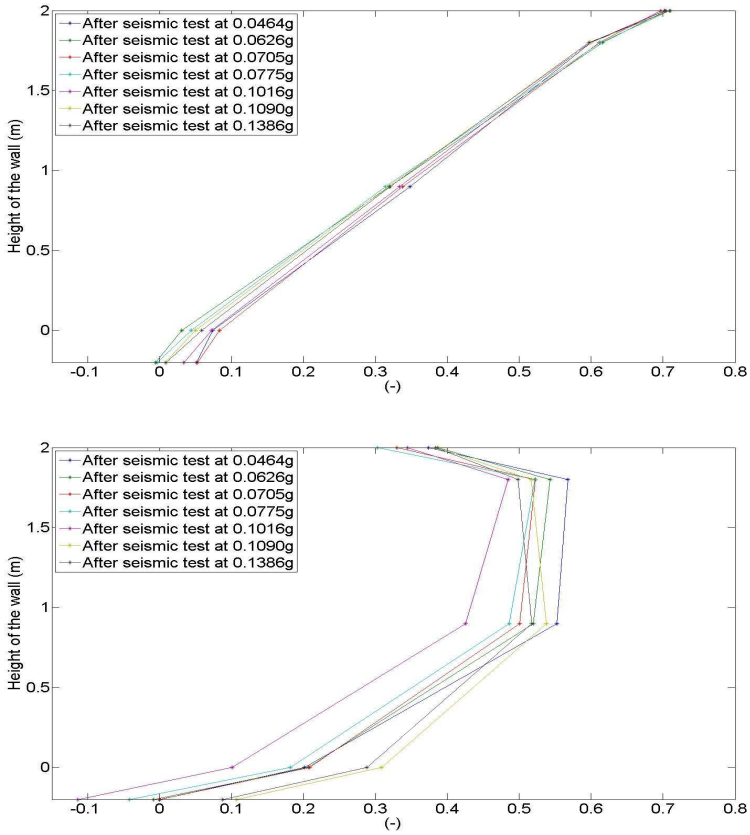


Figure 37 – 1er (above) and 2e (below) modal shapes (Short wall with SonicStrip)

Table 17 summarizes the main differences observed.

Table 17 – Comparison of the modal shapes

| Long wall without SonicStrips | |
|---|---|
| **Differences between the 1st modal shapes** | The slope of the line connecting the sensors placed on the wall changes after the third seismic test (at 0.097g). Therefore, there are two kind of shapes for the first Eigenmode. |
| **Differences between the 2nd modal shape** | All the acceleration level give a similar modal shape and no changing is observed. |
| **Alignment of the sensors placed on the wall** | The sensors placed on the wall seem to be almost on a straight line. |
| **Relative position of the captor at the wall bottom and the one on the beam** | For the first modal shape, the position of the sensor on the beam is nearly at the same place than the one place at the wall bottom. The maximum difference is about 0.05 (for the seismic test at 0.0485g).<br>For the second modal shape, the position of the sensor on the beam is also close to this of the captor on the wall bottom. The difference is at most 0.1. |
| **Relative position of the captor at the wall top and the one on the mass** | For the first modal shape, the position of the sensor on the mass and this of the sensor placed at the wall top are close. The maximum difference is about 0.1.<br><br>For the second modal shape, a huge difference is observed. It seems that the mass and the wall are in opposition phase. |
| **Conclusions** | The first modal shape looks like a straight line where the wall and the mass are in phase.<br>The second modal shaped is a broken line, with two segments, showing an opposition phase between the wall (first segment) and the mass (second segment)<br>The specimen may be replaced with a single degree of freedom structure. |

| Long wall with SonicStrips | |
|---|---|
| **Differences between the 1st modal shapes** | The slope changing of the line connecting the sensors placed on the wall is also observed after the third seismic test (at 0.097g). Nevertheless, the difference is smaller than in the case of the long wall without SonicStrips. |
| **Differences between the 2nd modal shape** | All the acceleration level give a similar modal shape and no changing is observed. |
| **Alignment of the sensors placed on the wall** | The sensors placed on the wall seem to be almost on a straight line. |
| **Relative position of the captor at the wall bottom and the one on the beam** | For the first modal shape, the difference increases a bit, but stays at most 0.1.<br><br>For the second modal shape, the sensors are quite far from each other. The first is at 0.1, whereas the second is close to 0.3. |
| **Relative position of the captor at the wall top and the one on the mass** | For the two modal shapes, a big difference is noticed between the position of the sensor on the beam and this of the captor on the wall bottom. The difference is about 0.2 for each Eigenmode. |
| **Conclusions** | Unlike the long wall without SonicStrips, the wall and mass behaviour look like different because of the presence of acoustic insulating devices.<br>Except for the mass, the first modal shape is the same for the long wall with or without SonicStrips.<br>The second modal shape of the long wall with acoustic insulating devices can be interpolated with a 3-segments broken line. The wall seems to move between the bottom beam and the mass. The specimen may be replaced with a three degrees of freedom structure. |

| | Short wall without SonicStrips |
|---|---|
| **Differences between the 1st modal shapes** | Like for the short wall with SonicStrips, the shapes are close from each other and the slope is the same for all acceleration levels. The general shape is similar to the first one of the first Eigenmode of the long wall without SonicStrip devices |
| **Differences between the 2nd modal shape** | The observations are also the same than those made for the short wall with SonicStrips. |
| **Alignment of the sensors placed on the wall** | The first modal shapes are close to a straight line.<br>For the second modal shapes, a break is observed. |
| **Relative position of the captor at the wall bottom and the one on the beam** | 1st modal shapes : The sensors are practically in a vertical straight line. It can be deduced that no movement exists between the wall and the bottom beam.<br>2nd modal shapes : The same comments can be said, but the straight line is not so vertical. |
| **Relative position of the captor at the wall top and the one on the mass** | The remarks made for the short wall with SonicStrips are valid. |
| **Conclusions** | The differences with the same wall with acoustic insulating devices are small or negligible. It can be explained by the low area of the wall-beam interface and by the low horizontal connection between the wall and the mass. |

| | Short wall with SonicStrips |
|---|---|
| **Differences between the 1st modal shapes** | The shapes are close from each other and the slope is the same for all acceleration levels. The shapes look like the first one of the first Eigenmode of the long wall without SonicStrip devices |
| **Differences between the 2nd modal shape** | All acceleration levels give a similar shape. They also look like the 2e modal shapes of the long wall without acoustic insulating devices. |
| **Alignment of the sensors placed on the wall** | The alignment is perfect for the first modal shapes, but a break is observed for the second one. |
| **Relative position of the captor at the wall bottom and the one on the beam** | For the first modal shape, the difference is small and about 0.05.<br><br>For the second modal shape, the position of the sensor at the wall bottom is far from the one on the beam (0.2) |
| **Relative position of the captor at the wall top and the one on the mass** | For the two modal shapes, a big difference is observed. The difference goes from 0.1 to 0.2 for each Eigenmode. |
| **Conclusions** | The modal shapes of the short wall with SonicStrips are very close to the ones of the long wall without SonicStrips.<br>The presence of acoustic insulating devices is observed thanks to the differences between the positions of the sensors placed on the wall or on the beam/mass. |

Some general comparisons and conclusions can be made between the walls of different length. The first and main one concerns the shape of the wall. The shapes of the Eigenmodes are nearly the same for all the acceleration levels. There is only a little difference in the first modal shape of the long walls.

For each tested wall, the presence of acoustic insulation device is shown with the comparison of the positions of the sensors placed on the bottom beam and the wall or the wall and the mass. With these devices, the stiffness of the wall decreases and, so, the displacements increases.

### 3.4.3. Comparison with the preliminary assessment

To remind, the Noise tests were done to characterize the walls. One of these characteristics is the natural frequency. The Table 18 gives the value of the natural frequencies of the structure (wall + mass) before the first seismic test.

Table 18 – Natural frequencies of the long wall obtained by the laboratory processing

| | | Wall without SonicStrip | | Wall with SonicStrip | |
|---|---|---|---|---|---|
| | | First peak | Second peak | First peak | Second peak |
| **Long wall** | **N3** | 9.01 Hz | 25.50 Hz | 5.26 Hz | 16.15 Hz |
| **Short wall** | **N2/3** | 3.81 Hz | 15.67 Hz | 2.53 Hz | 11.14 Hz |

In the preliminary assessment, the period of the single-freedom degree structure and, so, the natural frequency were calculated as follows :

$$T = \frac{1}{f} = 2\pi\sqrt{\frac{M}{K}}$$

Where $M\ [kg]$ is the mass (5000 kg)

$K\ [N/m]$ is the stiffness of the structure

The value of the stiffness is the sum of two contributions (Tomazevic, 1999) : the bending (1) one and the shear one (2). In the case of a wall built-in at the bottom and free at the top, we have :

$$\frac{H^3}{3EI}\ (1) \qquad \frac{H}{GA'}\ (2)$$

$$K = \frac{1}{\frac{H^3}{3EI} + \frac{H}{GA'}}$$

Where $H\ [m]$ is the height of the wall ;

$I\ [mm^4]$ is the inertia of the wall ;

$A'\ [mm^2]$ is the shear area of the wall, taken to $5/6$ of the wall area (Serge Cescotto & Charles Massonet, 2001) ;

$E\ [N/m^2]$ is the elastic Modulus of the masonry ;

$G\ [N/m^2]$ is the shear Modulus of the masonry.

In these formulas, the factor 3 is due to the support conditions of the wall (built-in at the bottom and free at the top). The value of the elastic modulus $E$ must be divided by 2 to take into account the cracking (Eurocode8*, 2004) and shear modulus may be taken as 40% of the elastic modulus (Eurocode6, 2004).

These formulae are directly usable for the walls without acoustic insulation devices. Some modifications are required to apply them to the walls with the devices. Due to the time, these modifications are not made in this work.

Table 19 – Natural frequency according to the EC & dynamic's equations

| Tested wall | Length [m] | M [kg] | Stiffness $K$ [N/m] | Period $T$ [s] | Frequency [Hz] |
|---|---|---|---|---|---|
| **Long wall** | 2.10 | 5000 | $52{,}76.10^6$ | 0.0642 | 15.59 |
| **Short wall** | 0.72 | 5000 | $3{,}84.10^6$ | 0.238 | 4.203 |

The comparison between the values of the frequency of the first peak [7] mentioned in Table 18 and those in Table 19 shows that the frequencies obtained thanks to the noise tests and the ones given by the preliminary assessment are uneven. The relative error is equal to :

- 45.69 % for the long wall
- 9.35 % for the short wall

The difference for the long wall is more important. Consequently, the shear contribution to the stiffness seems to be the problem. In the case of the long wall, this term is actually of the same order of magnitude than the bending one, as shows in the Table 20. In the case of the short wall, the shear contribution is about 10% of the bending one.

Table 20 – Stiffness of the wall according to the EC

| Tested wall | Bending contribution [m/N] | Shear Contribution [m/N] | Stiffness $K$ [N/m] |
|---|---|---|---|
| **Long wall** | $9{,}3799.10^{-9}$ | $9{,}5753.10^{-9}$ | $52{,}76.10^{6}$ |
| **Short wall** | $2{,}3273.10^{-7}$ | $2{,}7928.10^{-8}$ | $3{,}84.10^{6}$ |

To summarize, the assessment of the wall stiffness in accordance to the EC6 seems to give a wrong value of the shear stiffness. The mistake can come from the value of the shear or the one of the shear modulus. As the formula of the shear area stemmed from the materials strength, the second possibility may be the reason. These formulae were also developed for continuous materials and it can be a third reason.
Moreover, the values we used are suggested by Eurocode6 and are about unreinforced masonry walls. However, the tested walls have empty vertical joints. It involves a higher shear deformation and it confirms the idea of a wrong assessment of the shear modulus.

In Table 21, the results of the stiffness and frequencies are given for a value of the shear modulus equal, for example, to 10% of the elastic modulus.

Table 21 – Stiffness of the wall with the suggested value of the shear modulus $(0,1E)$

| Tested wall | Bending contribution [m/N] | Shear Contribution [m/N] | Stiffness $K$ [N/m] | Frequency [Hz] |
|---|---|---|---|---|
| **Long wall** | $9{,}3799.10^{-9}$ | $3{,}8301.10^{-8}$ | $20{,}973.10^{6}$ | 10.31 |
| **Short wall** | $2{,}3273.10^{-7}$ | $1.1172.10^{-7}$ | $2{,}903.10^{6}$ | 3.835 |

With that value of shear modulus, the relative error is equal to :

- 12.61 % for the long wall
- 0.65 % for the short wall

Although these results are better than the previous ones, the relative error is still too important in the case of the long wall. It can be concluded that the shear modulus value cannot be simply taken as a percentage of the elastic modulus. Other parameters must be taken into account. Obviously, the determination of the parameters and of this kind of rules needs more research and results.

[7] The comparison is made with the frequency of the first peak because of its Eigenmode. Indeed, the first eigen mode can be considered as a single-degree freedom structure, unlike the second Eigenmode.

## 3.5. Seismic tests

The analysis of the measurements taken during the seismic tests allows us to study the behaviour of the different tested walls in dynamic conditions. Considering the measurements and the preliminary assessment method of this series, the main subjects concern :

- the value of the compressive length ;
- the horizontal displacement of the wall ;
- the shear strength ;
- the behaviour of the dead load.

The comparison between the long and the short walls without SonicStrips devices highlights the differences of the behaviour of this kind of walls. Whereas the comparison between walls of same length, but with or without acoustic insulation devices, shows the influence of these devices.

### 3.5.1. Assessment of the compressive length

First of all, the main measurement to describe is the compressive length. As it could be seen in the preliminary assessment, this length has an influence in the strength of the wall. Indeed, each formula is a function of the value of the compressive length.

#### *3.5.1.1. Determination of useful parameters*

In order to calculate the compressive length, the LVDT devices 8, 10 and 12 are used.

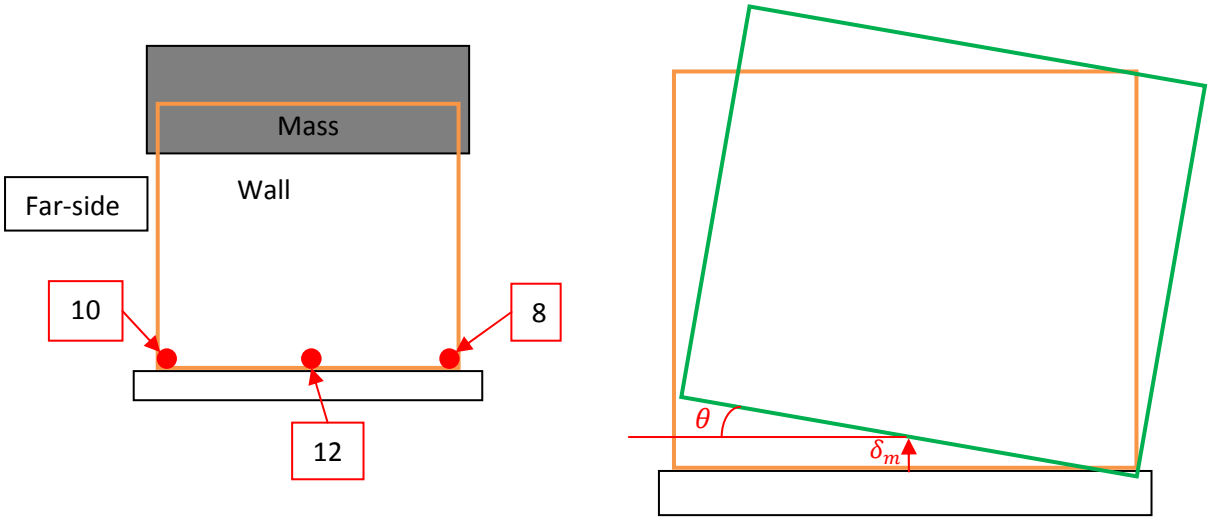


Figure 38 – Position of the used sensors (left) and deduced parameters

They measure the relative vertical displacement between the wall and the bottom beam. Therefore, there are three points of measurement, approximately located at the wall near end (8), the mid wall (12) and the wall far end (10).

From these points, a linear interpolation is made and it gives two parameters (Figure 38) : the mean displacement $\delta_m$ and the rotation (slope) $\theta$ of the wall basis. The wall is supposed to be a rigid body. The mean displacement is positive if there is an uplift of the wall and the slope is positive when the "far" side is uplifted.

To illustrate them, Figure 39 up to Figure 44 give the time evolutions of these parameters under three acceleration levels for the long wall without SonicStrip devices. The levels are chosen such as the first one is under the design acceleration, the second one is near it and the last is over it.

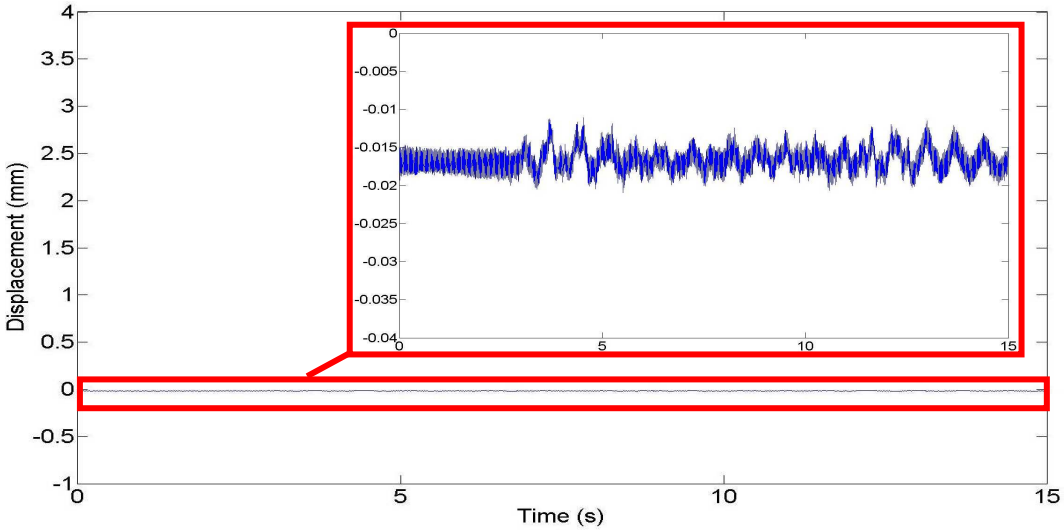


Figure 39 – Mean displacement during the seismic test at 0.0393g

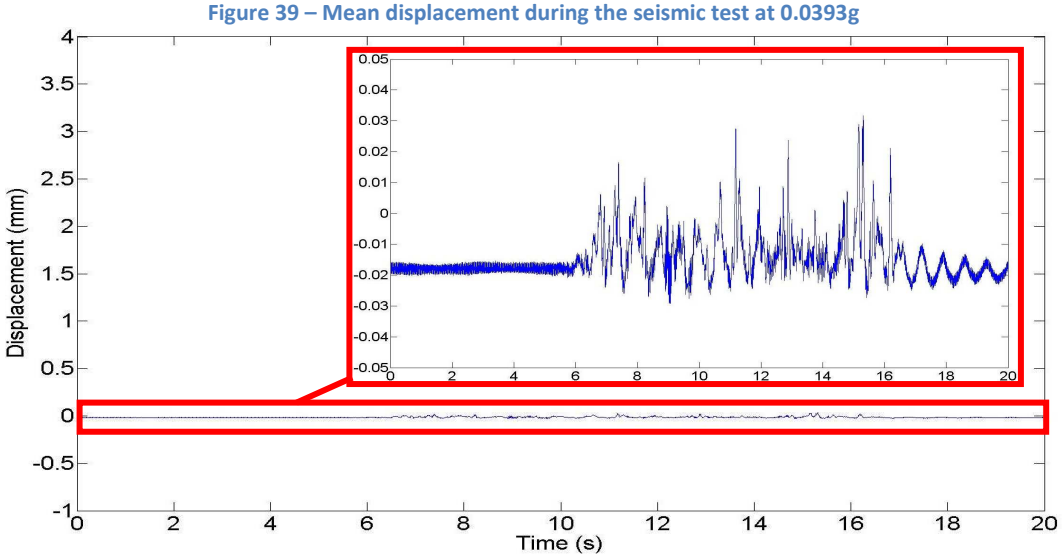


Figure 40 – Mean displacement during the seismic test at 0.2387g (Acceleration design = 0.2g)

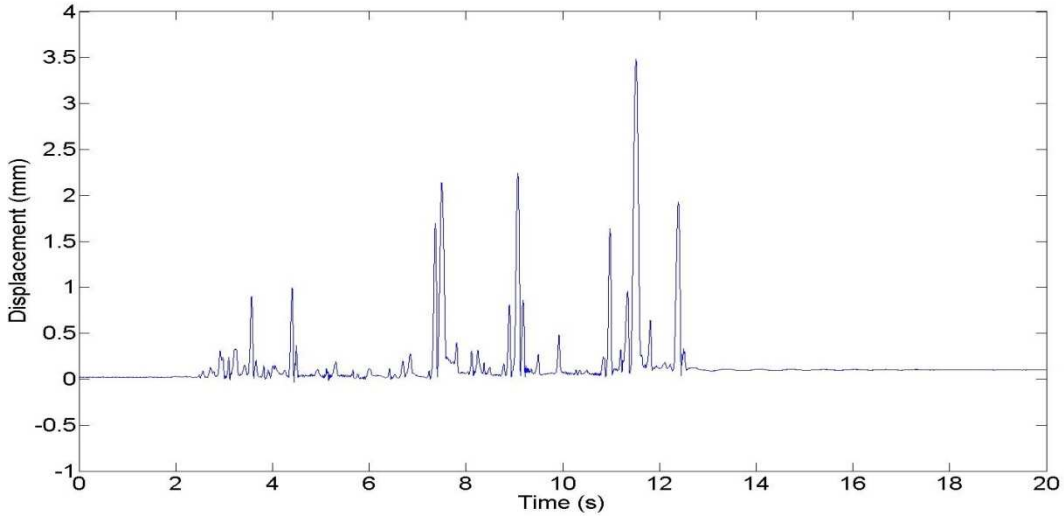


Figure 41– Mean displacement during the seismic test at 0.6878g

As it can be seen in Figure 39, Figure 40 and Figure 41, the mean displacement increases with the acceleration level. However, the displacement increment is not proportional to the acceleration one.

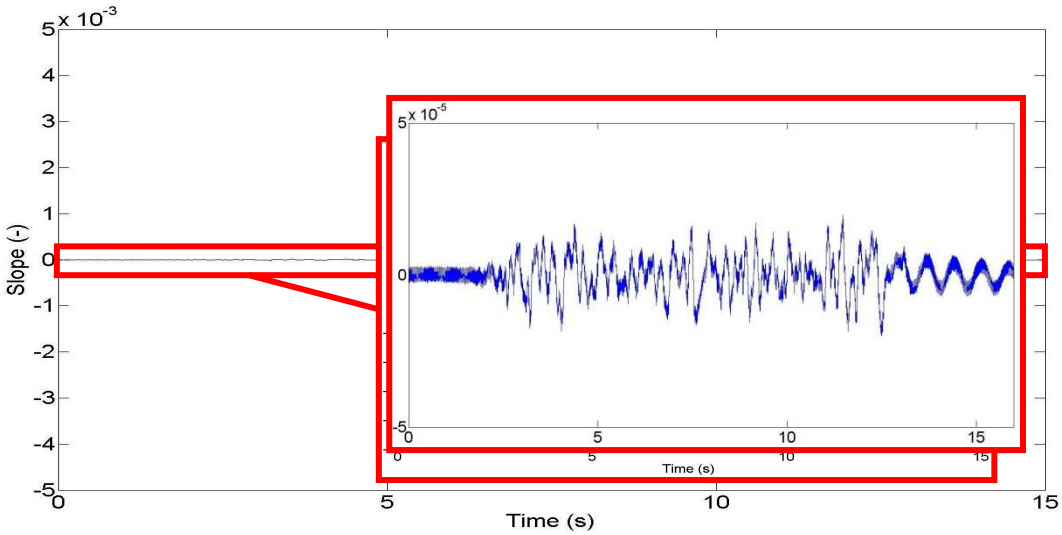


Figure 42 – Slope during the seismic test at 0.0393g

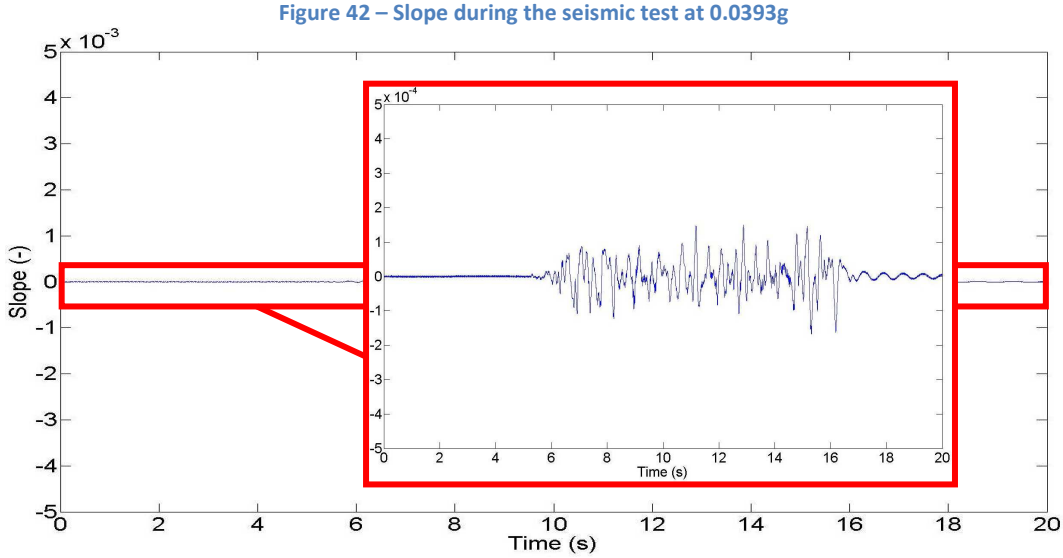


Figure 43 – Slope during the seismic test at 0.2387g (Acceleration design = 0.2g)

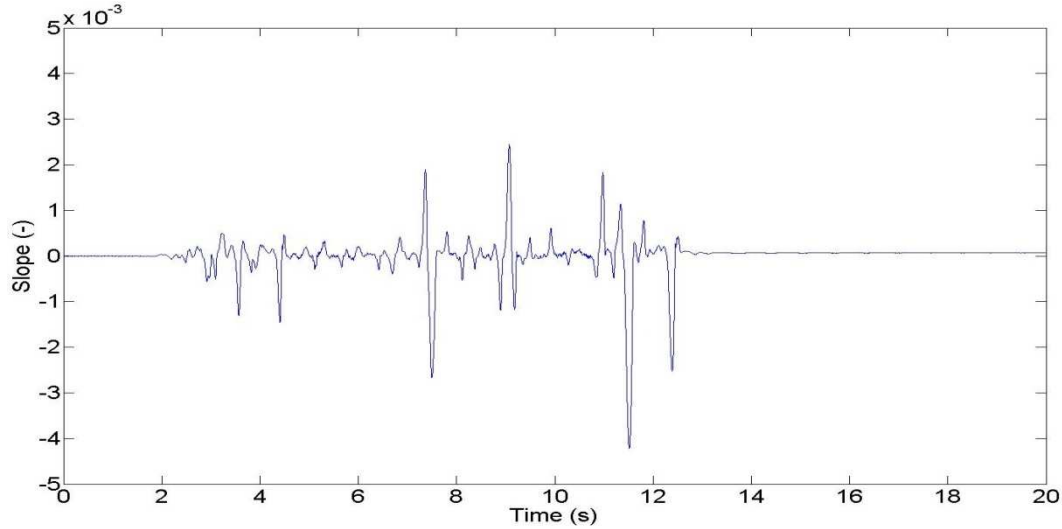


Figure 44 – Slope during the seismic test at 0.6878g

Like the mean displacement, the slope is higher when the acceleration level increases, but not in a proportional way. Indeed, if the acceleration level is multiplied by three, the mean maximum slope increases about twenty times or more. So, the phenomenon is clearly non-linear. It is confirmed thanks to the values given in Table 22, Figure 45 and Figure 46.

Table 22 – Value of the maximum slope according to the acceleration level

| Specimen | Acceleration level [g] | Maximum slope [-] |
|---|---|---|
| Long wall without SonicStrip | 0.0393 | $1{,}9954.10^{-5}$ |
| | 0.2387 | $1{,}6836.10^{-4}$ |
| | 0.6878 | $4{,}2200.10^{-3}$ |
| Long wall with SonicStrip | 0.0426 | $7{,}7180.10^{-6}$ |
| | 0.1871 | $5{,}2421.10^{-4}$ |
| | 0.6392 | $8{,}4000.10^{-3}$ |
| Short wall without SonicStrip | 0.0413 | $2{,}4416.10^{-4}$ |
| | 0.0635 | $4{,}5867.10^{-4}$ |
| | 0.1784 | $9{,}7000.10^{-3}$ |
| Short wall with SonicStrip | 0.0417 | $1{,}3000.10^{-3}$ |
| | 0.0607 | $2{,}4000.10^{-3}$ |
| | 0.1709 | $1{,}3800.10^{-2}$ |

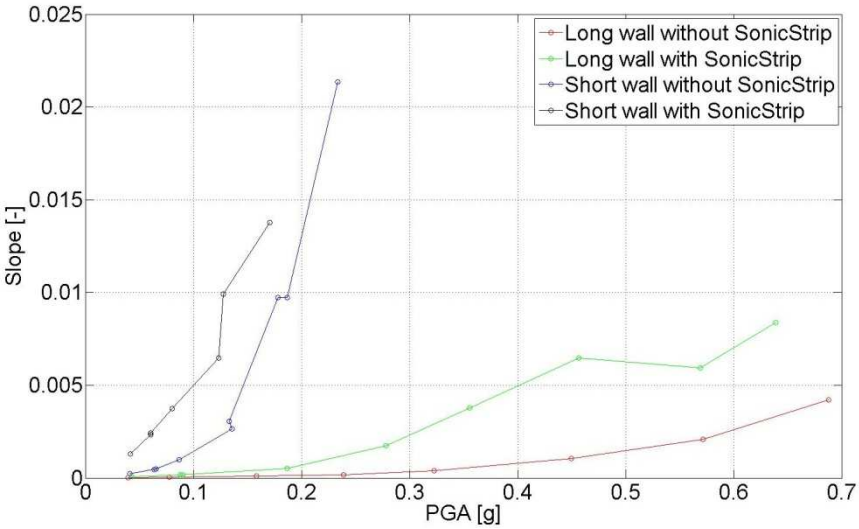


Figure 45 – Evolution of the maximum slope (absolute value) according to the PGA

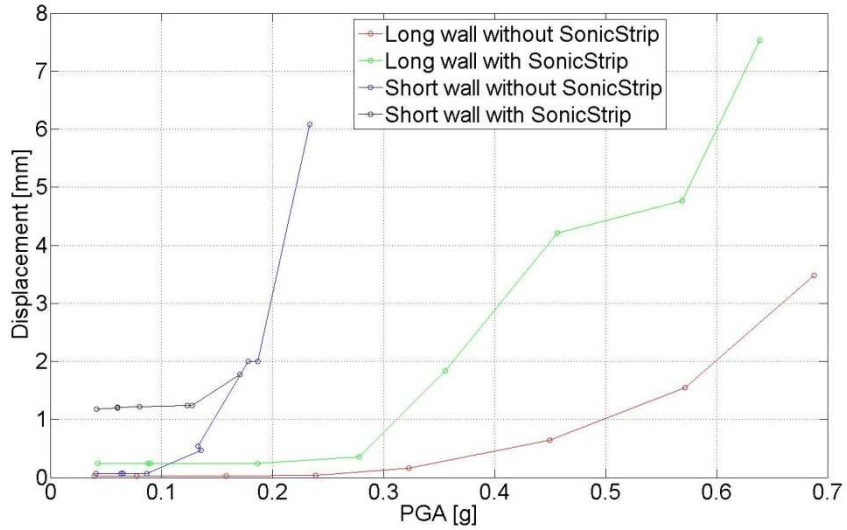


Figure 46 – Evolution of the maximum mean displacement(absolute value) according to the PGA

#### *3.5.1.2. Calculation of the compressive length*

Thanks to the mean vertical displacement and the slope, it is possible to deduce the compressive length. The deduction is done with the research of the root of the straight line. The time evolution of the compressive length is drawn under three acceleration levels for the long walls (Figure 47 to Figure 52) and for the short ones (Figure 53 to Figure 58) .

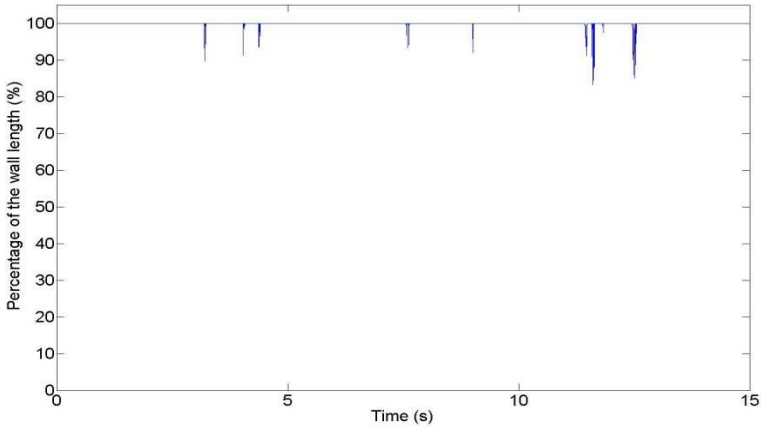


Figure 47 – Time evolution of the compressive length for the long wall without SonicStrip (0.0393g)

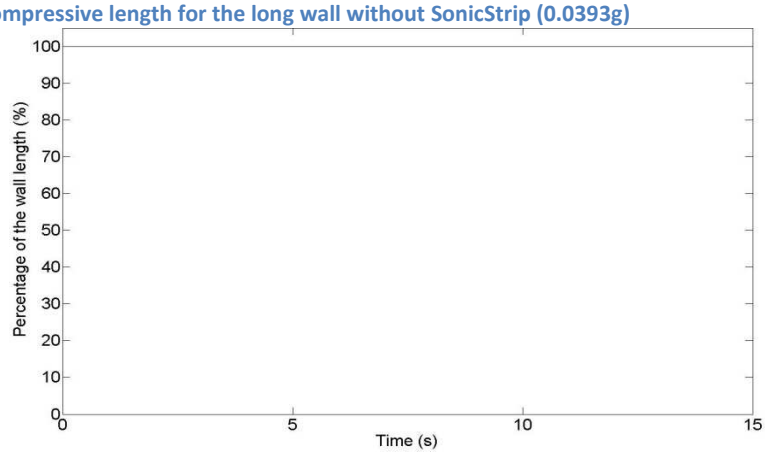


Figure 48 – Time evolution of the compressive length for the long wall with SonicStrip (0.0426g)

Figure 47 and Figure 48 show that the wall behaviour is different if acoustic insulation devices are installed. At the same level of PGA, the one-side-uplift is more important in the case of the wall without SonicStrip devices because the mortar layer allows a lower driving in than the rubber layer. The importance of the driving in is inversely proportional to the elastic modulus.

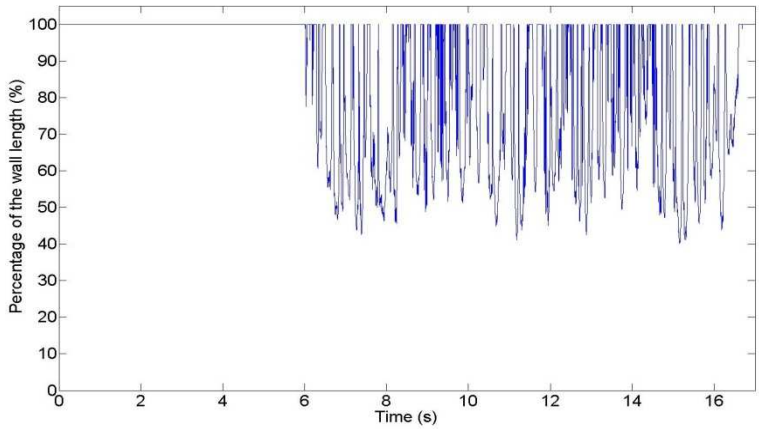


Figure 49 – Time evolution of the compressive length for the long wall without SonicStrip (0.2327g)

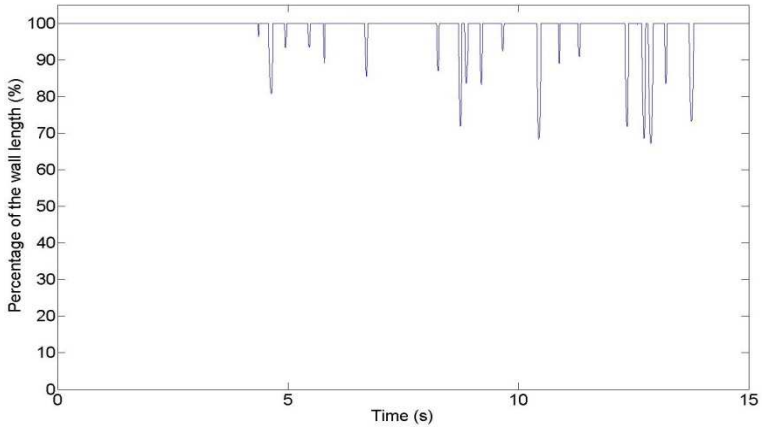


Figure 50 – Time evolution of the compressive length for the long wall with SonicStrip (0.1871g )

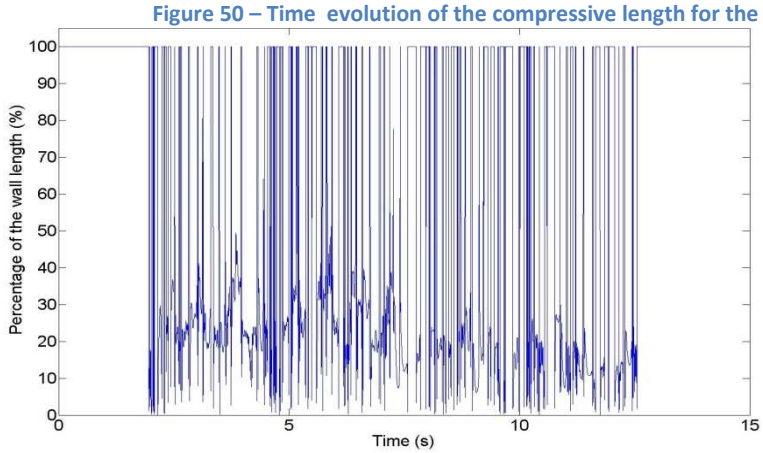


Figure 51 – Time evolution of the compressive length for the long wall without SonicStrip (0.6878g)

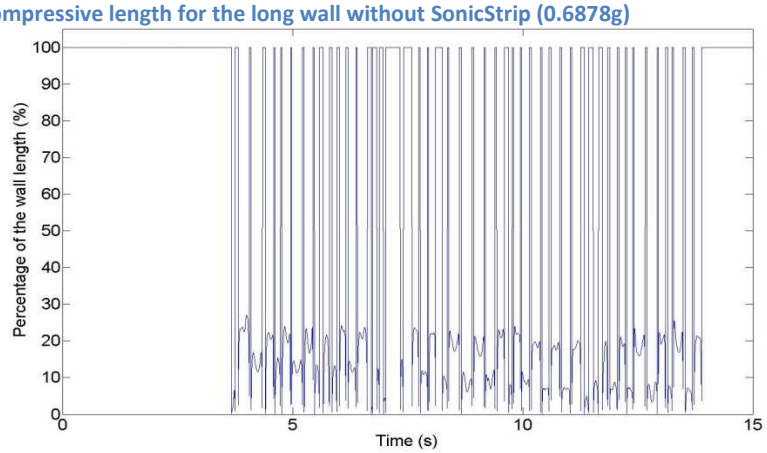


Figure 52 – Time evolution of the compressive length for the long wall with SonicStrip (0.6392g)

In Figure 51 and Figure 52, the compressive length becomes close to zero for the two long walls. Nevertheless, the compressive length of wall without SonicStrip devices is more often equal to 100%. It means that this wall comes more often back to its initial position (no one-side-uplift). This observation is explained thanks to the stiffness of the wall. The wall without acoustic insulation devices has a higher stiffness and, thus, its response is faster and more sensitive to quick changes of the acceleration direction.

In spite of their appearance, the compressive length is never null, even if it's very close to zero. To have an idea, the minimum value given by our method is 0.025% (without SonicStrip) and 0.05% (with SonicStrip).

The figures for the short walls can be seen here under.

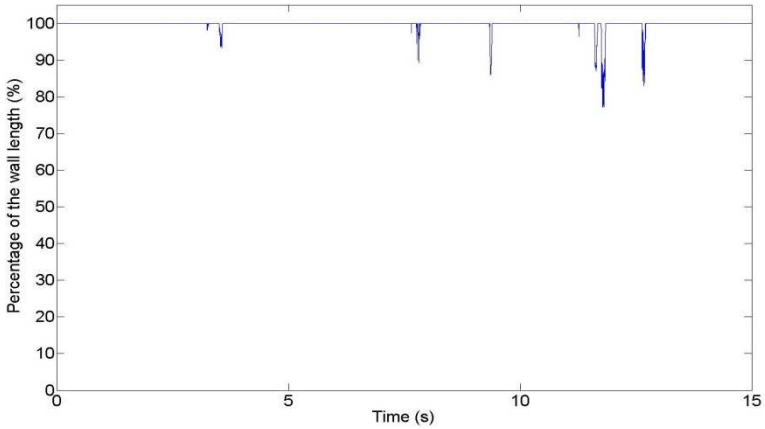


Figure 53 – Time evolution of the compressive length for the short wall without SonicStrip (0.0413g)

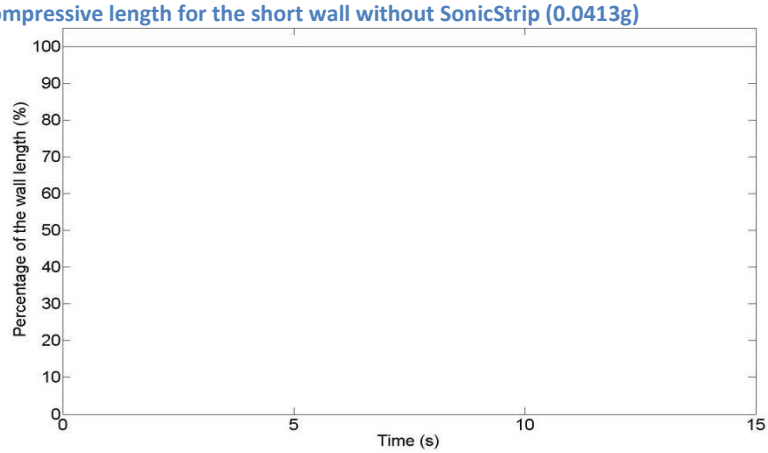


Figure 54 – Time evolution of the compressive length for the short wall with SonicStrip (0.0417g)

As for the case of the long walls, Figure 53 and Figure 54 show that there is a rocking of the wall if there are no acoustic insulation devices. If that kind of devices are present, the driving in of the wall is more important and the one-side-uplift is smaller.

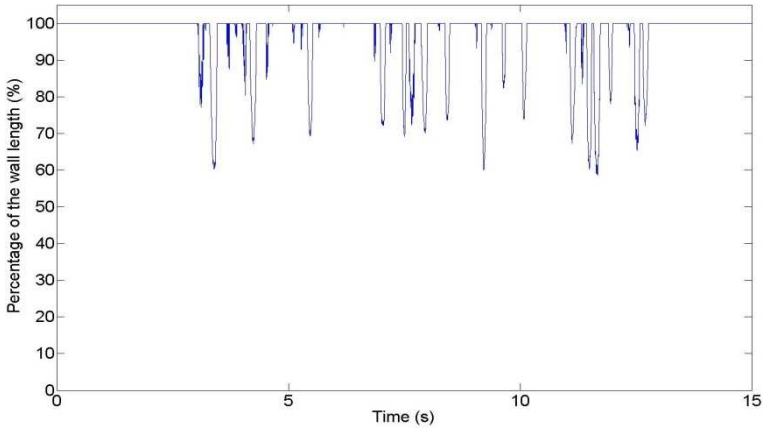


Figure 55 – Time evolution of the compressive length for the short wall without SonicStrip (0.0635g)

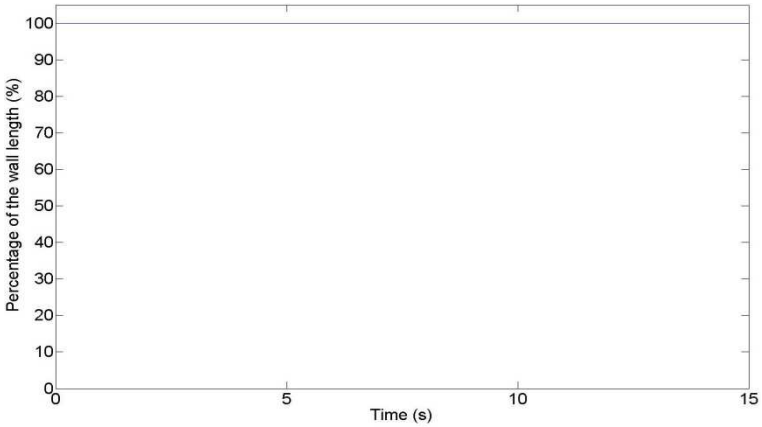


Figure 56 – Time evolution of the compressive length for the short wall with SonicStrip (0.0607g)

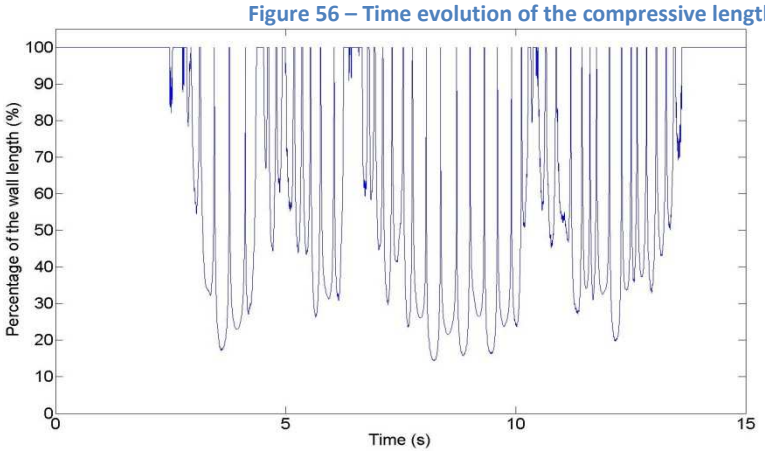


Figure 57 – Time evolution of the compressive length for the short wall without SonicStrip (0.1784g)

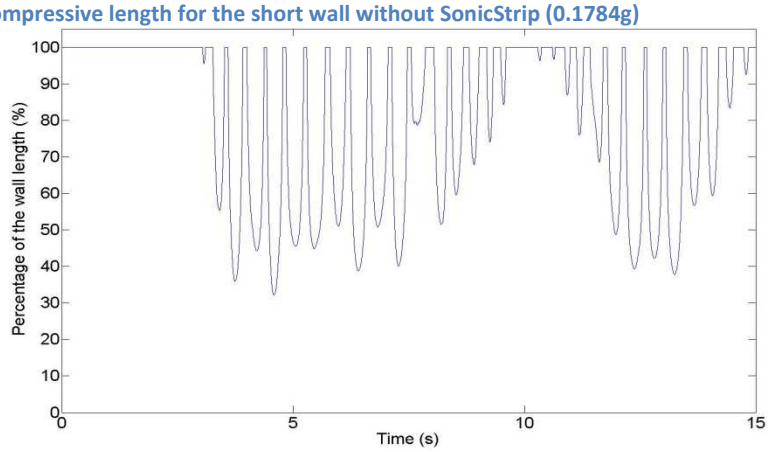


Figure 58 – Time evolution of the compressive length for the short wall with SonicStrip (0.1709g)

As for the case of the long walls, the compressive length is higher at the same acceleration level where acoustic insulating devices are present (Figure 55 to Figure 61). The reason is the same than in the case of the long wall.

Now, a comparison between the walls of different length is made (Table 23 and Figure 59). At a same PGA, it is remarked that the value of the compressive length is each time higher for long walls. The reason seems to be the relative importance of the eccentricity. Indeed, the formula used to assess the value of the compressive length is a function of the wall length and of the eccentricity of the compressive load.

$$L_c = \begin{cases} 0 & if\ e \geq L/2 \\ \left[3.\left(\frac{L}{2} - e\right)\right] & if\ e < L/2\ \wedge\ e > L/6 \\ L & if\ e \leq L/6 \end{cases}$$

When the acceleration level is the same, the eccentricity is the same. Therefore, the compressive length will decrease if the length of the wall is smaller.

To summarize all the figures and to have a value of the compressive length, Table 23 gives the minimum percentage in each studied cases. Figure 59 gives the evolution of the compressive length according to the PGA.

Table 23 - Minimum value of the compressive length

| Specimen | Acceleration level [g] | Compressive length [%] | Compressive length [mm] |
|---|---|---|---|
| Long wall without SonicStrip | 0.0393 | 83.2 | 1747.2 |
| | 0.2387 | 41.11 | 863.31 |
| | 0.6878 | 0.025 | 0.525 |
| Long wall with SonicStrip | 0.0426 | 100 | 2100 |
| | 0.1871 | 67.2 | 1411.2 |
| | 0.6392 | 0.05 | 1.05 |
| Short wall without SonicStrip | 0.0413 | 77.01 | 554.472 |
| | 0.0635 | 58.7 | 422.64 |
| | 0.1784 | 14.37 | 103.464 |
| Short wall with SonicStrip | 0.0417 | 100 | 720 |
| | 0.0607 | 100 | 720 |
| | 0.1709 | 32.13 | 231.34 |

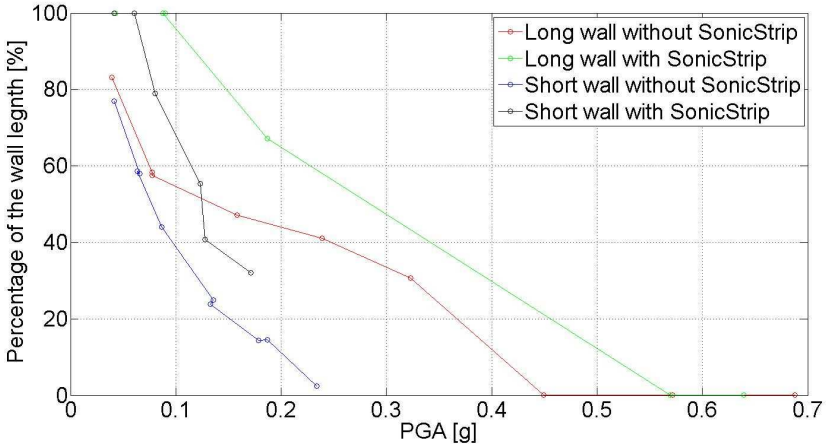


Figure 59 – Compressive length according to the PGA

Table 23 and Figure 59 lead to the following conclusions :

- at the same acceleration level , the compressive length is higher when there are acoustic insulation devices ;
- the value of the compressive length decreases less than proportionally to the increase of the value of the acceleration of the seismic test.

The main conclusion is about the behaviour of the walls. The tests show that the walls are rocking, whatever their length. This behaviour was not expected for the long walls.

Another main conclusion concerns the presence of the acoustic insulation devices. The results show that compressive length is longer when these devices are installed. So, the one-side uplift is delayed. Nevertheless, these devices lead to higher displacement and rotation.

#### *3.5.1.3. Amplitude of the rocking motion*

Figure 51 and Figure 52 point out that the compressive length of the long walls are close to zero when the acceleration level is approximately 0,65g. Nevertheless, the rocking is important if two conditions are fulfilled. The first one is a compressive length close to zero and the second one is a big rotation. Consequently, the time evolutions of the compressive length and of the slope on wall basis are put in parallel in Figure 60 and Figure 61.

In these ones, the rocking is more important for the long wall with acoustic insulation devices because its maximum slope is $8{,}37.10^{-3}$, namely $0{,}47°$, whereas the maximum slope of the long wall without devices is $4{,}22.10^{-3}$, namely $0{,}24°$. This observation can be explained thanks to the stiffness of the wall. With SonicStrip devices, the wall stiffness is lower and, so, the displacement and the slope are higher. A higher rotation is also the reason why the wall with devices stays longer in one-side-uplift (noting of Figure 51 and Figure 52).

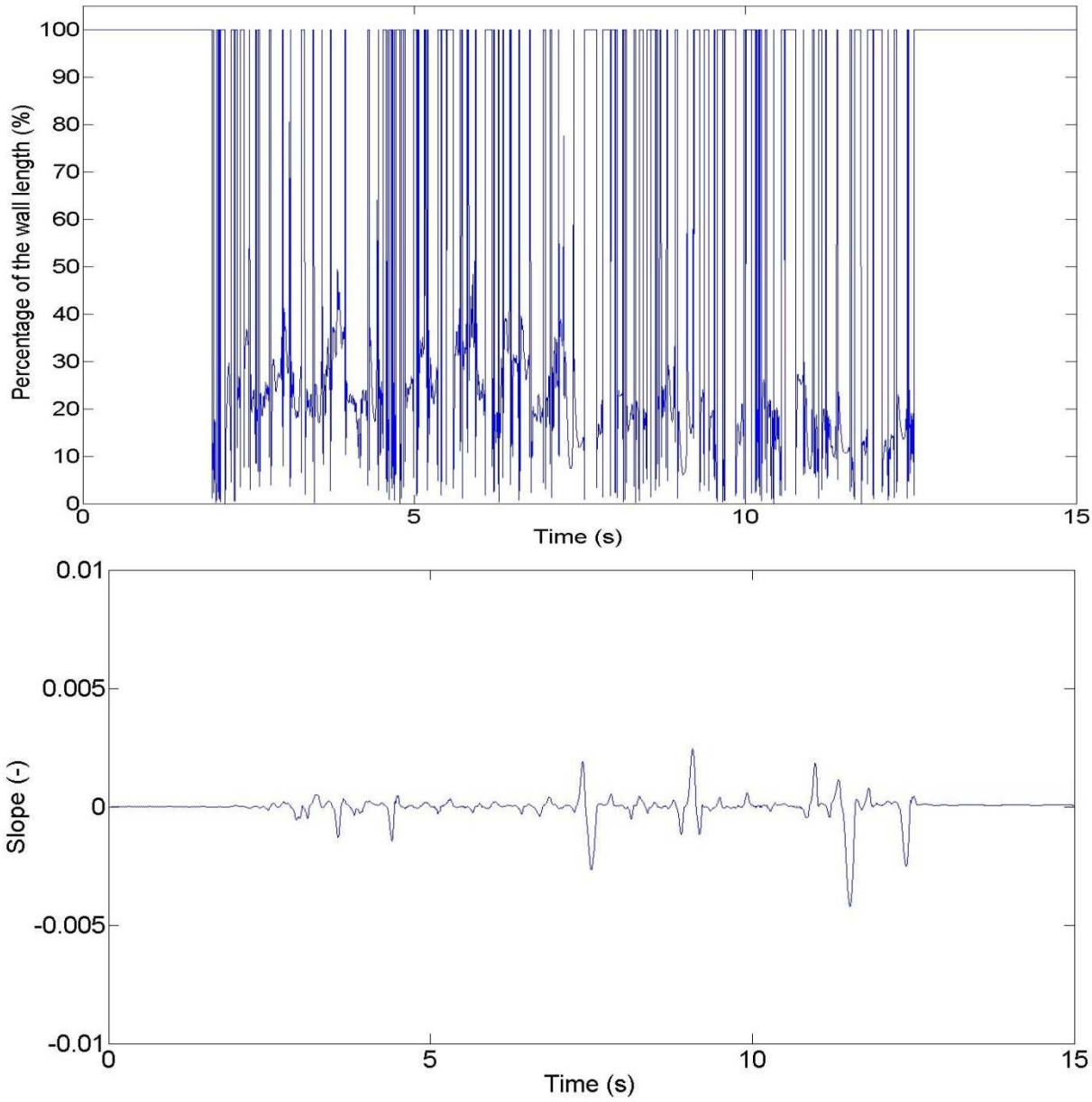


Figure 60 – Compressive length and slope of the long wall without SonicStrip (acceleration level : 0.6878g)

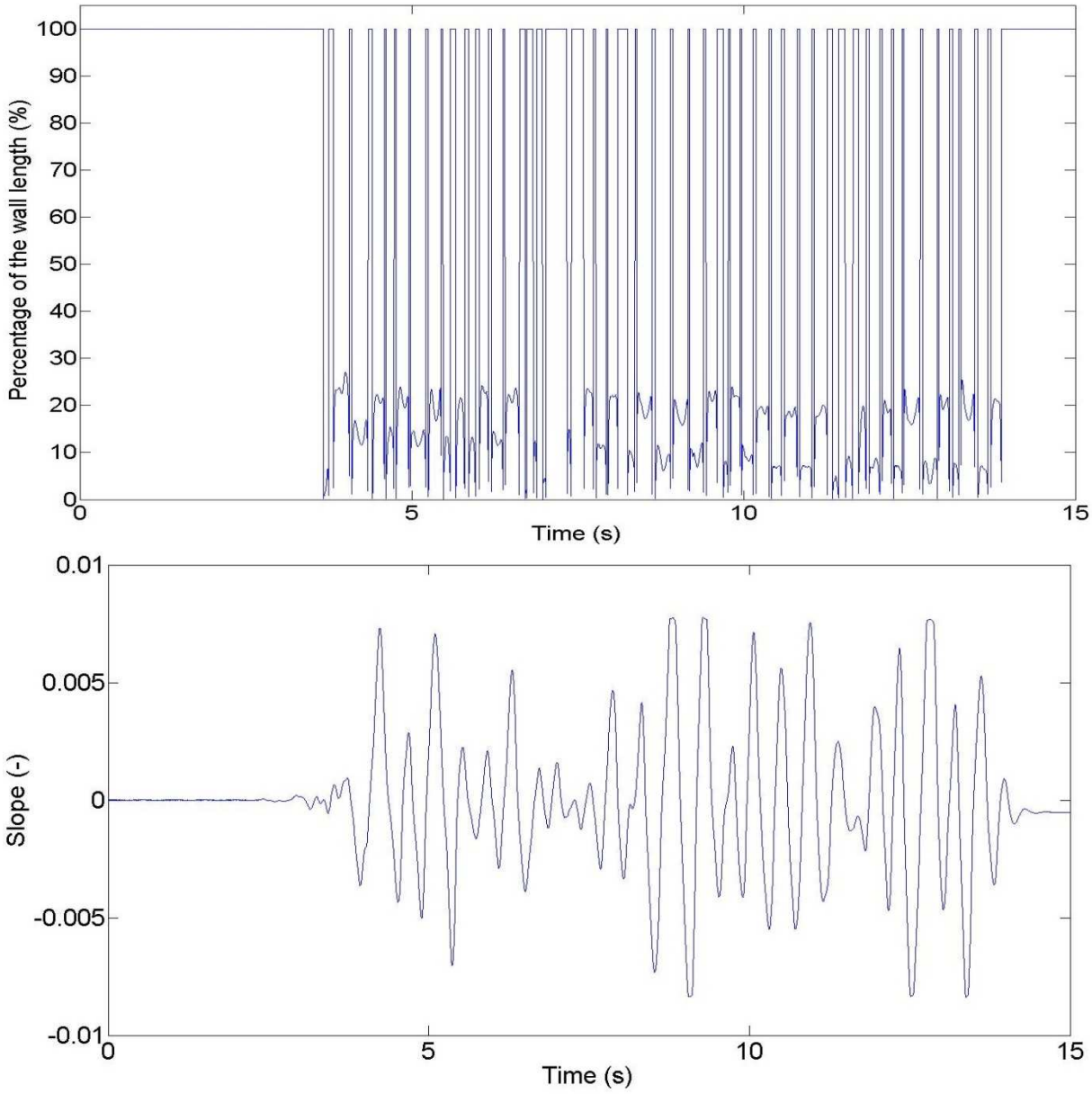


Figure 61 – Compressive length and slope of the long wall with SonicStrip (acceleration level : 0.6392g)

### 3.5.2. Horizontal relative displacements between the wall and the support beam

Three other sensors are placed at the wall bottom and measure the horizontal relative displacement between the wall and the support beam.
Once again, it can be interesting to draw the time evolution of this displacement under different acceleration levels and to compare it with the time evolution of the slope for the same wall and acceleration level. The comparison is possible because the rocking of the wall involves a horizontal displacement as shown in Figure 62.

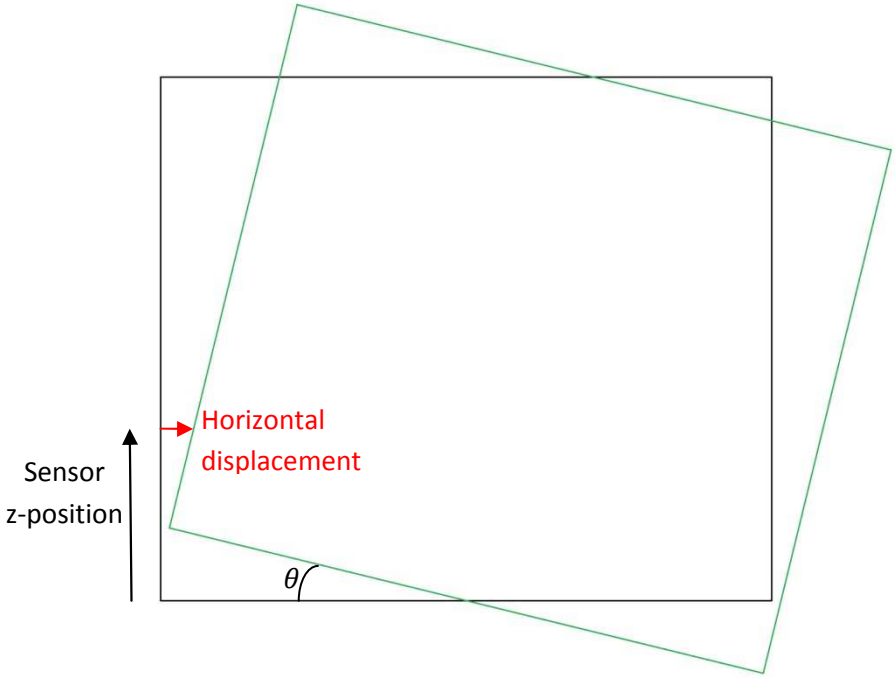


Figure 62 – Sketch of the horizontal displacement involved by the rocking

The value of the horizontal displacement caused by the rocking can be geometrically determined starting from the value of the slope. If $\theta$ is the angle representing the slope, the next formula gives the researched value :

$$\delta_{horizontal} = abs\left(\frac{WallLength}{2}.\tan\theta - z_{sensor}\right).\tan\theta + \frac{WallLength}{2}.(1-\cos\theta)$$

With the comparison of the calculated values of $\delta_{horizontal}$ and the ones of the horizontal displacement measured by the instrumental devices, it is possible to check if the wall is only rocking or if any horizontal displacement exists and when it happens.

In Figure 63 to Figure 66, the time evolution of the measured horizontal displacement and $\delta_{horizontal}$ are drawn for the long walls. The same thing is done for the small walls in Figure 67 to Figure 70.

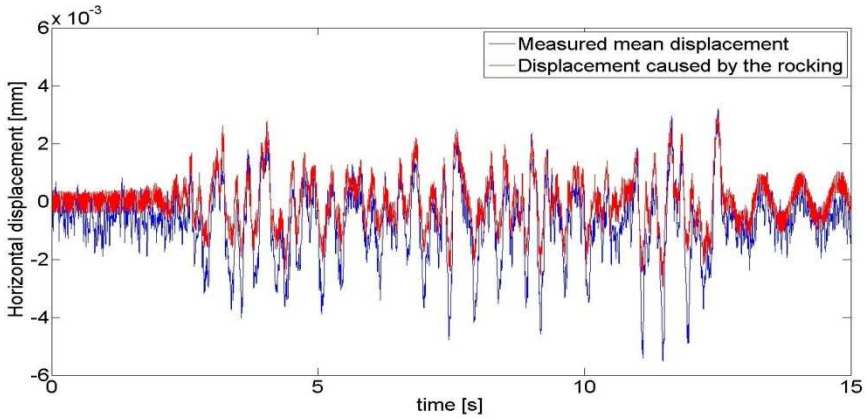


Figure 63 – Time evolution of the horizontal displacement (long wall without SonicStrip – 0.0393g)

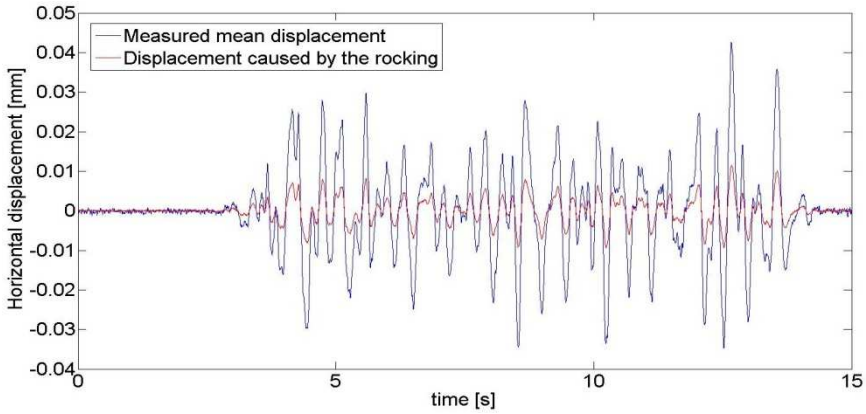


Figure 64– Time evolution of the horizontal displacement (long wall with SonicStrip – 0.0426g)

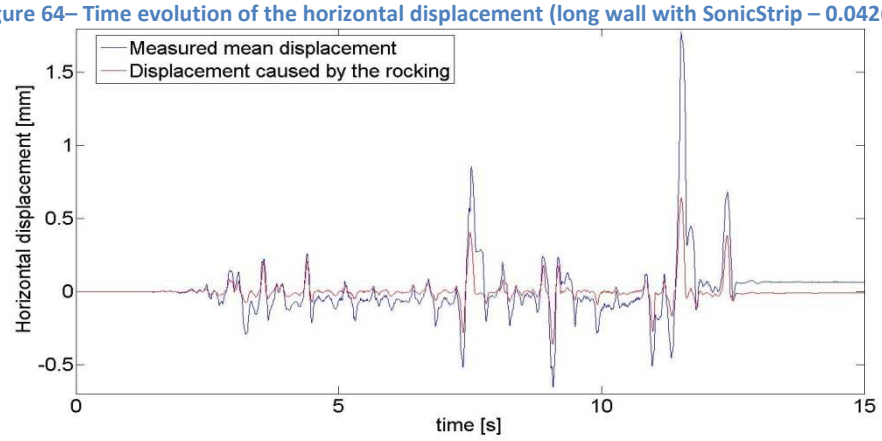


Figure 65– Time evolution of the horizontal displacement (long wall without SonicStrip – 0.6878g)

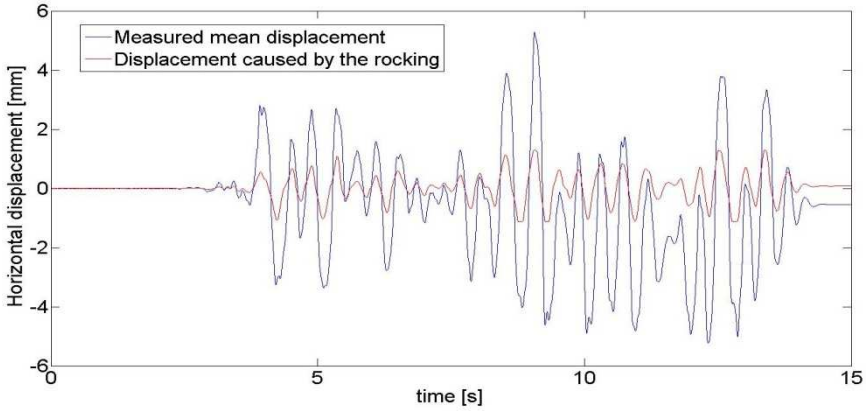


Figure 66– Time evolution of the horizontal displacement (long wall with SonicStrip – 0.6392g)

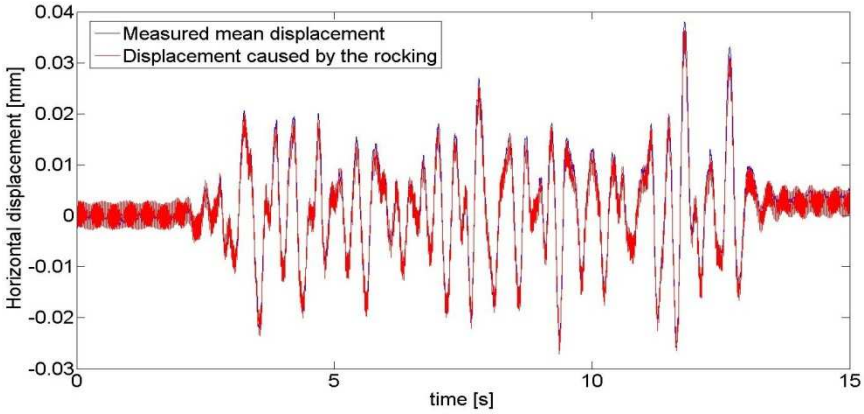


Figure 67 – Time evolution of the horizontal displacement (short wall without SonicStrip – 0.0413g)

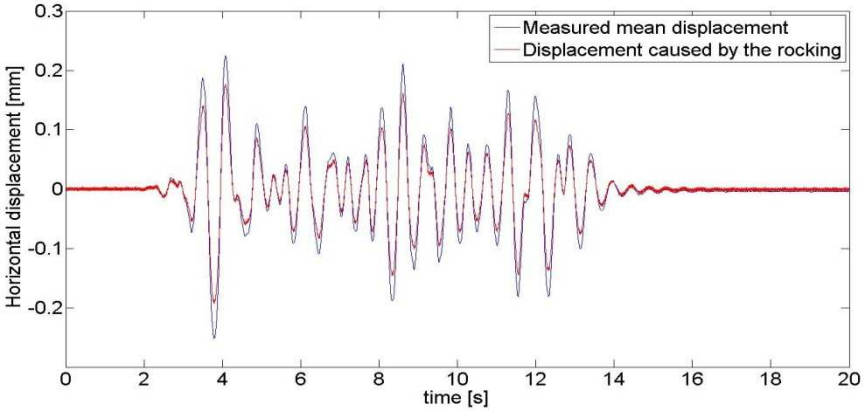


Figure 68 – Time evolution of the horizontal displacement (short wall with SonicStrip – 0.0417g)

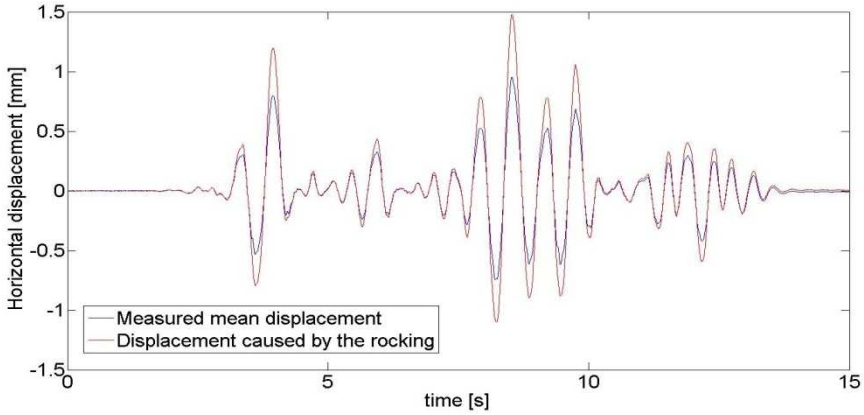


Figure 69 – Time evolution of the horizontal displacement (short wall without SonicStrip – 0.1784g)

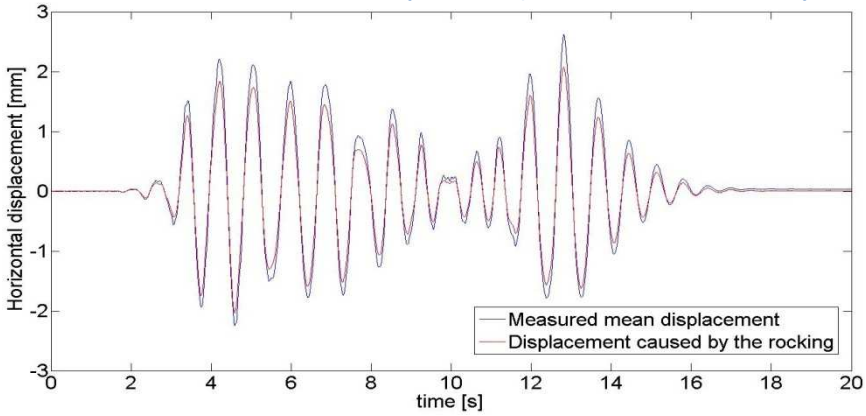


Figure 70 – Time evolution of the horizontal displacement (short wall with SonicStrip – 0.1709g)

For the figures from Figure 63 to Figure 70, the same main comments can be made. Indeed, the shape of the time evolution of the horizontal displacement calculated and caused by the rocking seems to be the same as the measured mean horizontal displacement. The outcome is that a horizontal displacement only happens when the wall is rocking.
If the value of the displacement are taken into account, the measured value has, most of the time, a higher absolute value. Two possibilities can explain this observation. The first one is a permanent displacement of the wall as a rigid body. Nevertheless, the second possibility seems to be more relevant. According to this one, the higher absolute value of the horizontal displacement is due to the shear of the wall or of the acoustic insulation devices. This also explains why the displacement is more important when there are acoustic insulation devices. The reason is the lower value of the shear modulus of the SonicStrip devices in comparison with the shear modulus of the masonry wall.
Another possibility is a sliding of the wall because the compressive length is small and, so, the contact area is also small.
Concerning the time evolution, the presence of acoustic insulation involves a longer response. For example, the comparison between Figure 69 and Figure 70 shows that the horizontal displacement comes back close to zero before 15 seconds for the first one (short wall without SonicStrips) and after 15 seconds for the second one(short wall with SonicStrips).

A last remark concerns the non-linear behaviour of the rocking. For example, when the acceleration level is multiplied by four, the response is ten times higher (Figure 68 and Figure 70). This remark confirms what was observed in the conclusions of the calculation of the compressive length.

### 3.5.3. Rocking of the mass

During the testing phases, a particular phenomenon happened when the long wall without acoustic insulation devices was tested, but not when the long wall with these devices was tested: the mass seemed to rock on the wall and it followed a kind of “impact” each time the mass went down. This phenomenon only appeared when the acceleration level reached a certain value.
As the walls plane was along the X-direction, the consequence was a high acceleration in the Y-direction. Figure 71 and Figure 72 illustrate the consequence by drawing the time evolution of the sensor 5. This sensor measures the Y-direction acceleration.

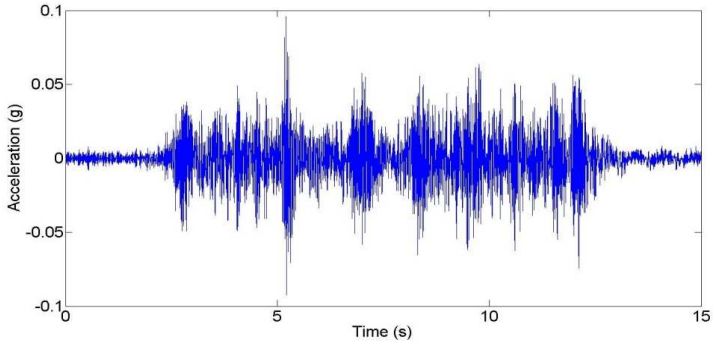


Figure 71 – Time evolution of the Y-direction acceleration (Long wall without SonicStrip – 0.1583g)

As illustrated in Figure 71, the maximum Y-direction acceleration is close to 0,1g. The value is more than the half of the acceleration level experimented on the shaking table.

If this value is compared with the one obtained when the tested wall has SonicStrip devices, it is about five times higher. Figure 72 actually shows a maximum value near to 0,02g for the same acceleration level.

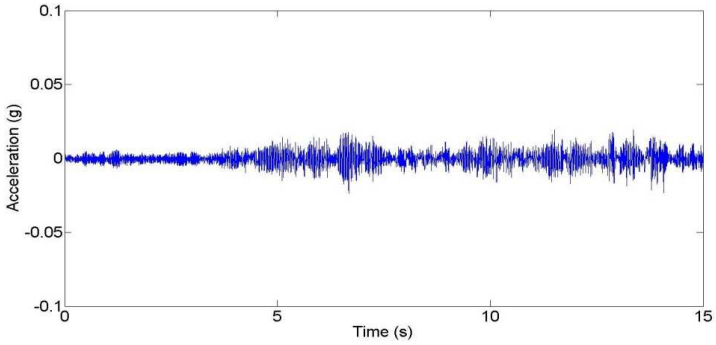


Figure 72 – Time evolution of the Y-direction acceleration (Long wall with SonicStrip – 0.1871g)

To confirm the feeling that mass is rocking on the wall, the sensors 9 and 11 are used (Figure 73). They were placed on the wall top and measured the vertical displacement between the wall and the mass. The followed procedure is the same than the one that has allowed the calculation of the compressive length of the wall.

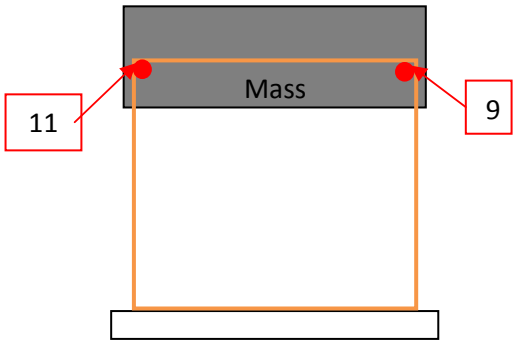


Figure 73 - Position of the sensors 9 and 11

Once again, the results are given for three different acceleration levels : one under the design acceleration, one close to it and one over it.

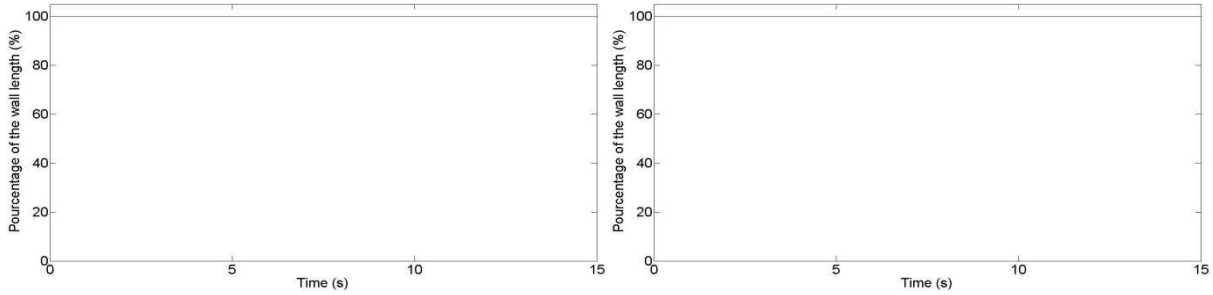


Figure 74 – Compressive length of the mass for the long walls without (left – 0.393g) and with (right – 0.0426g) SonicStrip

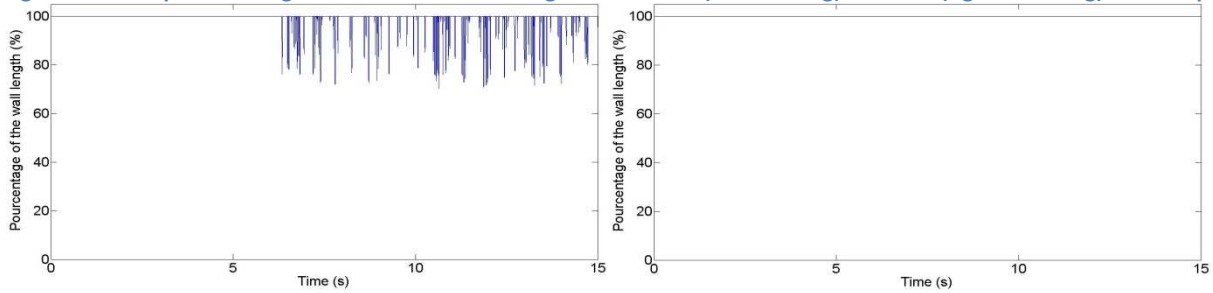


Figure 75– Compressive length of the mass for the long walls without (left – 0.2387g) and with (right – 0.1871g) SonicStrip

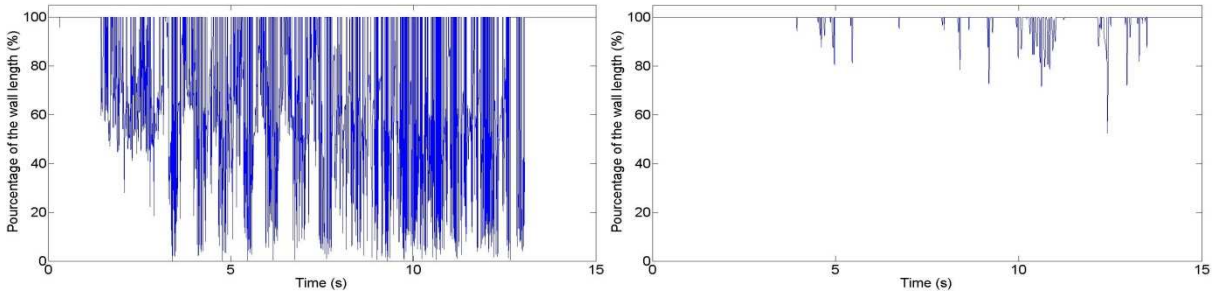


**Figure 76 – Compressive length of the mass for the long walls without (left – 0.6878g) and with (right – 0.6392g) SonicStrip**

The graph on the left side of the Figure 76 clearly proves the rocking of the mass when the long wall does not have acoustic insulation devices, whereas the graph on the right side only shows the presence of a little rocking. In the case of the long wall without SonicStrip devices, the impact is significant because the one-side-uplift is important and nothing absorbs it.
It may be concluded that the acoustic insulation devices have positive effect because they limit the impact and also the risk of buckling.

Concerning the short walls, the results show that no rocking of the mass appears. They confirm the observations made during the tests.

### 3.5.4. Horizontal shear

As the preliminary assessment method of the first test series is based on the "Push-Over" model, the calculation of the horizontal shear can be useful. Although it was shown that the walls have a rocking behaviour, they are still subjected to the horizontal shear.

#### *3.5.4.1. Horizontal shear in the wall*

Thanks to the "Celesco" devices, which measure the diagonal displacement of the wall, we are able to determine the horizontal shear in the wall. Considering that the displacement along the two diagonal of the wall is measured, it's possible to know if there is only shear deformation or if a bending deformation exists too. The difference between these two types of deformation is done with the comparison of the diagonal. If the extension of the first one is equal to the reduction of the second one, there is only shear deformation. In other case, there is also bending deformation.
Nevertheless, we are not able to do it in our case because the dead load owns some eccentricity. Therefore, one of the diagonal sensors will measure a bigger displacement. To avoid this problem of loading, the mean of the diagonal displacement is taken.
From the mean diagonal displacement, it's possible to deduce the horizontal one. Figure 77 explains the geometrical method used to do it. The horizontal displacement is obtained by projecting the diagonal displacement $\delta_d$, measured by a wire between two points, A and B.

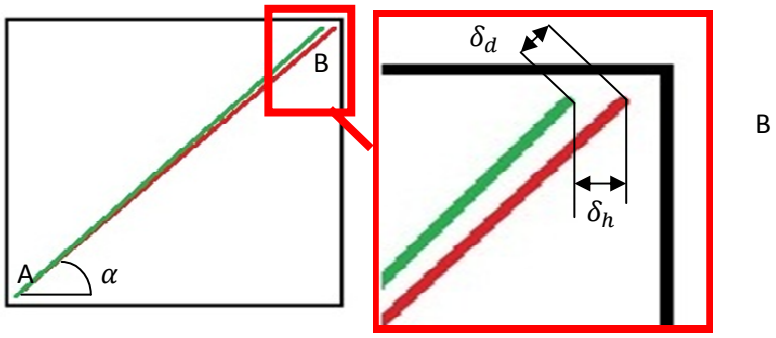


Figure 77 – View of diagonal and horizontal displacements

Assuming the vertical displacement and the variation of the angle $\alpha$ are not significant, the next relation is valid : $\delta_h = \delta_d . \cos\alpha$

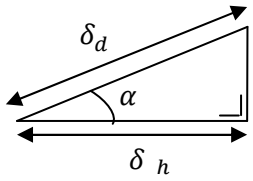


Figure 78 – View of diagonal and horizontal displacements

Once the horizontal displacement is known, the drift can be calculated with the height of the wall and, then, the horizontal shear (Serge Cescotto & Charles Massonet, 2001) :

$$\gamma = \delta_h \,/\, height_{wall}$$
$$V = \gamma . G . A'$$

Where $G\ [N/mm^2]$ is the shear modulus of the masonry, taken to the 40% of the Young Modulus (Eurocode6, 2004).

$A'\ [mm^2]$ is the shear area, taken to 5/6 of the area.

#### 3.5.4.1.1. Horizontal shear in the long walls

The Figure 79 to Figure 82 show the time evolution of the horizontal shear in the long walls during the seismic tests (S1) and (S9). The same observation can be made for all these figures : if there is a shear stress (in red), its value is below what we can expect in the case of a long wall subjected to a horizontal shear (in blue).

The rocking behaviour of the wall may be the reason of the difference and it explains why the maximum acceleration level sent to the table during the tests is higher than the design one.

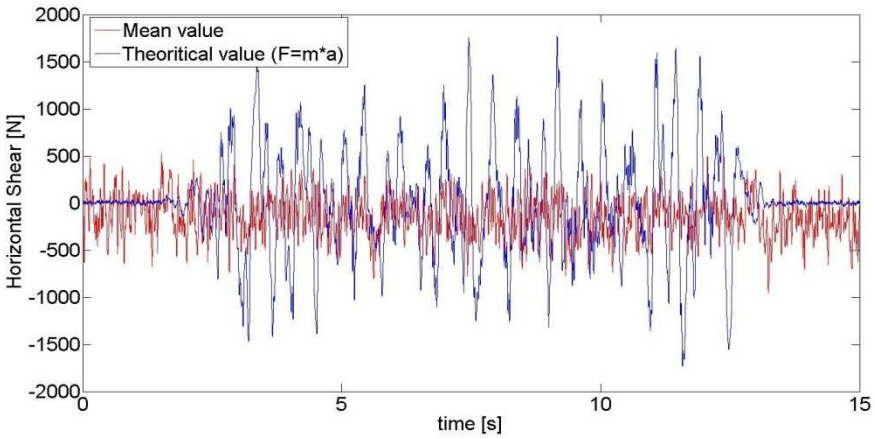


Figure 79 – Time evolution of the horizontal shear (long wall without SonicStrip – 0.0393g)

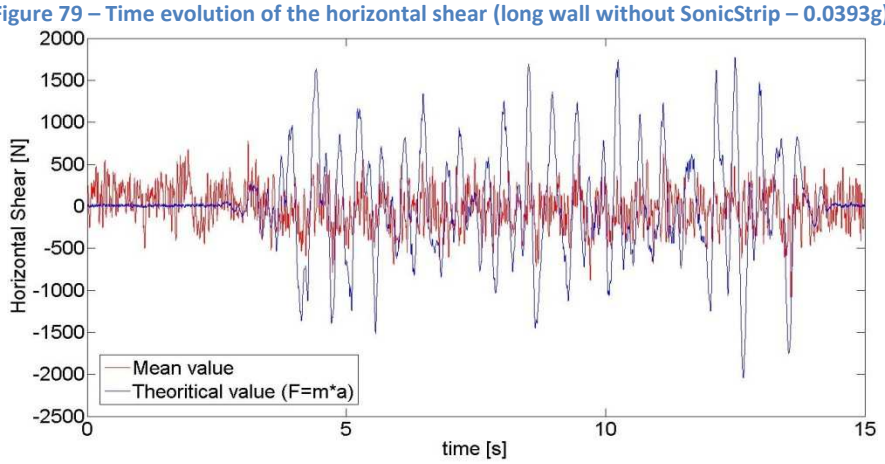


Figure 80 – Time evolution of the horizontal shear (long wall with SonicStrip – 0.0426g)

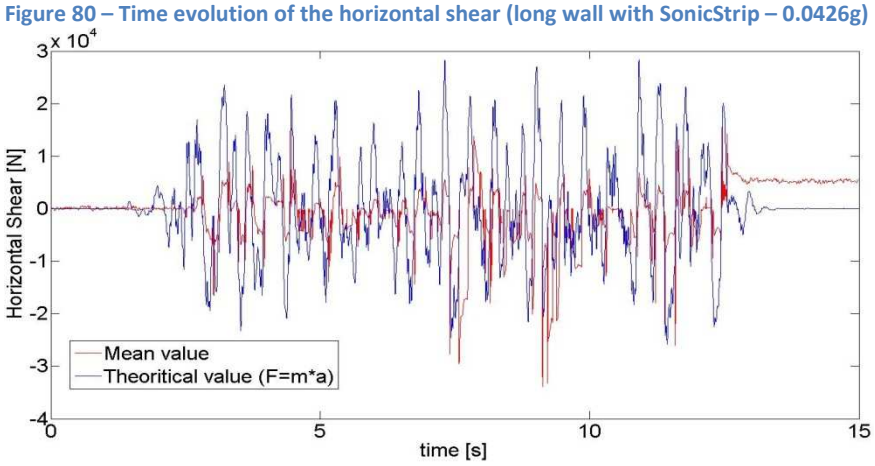


Figure 81 – Time evolution of the horizontal shear (long wall without SonicStrip – 0.6878g)

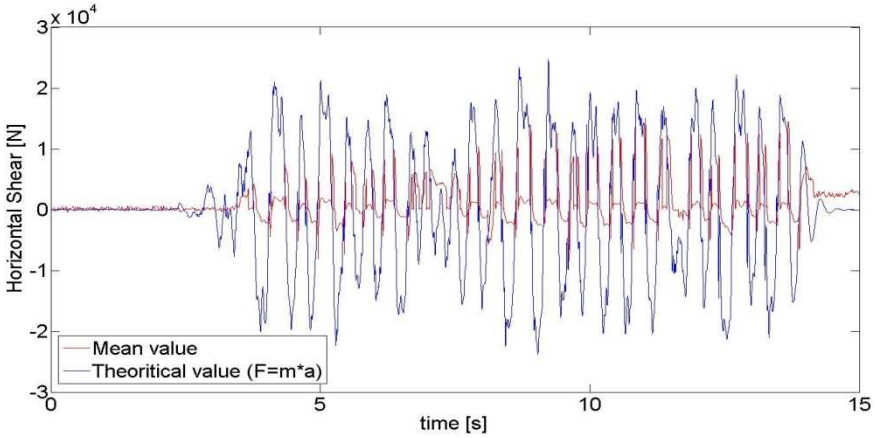


Figure 82 – Time evolution of the horizontal shear (long wall with SonicStrip – 0.6392g)

#### 3.5.4.1.2. Horizontal shear in the short walls

The Figure 83 to Figure 86 show the time evolution of the horizontal shear in the short walls during the seismic test (S1) and (S7). For these figure, the same observation is valid : the value of the shear stress (in red) is low, even close to zero.
This explanation of the observation is given after the figures.

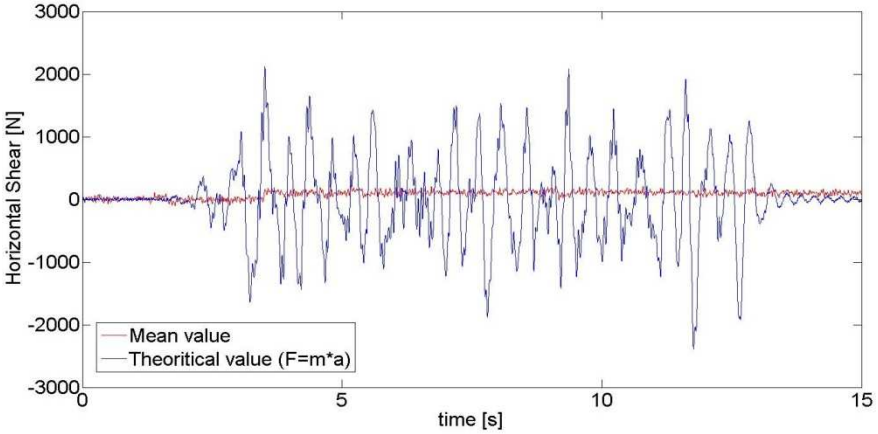


Figure 83 – Time evolution of the horizontal shear (short wall without SonicStrip – 0.0413g)

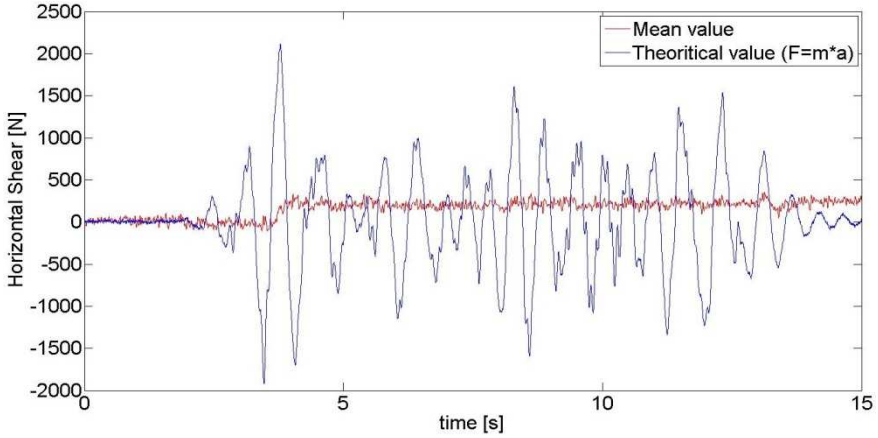


Figure 84 – Time evolution of the horizontal shear (short wall with SonicStrip – 0.0417g)

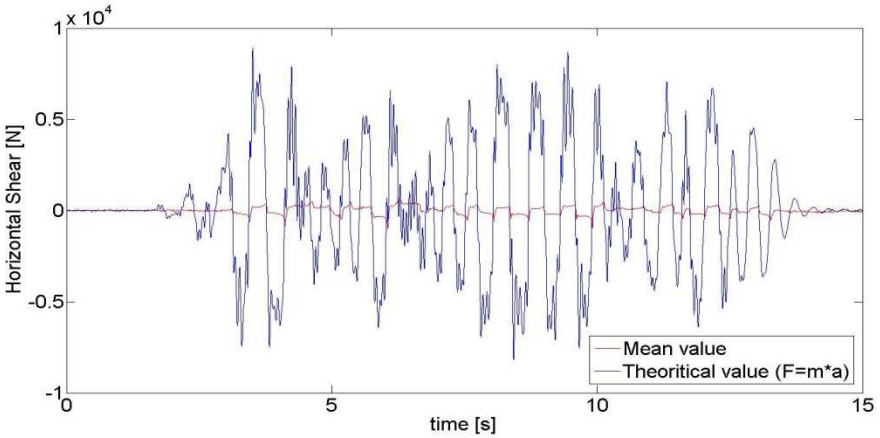


Figure 85 – Time evolution of the horizontal shear (short wall without SonicStrip – 0.1784g)

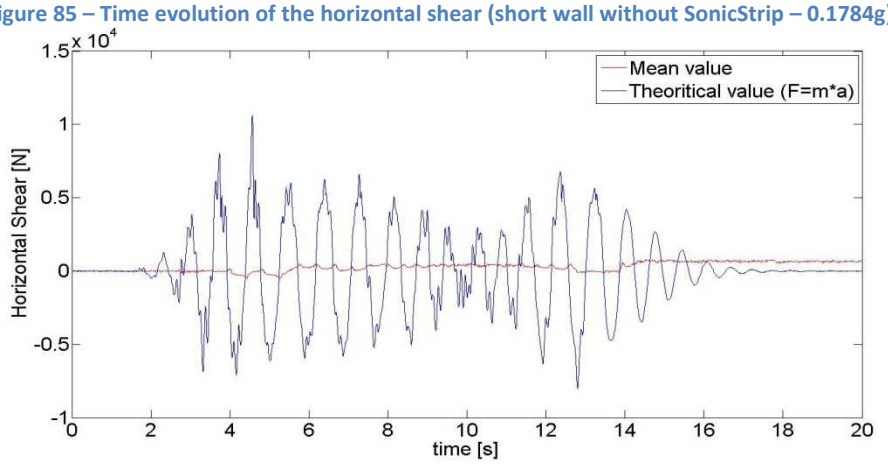


Figure 86 – Time evolution of the horizontal shear (short wall with SonicStrip – 0.1709g)

With the observations of Figure 79 to Figure 86, several comments can be made. The main one is the difference between the value of the horizontal shear measured and the value given by the theoretical approach. The difference is due to the presence of two types of transfer mechanisms.

The first mechanism is the classic one. The rectangular shape of the wall becomes a parallelogram. Nevertheless, the figures show that this first mechanism is not sufficient because of the differences observed.

The second mechanism is based on the strut and tie model. Indeed, as the walls are rocking, the shear stress is not perfectly horizontal and a vertical component exists. Therefore, the shear stress is equilibrated by a horizontal stress and a vertical one at the bottom corner where there is no uplift (Figure 87).

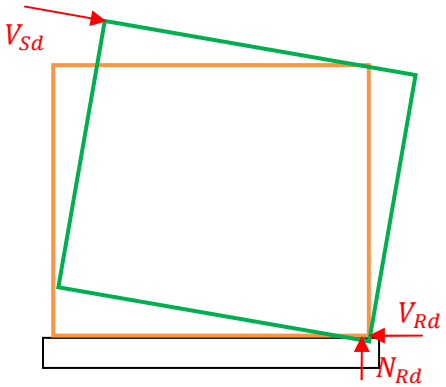


Figure 87 –Illustration of the strut and tie model

Now, we can understand why a difference is observed. It's because the way of calculation does not take the vertical component into account. It also explains why the shear stress is lower in the case of the short wall. In that case, the rocking is more important and it follows a higher vertical component.

In conclusions, the model of the shear strength must include the two types of the transfer mechanisms. Unfortunately, it is not made in this work due to a lack of time.

#### *3.5.4.2. Horizontal shear in the acoustic insulation devices*

The method used to calculate the horizontal shear in the acoustic insulation devices is nearly the same than the one used for the horizontal shear in the wall. Three differences exist :

- it's not necessary to do some geometrical projections because there are sensors which directly measure the horizontal displacement ;
- the horizontal displacement due to the rocking of the wall doesn't have to be taken into account ;
- the shear modulus of the masonry must be replaced with the one of the SonicStrip devices.

If these differences are taken into account, the same formula can be used.

##### 3.5.4.2.1. Horizontal shear in the bottom SonicStrip

The results of the calculation of the shear in the acoustic insulation devices at the wall bottom are given in :

- Figure 88, Figure 89 and Figure 90 for the long wall ;
- Figure 91, Figure 92 and Figure 93 for the short wall.

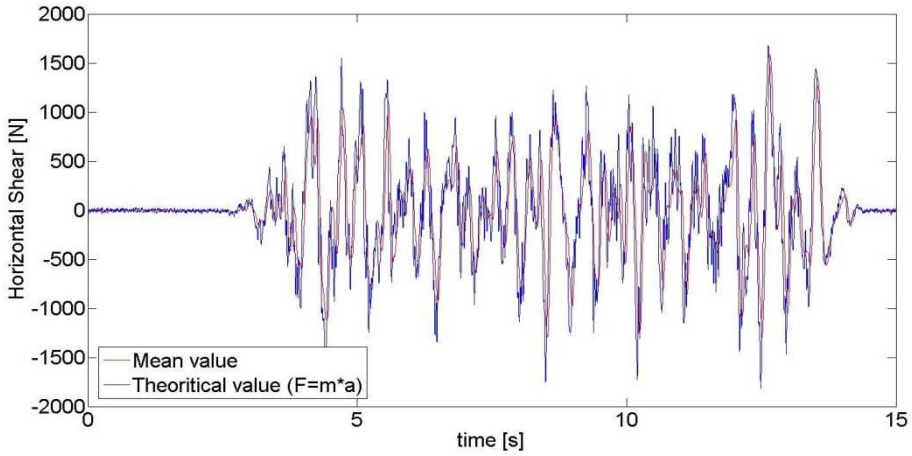


Figure 88 – Time evolution of the horizontal shear (bottom of the long wall – 0.0426g)

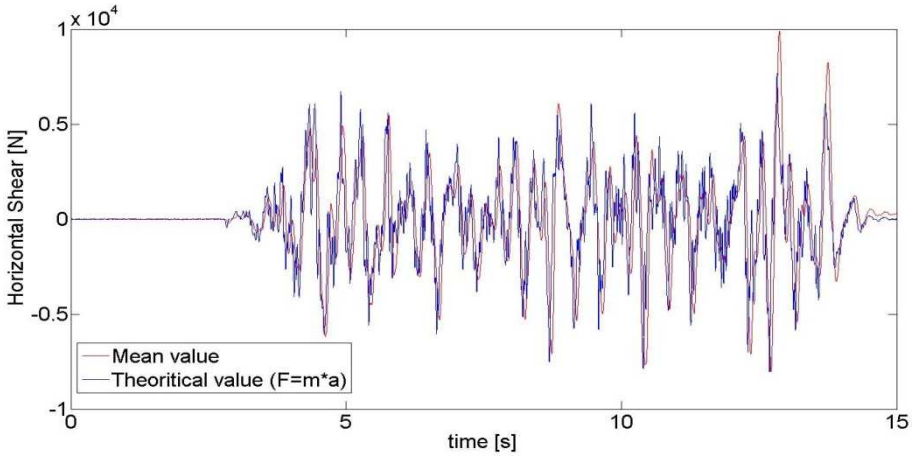


Figure 89 – Time evolution of the horizontal shear (bottom of the long wall – 0.2387g)

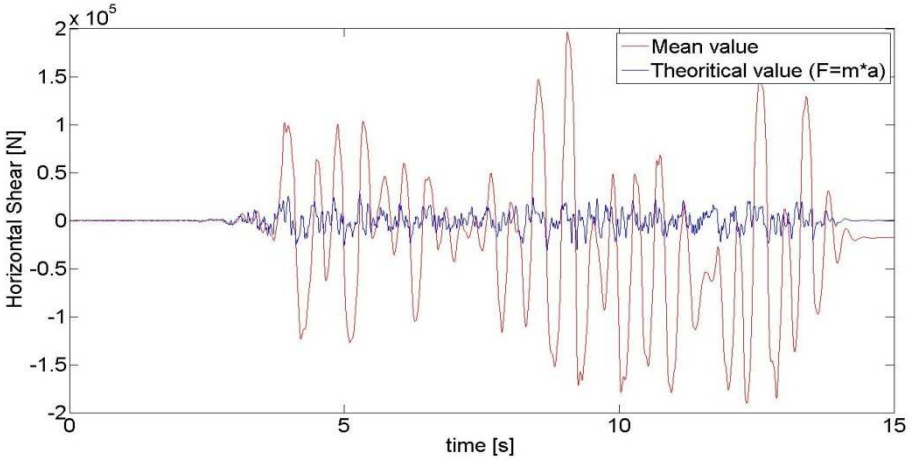


Figure 90 – Time evolution of the horizontal shear (bottom of the long wall – 0.6878g)

In the case of the long wall with acoustic insulation devices, the value of the horizontal shear is equal to the one expected if the acceleration level is low. On the contrary, the value is higher than the expected one when the acceleration level increases.

The reason is the assumption made with the method used to calculate the shear stress from the displacement. This assumption assumes a homogeneous shear along the wall. However, it's no more valid when rocking appears because only a part of the SonicStrip devices is stressed. The part where there is a one-side-uplift of the wall is no more stressed.

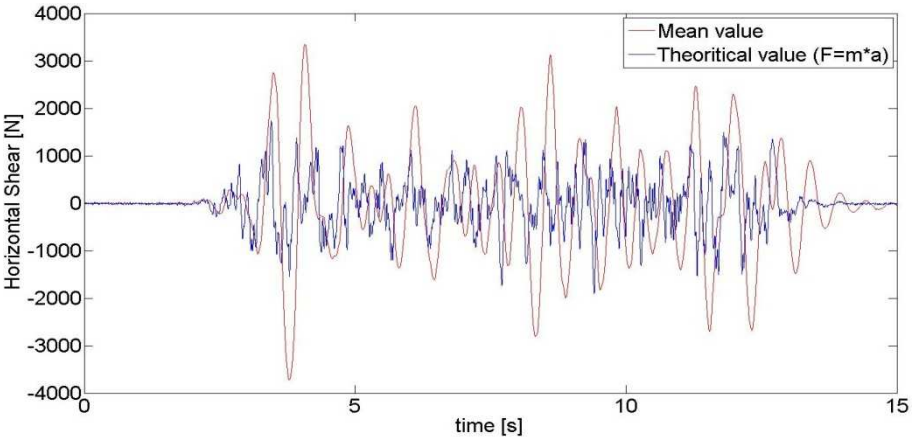


Figure 91 – Time evolution of the horizontal shear (bottom of the short wall – 0.0417g)

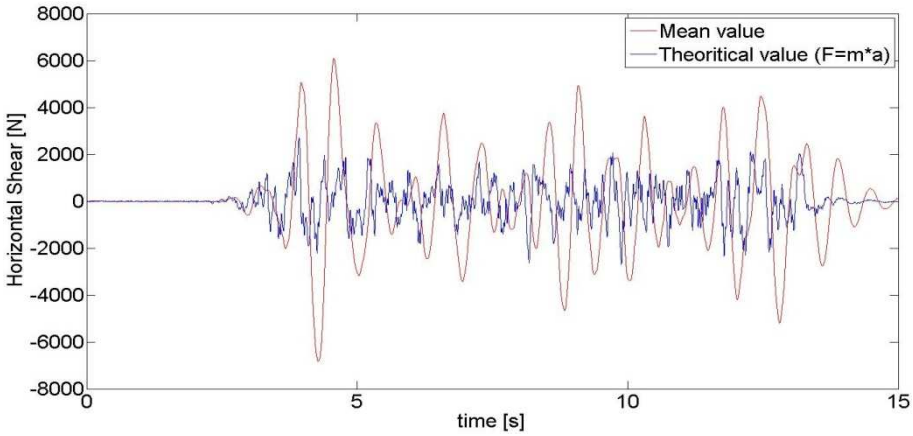


Figure 92 – Time evolution of the horizontal shear (bottom of the short wall – 0.0607g)

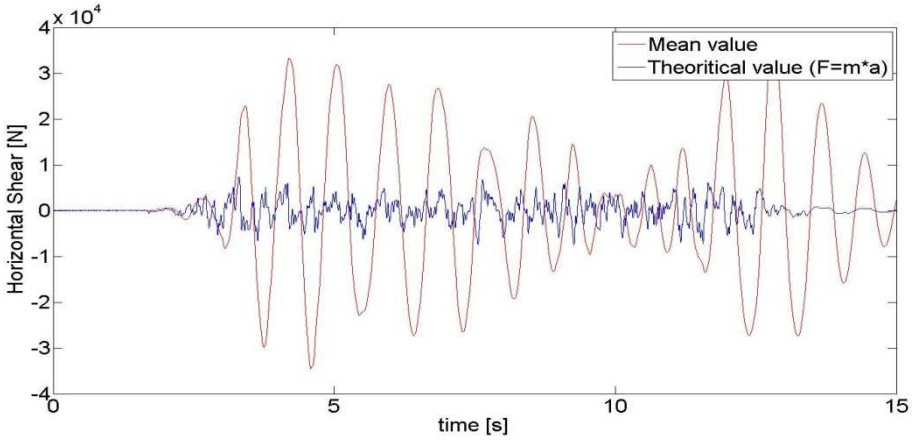


Figure 93 – Time evolution of the horizontal shear (bottom of the short wall – 0.1709g)

In the case of the short wall with acoustic insulation devices, the value of the horizontal shear is more or less equal to the one expected if the acceleration level is low. On the contrary, the value becomes higher than the expected one when the acceleration level increases.
The reason of these observations are the same than the one given for the long walls.

#### 3.5.4.2.2. Horizontal shear in the top SonicStrip

The results of the calculation of the shear in the acoustic insulation devices at the wall top are given in :

- Figure 94, Figure 95 and Figure 96 for the long wall ;
- Figure 97, Figure 98 and Figure 99 for the short wall.

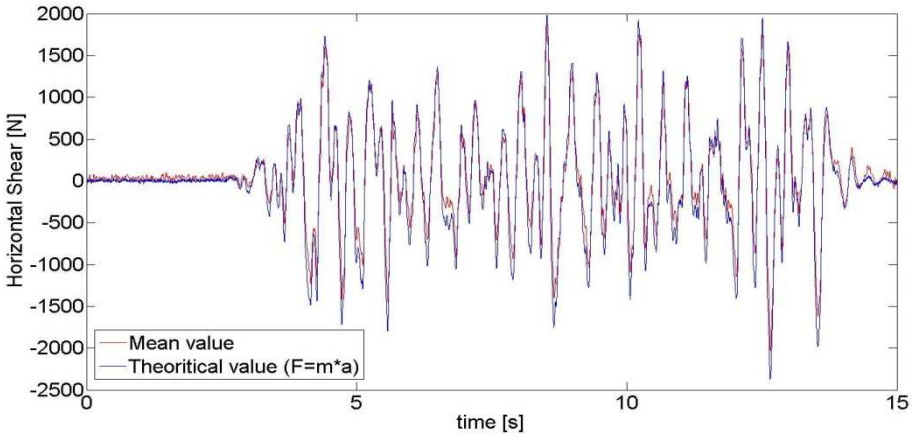


Figure 94 – Time evolution of the horizontal shear (top of the long wall – 0.0426g)

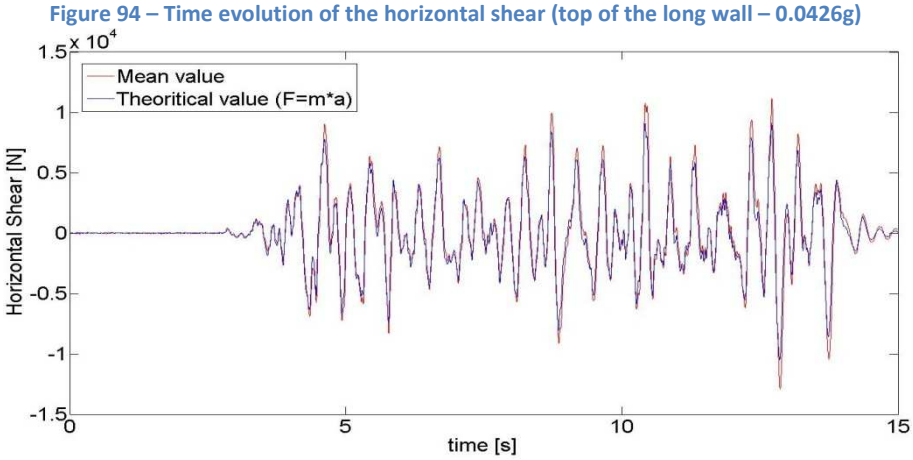


Figure 95 – Time evolution of the horizontal shear (top of the long wall – 0.1871g)

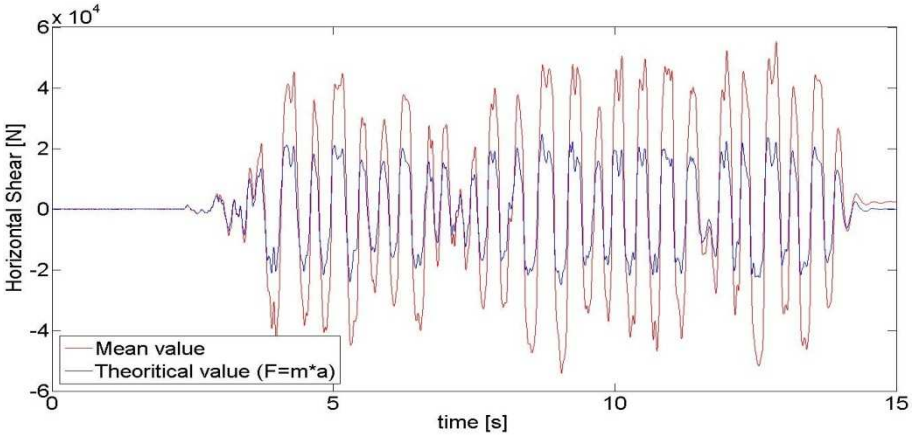


Figure 96 – Time evolution of the horizontal shear (top of the long wall – 0.6392g)

For the acoustic insulation devices at the top of the long wall, the calculated value of the shear stress is very close to the expected one, except for the Figure 96. The explanation is the same than the one given for the SonicStrip devices at the bottom. The results shown in Figure 94 and Figure 95 are nearer to the theoretical values because the rocking of the mass is less important than the rocking of the wall. Therefore, the assumption of a homogeneous shear along the wall is longer verified and the results are closer.

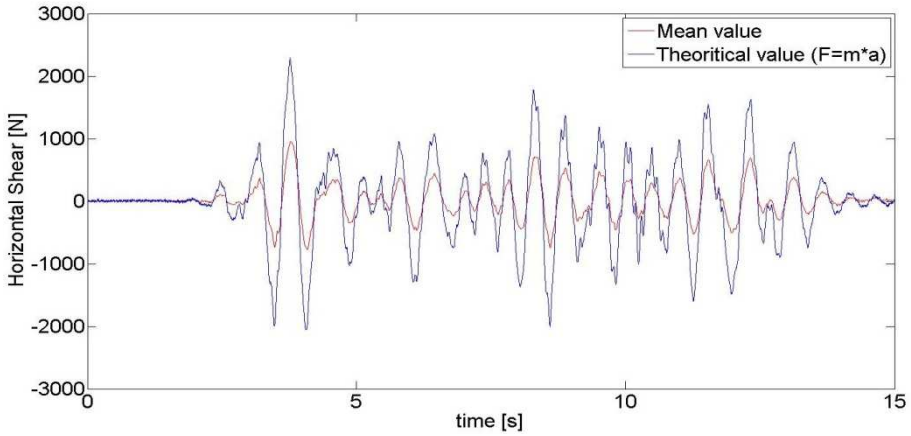


Figure 97 – Time evolution of the horizontal shear (top of the short wall – 0.0417g)

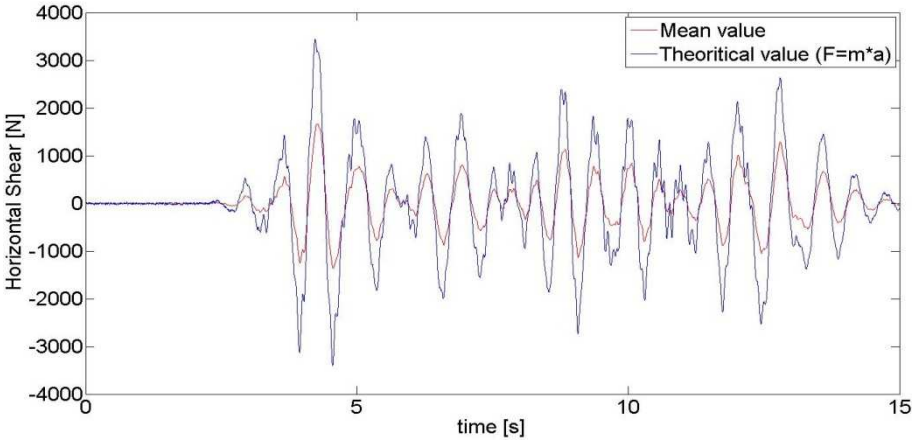


Figure 98 – Time evolution of the horizontal shear (top of the short wall – 0.0607g)

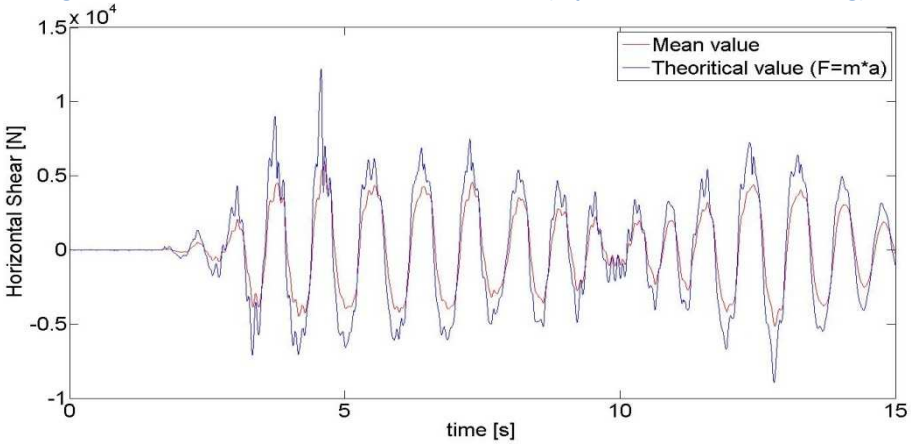


Figure 99 – Time evolution of the horizontal shear (top of the short wall – 0.1709g)

In Figure 97, Figure 98 and Figure 99, it can be seen that the time evolution is the same in both approaches, but the value of the horizontal shear is lower than the theoretical one.

As the rocking of the mass is null for the short wall, we could expect that the results are the same. Nevertheless, a difference exists. It is due to the compression level. Indeed, the shear modulus of the acoustic insulation devices is a non-linear function of the compression level and of the thickness of the devices. The shear modulus increases if the compression level becomes higher. Thus, the value of the shear modulus must be multiplied by a factor to take into account the compression level.

It follows :

$$G = \alpha \frac{E}{2(1-\nu)}$$

Where $E\ [MPa]$ is the elastic modulus

$\nu$ is the coefficient of Poisson

The value of $\alpha$ is unknown, but it must be over the unit if $\alpha = 1$ in the case for the devices on the long wall. Thanks to this factor, the calculated values and the theoretical ones are equal. In our case, the coefficient $\alpha$ is equal to 1.5 for the short wall if it is equal to the unit for the long wall. This value have been found after several attempts.

To summarize, the calculation of the shear stress in the SonicStrip devices depends on the rocking and on the compression level. Firstly, when the rocking becomes important, the main assumption of the calculation is no more valid and some modifications must be done to take into account the non homogeneous distribution of the shear along the devices. Secondly, the shear modulus must be multiplied by a factor to consider the influence of the compression level and the thickness of the devices.

Some research are necessary to study the influence of the rocking and of the compression level. Nevertheless, a calibration of our results gives the value of the coefficient $\alpha$ to apply in order to consider the compression level. If the compression level is about three times higher, the coefficient $\alpha$ seems to be 1.5.

### 3.5.5. Comparison with the vision system

The comparison with the vision system is the last subject of this chapter dedicated to the "Processing of the results of first test series". The data given by the vision system are only used to confirm the results obtained thanks to the sensors placed on the wall (compressive length, etc.). In fact, we receive these data later than the others because they need a more important post-processing.

#### *3.5.5.1. Justification of the comparison*

As it was explained in Chapter 2, the instrumentation layout includes a vision system data. This one measures the horizontal and vertical global displacements of the mass and the frame. Considering that the frame is connected to the table, their displacements are assumed equal. The global displacements of the wall top can be deduced from the ones of the mass thanks to the measurements of the relative displacement between the wall top and the mass.
Therefore, it is possible to compare the results given by the LVDT devices and the vision system data.

#### *3.5.5.2. Scaling of the time*

The data acquisition system of the Seismic test and the Imetrum Video-Gauge Vision System are independent. A time difference is the main consequence of this independence. It's illustrated in the Figure 100 and 101. The time difference is clearly obvious.

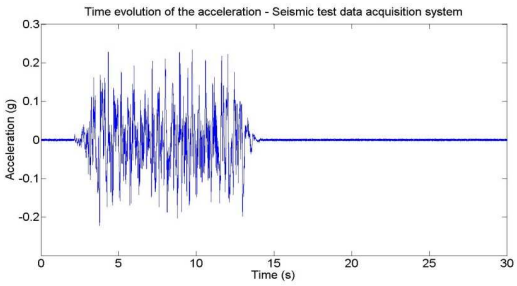


Figure 100 - Example with the Seismic test data acquisition system (Short wall without SonicStrip – 0.2425g)

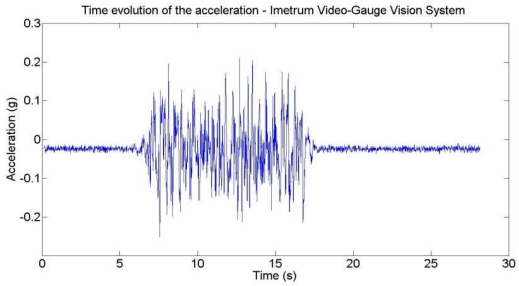


Figure 101 – Example with the Imetrum Video-Gauge Vision System(Short wall without SonicStrip – 0.2425g)

For every seismic test of each wall, one of the two data vectors must be shifted in order to compare the measurements. The values of the shift are given in Table 24 and must be applied to the vector of the Imetrum Video-Gauge Vision System.
NB : the values are obtained after manual trials and errors procedure.

Table 24 - Values of the time shift

| Seismic test | Long wall without SonicStrip [s] | Long wall with SonicStrip [s] | Short wall with SonicStrip [s] | Short wall without SonicStrip [s] |
|---|---|---|---|---|
| S1 | -8.355 | -7.0965 | -9.5942 | -6.405 |
| S2 | -6.035 | - 6.1207 | -5.223 | -5.4195 |
| S3 | -5.533 | -5.016 | -5.226 | -4.7985 |
| S4 | -6.6501 | -5.126 | -6.0684 | -7.1124 |
| S5 | -5.465 | -7.04 | -4.137 | -2.06 |
| S6 | -11.8 | -3.7 | -6.7515 | -3.848 |
| S7 | -7.0505 | -6.3645 | -5.745 | -4.8855 |
| S8 | -5.74 | -6.633 | / | -4.064 |
| S9 | -7.0465 | -10.12 | / | -3.8375 |

### *3.5.5.3. Post-processing and comparison of the results*

Once the scaling time is done, the post-processing can begin. It consists in two part. The first is based on the vertical displacement and the second one, on the horizontal displacement.
Remark : the global displacement of the target fixed on the frame are subtracted to one of the target fixed on the mass. So, the global displacements gives the motion of the wall relative to the table.

#### 3.5.5.3.1. Using of the vertical displacements

On one hand, the measurement in four points of the vertical global displacement allows the calculation of a slope of the wall top and also its rotation. This slope (angle $\alpha$) can be compared with the ones calculated for the rocking (angle $\gamma$) of the wall and the mass (angle $\beta$). Indeed, the sum of the slopes due to the rocking of the wall and of the mass should be the same than the slope deduced with the vertical global displacements, as it is shown in Figure 102.

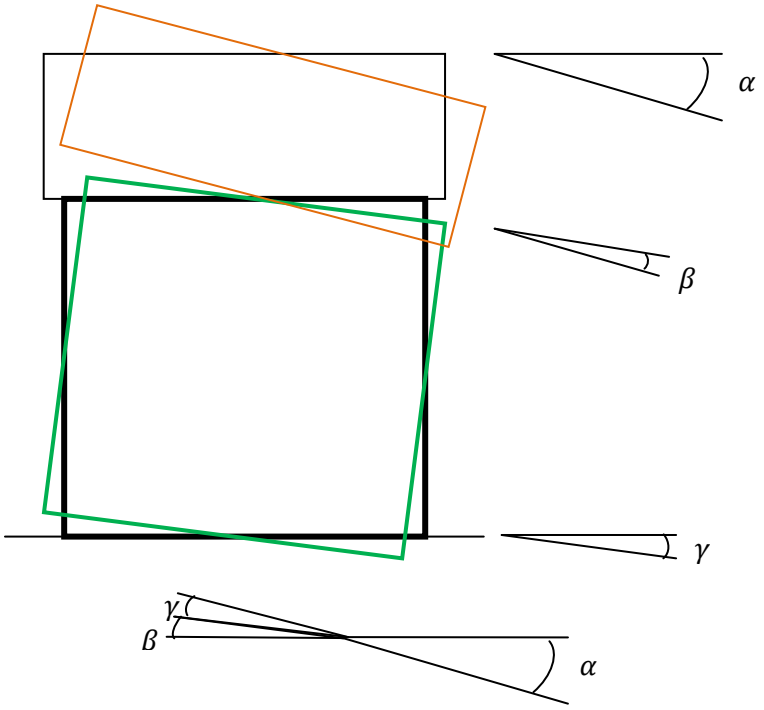


Figure 102 – Relation between the slope

In Figure 102, $\alpha$ is the angle corresponding to the slope given by the vertical global displacements, $\beta$ is the equivalent angle to the slope of the mass rocking and $\gamma$ is the equivalent one to the slope of the wall rocking. The obvious relation is

$$\gamma + \beta = \alpha$$

An example of the comparison is done for each wall, with results obtained under the maximum acceleration level reached during the test of a wall (from Figure 103 to Figure 105). In this figures, the slope calculated with the data acquisition systems of the Seismic test and the one given by the Imetrum Video-Gauge Vision System are nearly the same. It confirms the results obtained previously with the developed method.
The observation can be extended to this other seismic test, but the precision of the data acquisition system must be warily considered.

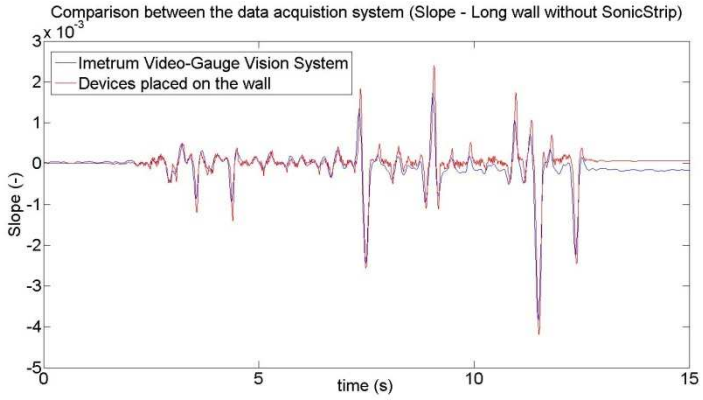


Figure 103 – Example with the long wall without SonicStrip (0.6878g)

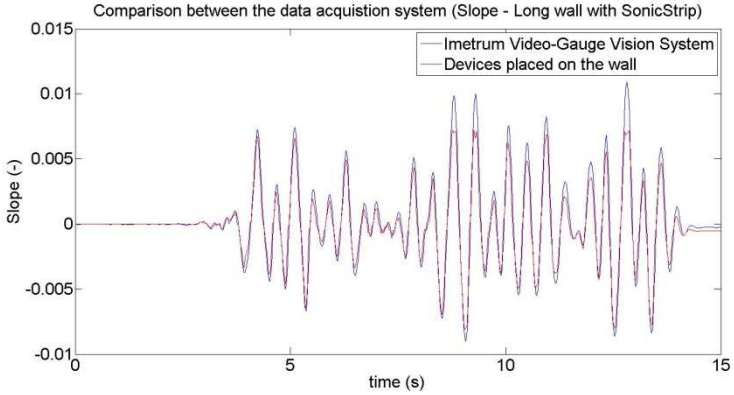


Figure 104 – Example with the long wall with SonicStrip (0.6392g)

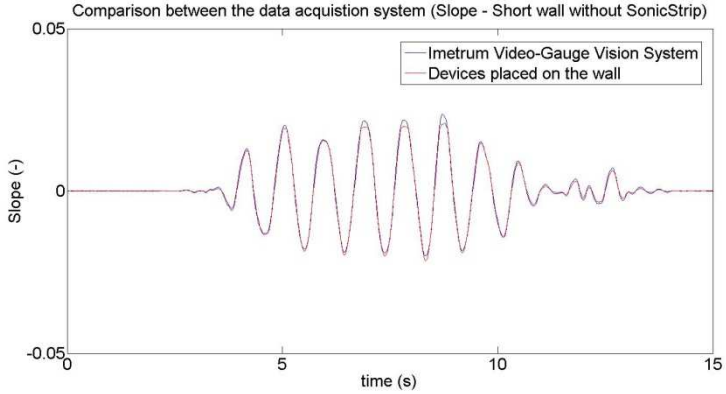


Figure 105 – Example with the short wall without SonicStrip (0.2336g)

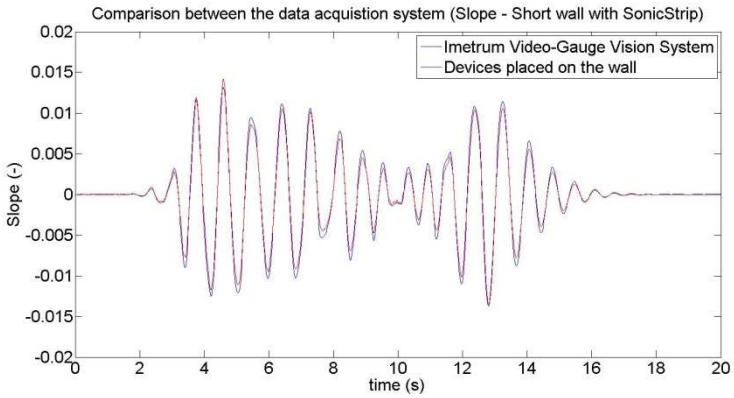


Figure 106 – Example with the short wall with SonicStrip (0.1709g)

The comparison between the vertical displacements of the two acquisition system data leads to the following conclusion. As the slopes are the same at the bottom and the top of the wall, the phenomenon observed is the rocking of a rigid body.

#### 3.5.5.3.2. Using of the horizontal displacement

On the other hand, the data also include the measurement of the horizontal global displacement in the same four points. As the support of the target can be considered as a rigid body, we expect that this measurement is the same for each target and the comparison will be made with the mean value.

The horizontal displacement calculated with the sensors placed on the specimens can be found with the following method. The value is not directly given by a sum because all the phenomena must be taken into account, like the rocking of the wall. Actually, the horizontal displacement at the wall top is caused by :

- the rocking of the wall ;
- the relative displacement between the wall and the support beam (not caused by the rocking) ;
- the relative displacement between the wall and the mass.

Here again, the example of the comparison is done, for each wall, with measures taken when the maximum acceleration level reached during the test of a wall is sent to the table (from Figure 107 to Figure 110)

In these figures, the horizontal displacement calculated with the data acquisition systems of the Seismic test and the one given the Imetrum Video-Gauge Vision System are very close. As it is the case for the comparison of the slope, it confirms the results obtained previously with the developed method.
The observation can be extended to this other seismic test, but the precision of the data acquisition system must be warily considered.

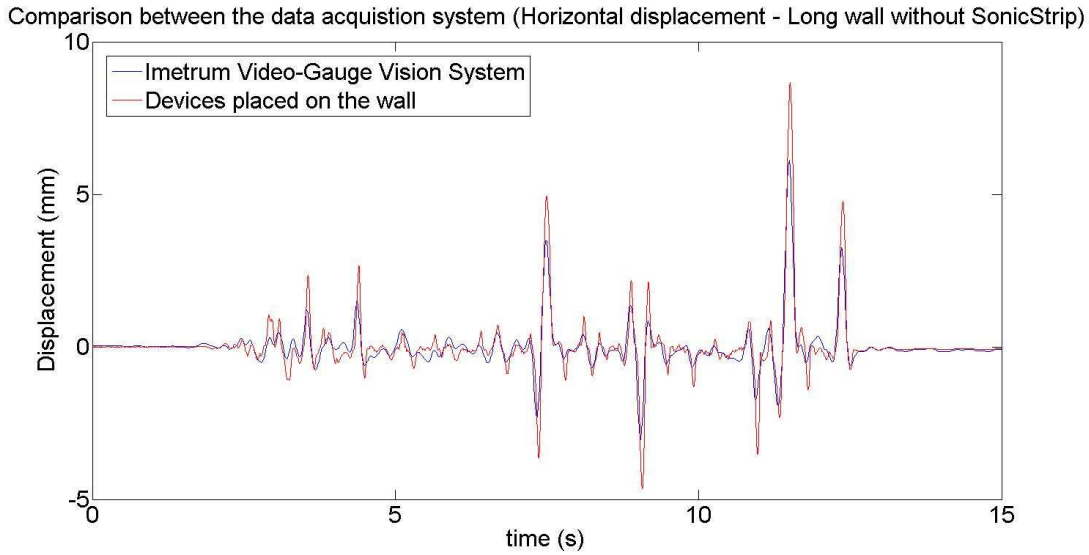


Figure 107 – Example with the long wall without SonicStrip (0.679g)

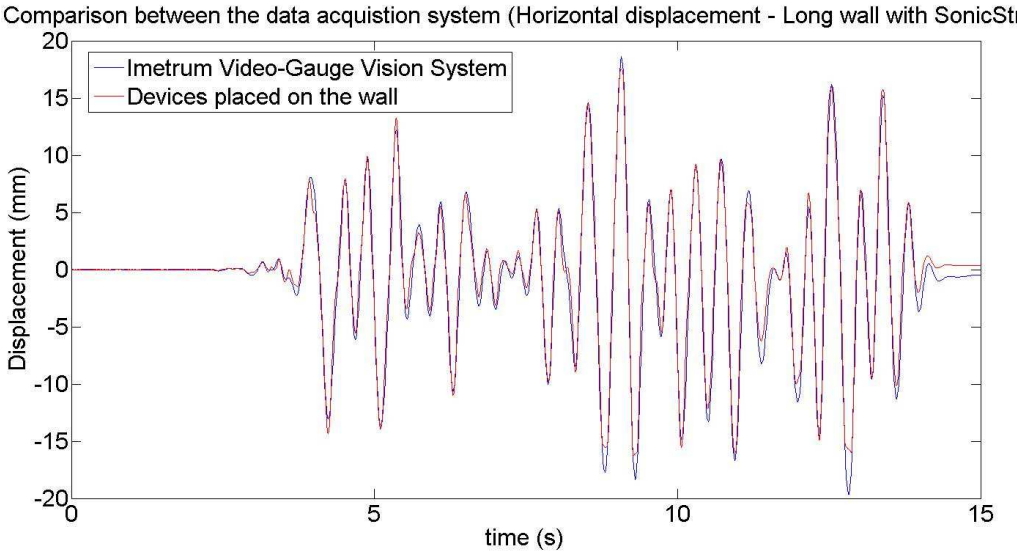


Figure 108 – Example with the long wall with SonicStrip (0.679g)

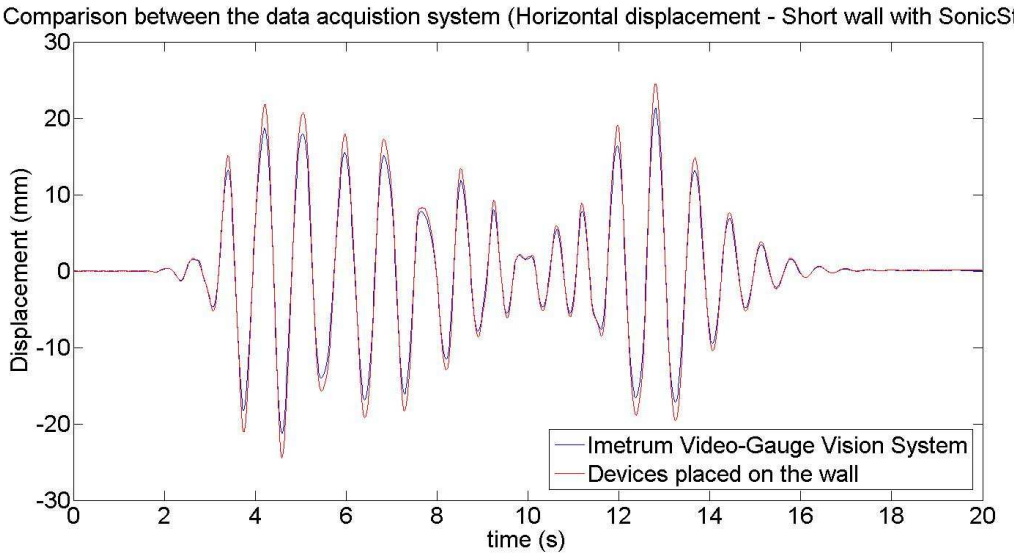


Figure 109 – Example with the short wall with SonicStrip (0.294g)

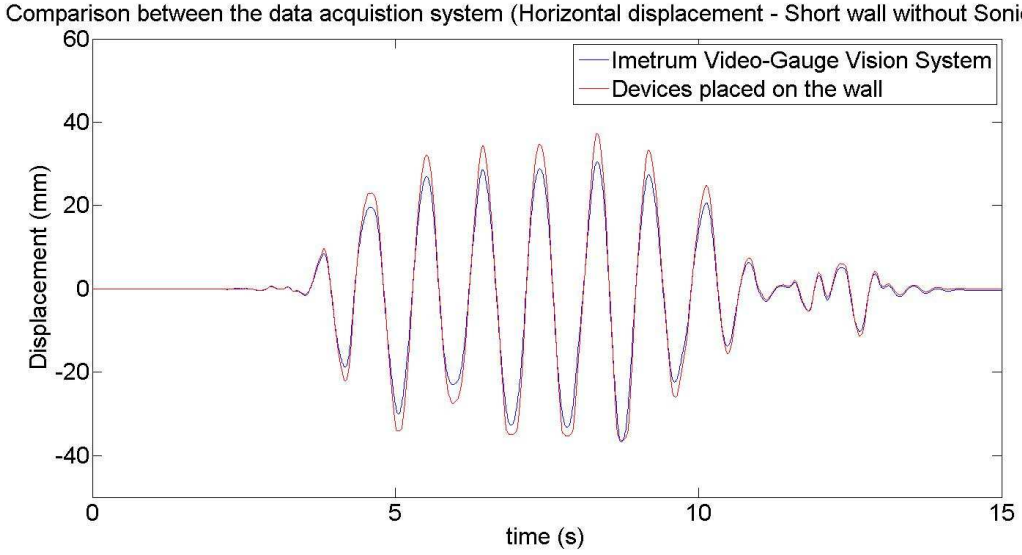


Figure 110 – Example with the short wall without SonicStrip (0.2425g)

### 3.5.6. Comparison with the preliminary assessment

The seismic tests provide some results about the compressive length, the shear strength and, sometimes, about the compressive strength. However, the absence of collapse, like the crushing of the units or the cracking along the diagonal, does not allow the exploitation of the results for the compressive and shear stress.
Two subjects can be exploited : the compressive length in dynamic's conditions and the rocking behaviour.

#### *3.5.6.1. Compressive length*

The sensors placed at the wall bottom have measured the relative vertical displacement between the bottom beam and the wall. These measurements led to the calculation of a compressive length which values are reminded in Table 25.

Table 25 - Minimum value of the compressive length (deduced from the seismic tests)

| Specimen | Acceleration level | | Compressive length | |
|---|---|---|---|---|
| | Theoretical [g] | Real [g] | [%] | [mm] |
| Long wall without SonicStrip | 0.0485 | 0.0278 | 83.2 | 1747.2 |
| | 0.194 | 0.1471 | 47.15 | 990.15 |
| | 0.679 | 0.6592 | 0.025 | 0.525 |
| Short wall without SonicStrip | 0.0485 | 0.0071 | 77.01 | 554.472 |
| | 0.07275 | 0.0244 | 58.7 | 422.64 |
| | 0.194 | 0.1444 | 14.37 | 103.464 |

In the preliminary assessment, a compressive length was calculated with the next formulae :

$$M = V.H \qquad e = \frac{M}{N}$$

$$L_c = \begin{cases} 0 & if\ e \geq L/2 \\ \left[3.\left(\frac{L}{2} - e\right)\right] & if\ e < L/2\ \wedge\ e > L/6 \\ L & if\ e \leq L/6 \end{cases}$$

These ones are deduced from the equilibrium equations for materials without tensile strength, where Navier's equations are not valid. They are based on the assumption of a linear distribution of the stresses.
To compared with the results of Table 25, the calculations with the same acceleration level (real) are done and their results are presented in Table 26. The results are only available for the walls without acoustic insulation devices.

Table 26 – Compressive length calculated in preliminary assessment (linear distribution)

| Tested wall | $a_g$ [g] | $V_{Sd}$ [N] | Assessed compressive length [mm] | [%] | Measured compressive length [mm] | [%] |
|---|---|---|---|---|---|---|
| Long wall | 0.0278 | 3409 | 2100 | 100.00 | 1747.2 | 83.2 |
| | 0.1471 | 18038 | 1201.88 | 57.23 | 990.15 | 47.15 |
| | 0.6592 | 80834.4 | 0 | 0.00 | 0.525 | 0.025 |
| Short wall | 0.0071 | 871 | 720 | 100.00 | 554.472 | 77.01 |
| | 0.0244 | 2992 | 720 | 100.00 | 422.64 | 58.7 |
| | 0.1444 | 17707 | 0 | 0.00 | 103.464 | 14.37 |

The comparison between Table 25 and Table 26 leads to the conclusion that the method used for the preliminary assessment overvalues the compressive length, except for the maximum acceleration. For this last value, a null compressive length means that the wall is rocking and turns around its bottom corners, as it was observed during the tests.

Another way to assess the compressive length is possible by changing the assumption of a linear distribution of the stresses. The new assumption is a constant distribution of the stresses and gives the next formulas and results (Table 27) :

$$M = V.H \qquad e = \frac{M}{N}$$

$$L_c = \begin{cases} 0 & if\ e \geq L/2 \\ \left[2.\left(\frac{L}{2} - e\right)\right] & if\ e < L/2\ \wedge\ e > 0 \\ L & if\ e \leq 0 \end{cases}$$

Table 27 – Compressive length calculated in preliminary assessment (constant distribution)

| Tested wall | $a_g$ [g] | $V_{Sd}$ [N] | Assessed compressive length [mm] | Assessed compressive length [%] | Measured compressive length [mm] | Measured compressive length [%] |
|---|---|---|---|---|---|---|
| Long wall | 0.0278 | 3409 | 1854.55 | 88.31 | 1747.2 | 83.2 |
| | 0.1471 | 18038 | 801.25 | 38.15 | 990.15 | 47.15 |
| Short wall | 0.0071 | 871 | 657.31 | 91.29 | 554.472 | 77.01 |
| | 0.0244 | 2992 | 504.57 | 70.08 | 422.64 | 58.7 |

Table 27 gives two main results. On one hand, in the case of the long wall, the calculated compressive length is close or under the length measured during the test. So, we can conclude that the distribution of the compressive stresses in the wall is between the constant one and the linear one.
For example, a distribution of the type “parabola-rectangle” could be considered. The idea comes from what it do with the concrete structures.

On the other hand, in the case of the short wall, the calculated compressive length remains bigger than the measured one. Thus, the assumption of a constant distribution of the stresses is wrong. The relative error is the following :

- $15.6\ \%\ (a_g = 0.0071)$
- $12.27\%\ (a_g = 0.0244)$

A possible solution is to apply a reduction factor to the value given by the equilibrium equations with the assumption of a constant distribution of the stresses. This factor will depend on a few parameters like the aspect ratio and the acceleration level. It can be imagined that the factor becomes equal to the unit if the aspect ratio is over a given value. It seems that the factor will also decrease if the acceleration increases.

Another idea is to consider the “shear “length instead of the wall length. The shear length is equal to 5/6 of the wall length. It can be seen that the factor is the one of the “shear area”. The origin of this idea comes from the behaviour of the wall. As the short wall behaviour should be in bending, a part of the length does take part to the shear strength. Now, the shear strength depends on the compressive length.

In order to improve the idea, all the seismic tests are studied. It follows the results in Table 28.

Table 28 – Compressive length calculated in preliminary assessment (short wall – with shear length)

| $a_g$ [g] (PGA) | $V_{Sd}$ [N] | Compressive length [mm] (linear distribution) | | Compressive length [mm] (constant distribution) | | Compressive length [mm] (measured) | |
|---|---|---|---|---|---|---|---|
| **0,0071** | 871 | 720.00 | 100.00 % | 537.31 | 74.63 % | 554.472 | 77.01 % |
| **0,0287** | 3519 | 519.91 | 72.21 % | 346.61 | 48.14 % | 417.24 | 57.95 % |
| **0,0244** | 2992 | 576.86 | 80.12 % | 384.57 | 53.41 % | 422.496 | 58.69 % |
| **0,0479** | 5874 | 265.64 | 36.89 % | 177.09 | 24.60 % | 316.944 | 44.02 % |
| **0,0928** | 11380 | 0 | 0 % | 0 | 0% | 178.848 | 24.87 % |
| **0,0955** | 11711 | 0 | 0 % | 0 | 0% | 171.648 | 23.84 % |
| **0,1444** | 17658 | 0 | 0 % | 0 | 0% | 103.464 | 14.37 % |
| **0,1532** | 18786 | 0 | 0 % | 0 | 0% | 104.832 | 14.56 % |
| **0,1984** | 24329 | 0 | 0 % | 0 | 0% | 18 | 2.5 % |

Table 28 leads to the following comments. Except for the case with $a_g = 0.0479g$, the measured compressive length is always between the calculated ones, as in the case of a long wall. Indeed, the measured values are in an interval where the lower bound is the value obtained with the constant distribution of the stresses and the upper bound is the value obtained with the linear distribution of the stresses.
Once the PGA is over the design acceleration, the calculated compressive length is null because the used model is a static one.

In conclusion, the compressive length of wall can be assessed thanks to the equilibrium equations for materials without tensile strength. The criterion used to know if the wall is a short or a long one, is the aspect ratio and it has an influence on the results. According to the aspect ratio, the wall length to consider will be :

- the real length if it's a "long" wall ;
- the shear length if it's a "short" wall.

Once the acceleration reaches a certain value, the compressive length becomes equal to zero, but it doesn't mean the collapse of the wall.
Here again, the development of such a model obviously needs more research and results.

#### *3.5.6.2. Rocking behaviour*

If the acceleration level gradually increases, there is a moment where the equations of the static equilibrium give a compressive length equal to zero. With the "Push-over" method, it means the overturning of the wall and also its collapse. Nevertheless, the wall was still in place after the dynamic tests we did. Therefore, it was an additional reason to think that the use of a static equivalent method is no more valid if the acceleration level is too high and the dynamic equations must be explicitly solved.

The resolution of these equations is done by the computer program developed by Sophie Grigoletto (Grigoletto, 2006). This program can't be used directly and some modifications are necessary to take into account that the mass is applied at the wall top. The main unknown is the value of the coefficient of plastic dissipation. There is no way to assess it, also we take a value of 0.91 for the wall without SonicStrip devices and of 0.87 for the walls with these devices. The choice of the values implicitly makes the assumption that the presence of acoustic insulation devices lead to a higher dissipation. These values are obtained after a trials and errors procedure.

The inputs of the program are the geometry of the wall, the time evolution of the acceleration experimented at the table and the coefficient of plastic deformation.

The main result of the use of this program is the time evolution of the angle $\theta$ between the horizontal and the wall bottom during the test. This value can be compared to the slope calculated from the sensors 8,10 and 12 (placed at the bottom of the wall). To remind, these sensors are used to assess the compressive length.

For example, the results for the long walls under the maximum acceleration level are drawn in Figure 111 and their maximum value is given in Table 29.

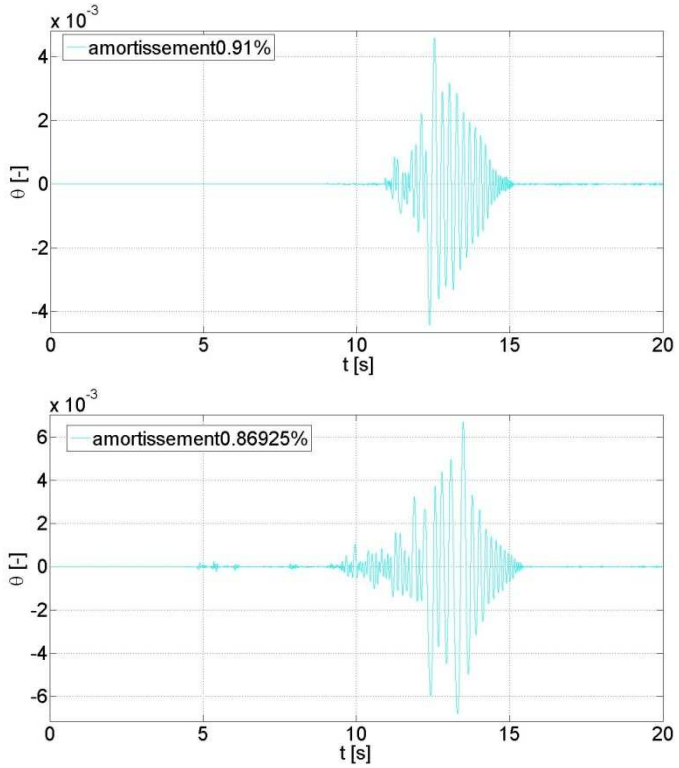


Figure 111 - Results given by the program of Sophie Grigoletto

Table 29 – Value of the maximum slope according to the acceleration level

| Specimen | Acceleration level [g] | Maximum slope [-] | Maximum $\theta$ [-] |
|---|---|---|---|
| Long wall without SonicStrip | 0.6878 | $4{,}2200.10^{-3}$ | $4.59.10^{-3}$ |
| Long wall with SonicStrip | 0.6392 | $8{,}4000.10^{-3}$ | $6.69.10^{-3}$ |

In Table 29, it is observed that the values of the slope and of the angle $\theta$ are very close. It means that the walls behaviour can be considered as the rocking of a rigid body. The conclusion is the same for the short walls.

# Chapter 4 :
# Design of the second test series

## 4.7. Geometry of the specimens

As said in the introduction, two specimens are tested during the second test series and our first aim is to study the behaviour of T- and L-shaped walls. Besides this requirement, we add the wish to investigate the influence of an opening. The Annex B gives a few ideas of frames with T- or L-shaped walls. From these configurations, we deduce a few parameters that we can change to have the different drawn configurations. Among these parameters, there are :

- Type of units and mortar ;
- Length, width and height of the "shear walls" ;
- Length, width and height of the "flanges" ;
- Span of the lintel or size of the hole ;
- Relative position of "shear wall" and "flange" ;
- ...

In this non-exhaustive list, the "shear wall" means the wall which is in the plan of frame and the "flange" is the wall perpendicular to the "shear wall".

Now we must choose the two configurations to test. To help us in this choice, some technical thoughts have to be taken into account. For example, the frame length must obviously be smaller than the shaking table length. Nevertheless, it's not the only constraint. Indeed, to ensure the security of the laboratory team and to avoid the risk of damages to the table, the dead load put on the specimens must be lighter than or equal to 5 tons. This limit has some repercussions on the geometry because it influences the compression level of the masonry, which is usually between 0.1 and 1 MPa.
Therefore, the dimensions of our specimens have to respect the three following criteria :

- $l_{shear\ wall,1} + l_{span} + l_{shear\ wall,2} < 3\ m$
- $A_{base,cross\ section} < 50\ 000\ mm^2$
  $0{,}05\ m^2$
- $A_{base,cross\ section} > 500\ 000\ mm^2$
  $0{,}5\ m^2$

Despite the fact that we want to study T- and L-shaped walls and, so, we don't have to take a decision about the relative position of the "shear wall" and the "flange", the geometrical possibilities are still numerous. In order to select some configurations from the Annex B, two other ideas are develop.

The first one concerns the value of the span. If we refer to the technical recommendations for doors width, we learn that the openings, like doors, in masonry walls are at least 0,9m wide. From this value, we can deduce the length of the "shear walls".
The second one is about the wish to compare the results of this test series with those of the first one. In the first test series, our specimens were simple walls of 0.72m or 2.1m long. Considering that we want to compare the behaviour of a single wall and the one of the same wall connected to a perpendicular wall, it seems logical to take T- or L-shaped walls which "shear wall" has the same dimensions than the walls tested in the first test series.

At this step, the geometry of the “shear walls” is determined. Their dimensions are :

- $length : 0{,}72\ m$
- $width : 0{,}138\ m$
- $height : 1{,}8\ m$

We choose the length of the short walls of the first test series to respect the length of the shaking table.

For the dimensions of the “flange”, we decide to take the same ones than those of the “shear wall” for the next reason. According to the EN 1996-1-1 : “*Eurocode 6 : Design of masonry structures – Part 1-1 : Common rules for reinforced and unreinforced masonry structures*”, we can assume that a perpendicular wall takes part in the strength as “flange” if the connection between this wall and the shear one resists to the shearing actions and if the “flange” doesn’t buckle within the length assumed. EN 1996-1-1 also gives a criterion to calculate the length of the perpendicular wall which contributes to the strength [EN 1996-1-1, 2010].
With this criterion, we are aware that it’s not interesting to build a 2,1m long “flange” because only a part of this wall will act as flange of the shear wall. Thus, the dimensions of the perpendicular wall are the following :

- $length : 0{,}72\ m$
- $width : 0{,}138\ m$
- $height : 1{,}8\ m$

The last, but not the least, decision to take for the geometry of the specimens we want to test, is about their general configuration. To reduce the number of possibilities, we decide that the first specimen is made of two T-shaped walls and the second one, of two L-shaped walls.
In the case of the specimen with two T-shaped walls, the T-shaped walls are non-symmetrically built because we want to study the seismic behaviour of a frame which the walls have different bending inertia.
For the specimen with the L-shaped walls, the walls are built so that the frame has an axis of symmetry perpendicular to the lintel. The detail of this specimen lies in the connection of the “shear wall” and the “flange”. One L-shaped wall has its “flange” glued to the “shear wall”, whereas the other has its “flange” meshed with (built in) the “shear wall”.

From the Figure 112 to the Figure 115, we give the geometry of the specimens.

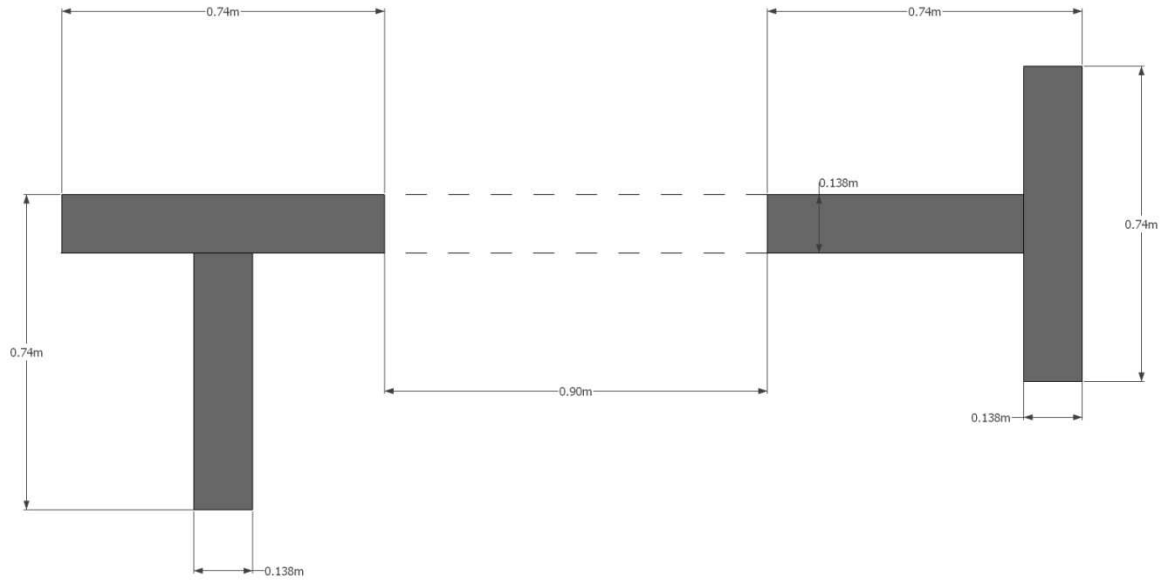


Figure 112 – Geometry of the first specimen (plan view)

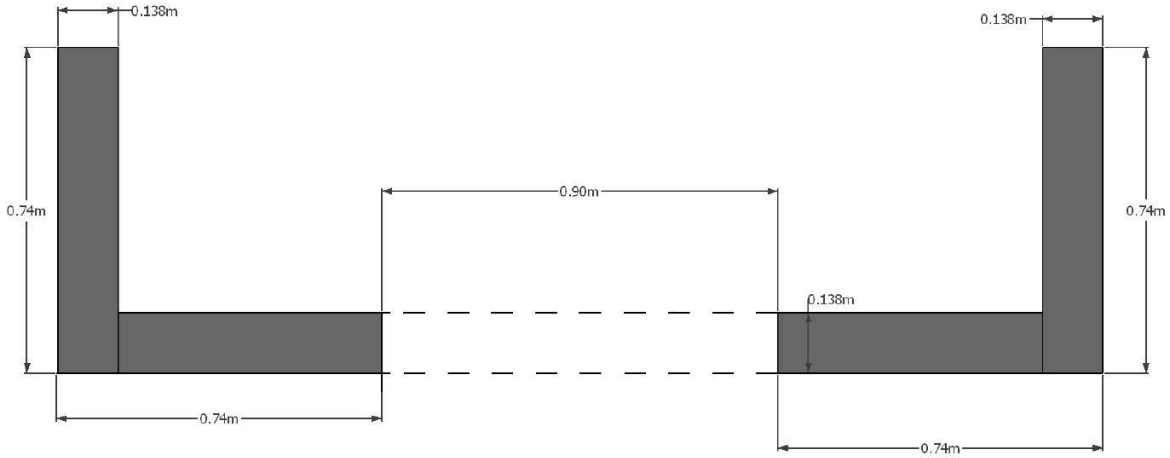


Figure 113– Geometry of the second specimen (plan view)

In Figure 112 and Figure 113, it is observed that the “shear” wall and “flange” length is not 0.72m, but 0.74m. This difference is due to the thickness of the used units, 138 mm, and the length of units, about 300mm. Therefore, the “shear wall” and the “flange” are a little bit longer to make the construction easier and to ensure a good connection between the wall parts.

Concerning the lintel, this one is not prefabricated because this kind of elements are economically built to reduce the costs. Therefore, the strength is equal to the minimum required. In our case, the goal is to study the behaviour of masonry buildings, not to collapse a lintel. That’s why, the lintel of the specimens is design by ourselves. The plans and the calculus are in Annex C.

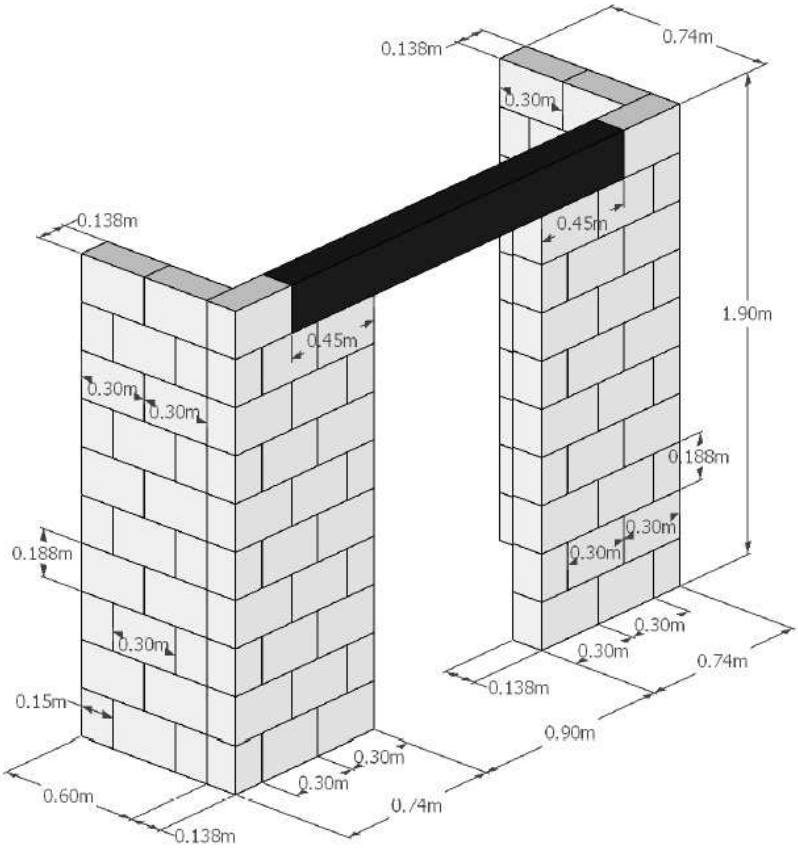


Figure 114 – Geometry of the first specimen (3D view)

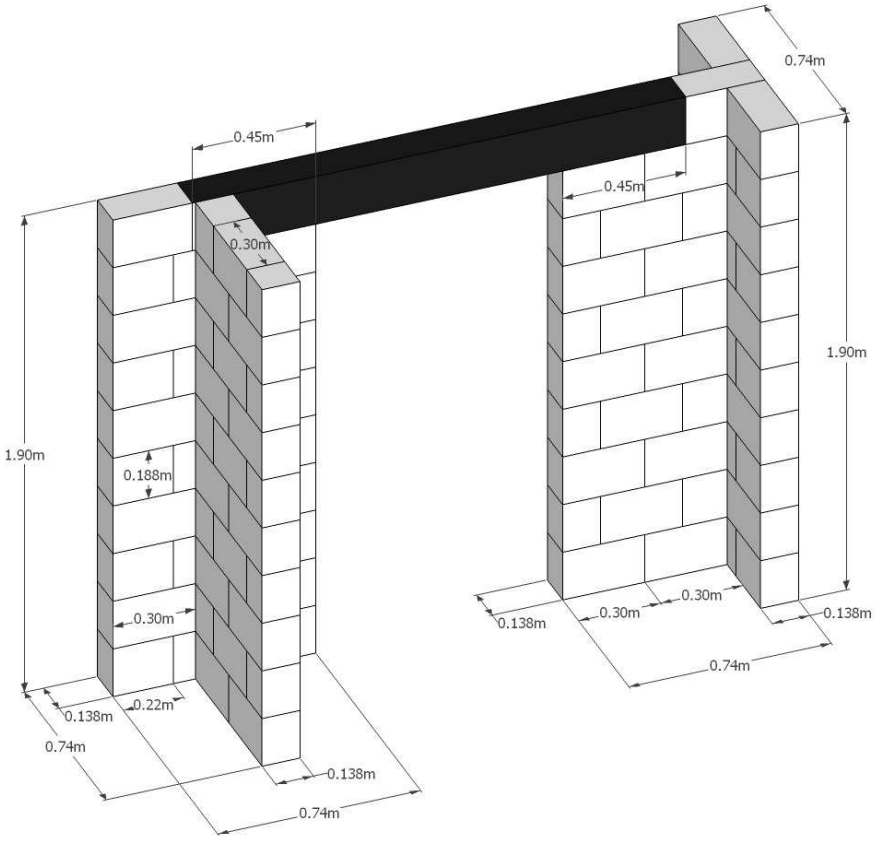


Figure 115 – Geometry of the second specimen (3D view)

## 4.8. Dead load

As it was done to emulate the structural floor load in the first test series, we have to load the frame with a mass. Nevertheless, the loading is more complicated for this second test series for two main reasons.

On one hand, the area to be loaded is not rectangular, especially in the case of the frame with T-shape walls. This has consequences on the position of the gravity centre of the mass, now we have to know where it is exactly because its position is the application point of the seismic action.

On the other hand, we want to test the structure under a X- and/or Y-direction earthquake and under different loading cases. If the earthquake direction is easy to change because the table can move in X- and Y-direction, modifying the loading case is more difficult. However, the modifying seems important to us because it allows the simulation of masonry structures in real situations. Indeed, everybody knows that, in masonry building, the structure is usually composed of parallel walls in one direction. The walls can be in the same direction than the earthquake or be perpendicular to it. Obviously, the direction of loaded walls compared with the one of the earthquake will affect the strength of the structure.

For the second test series, the dead load will be applied thanks to a concrete slab ( plans in Annex D).

To be able to simulate all loading cases, steel parts are put between the wall top and the concrete slab. Thanks to them, the vertical load is transferred to the “shear wall”, the “flange” or both of them. A sketch of the steel part is drawn in Figure 116.

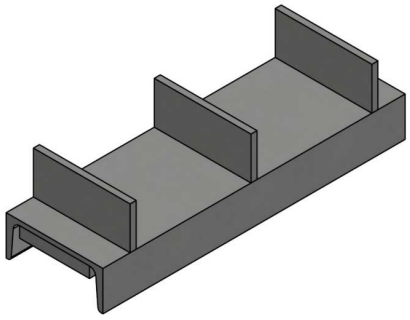

Figure 116 – Steel part

The U-shaped piece was chosen to avoid the risk of out-of-wall-plan displacement. In Figure 116, a expanded metal panel is welded in the hole of the U-shaped piece and of steel plates are welded perpendicular to the main axis of U-shaped piece. The expanded metal panel increases the friction between the piece and the wall top. The steel plates connect the piece to the slab thanks to some holes where they can go in.

With that system and a mass of 5 tons, the compression level of the structure is calculated for each loading cases in Table 30.

Table 30 - Compression level of different loading cases

| | Loaded wall | Compression level |
|---|---|---|
| **Frame with T-shaped walls** | Shear wall | 0.245MPa |
| | Flange | 0.245MPa |
| | Both | 0.135 MPa |
| **Frame with L-shaped walls** | Shear wall | 0.245MPa |
| | Flange | 0.245MPa |
| | Both | 0.135 MPa |

The values of compression level are included in the usual boundaries of the compression level in masonry.

Remark : the dead load will be hung from the crane throughout the duration of the tests, like it was during the first test series.

## *4.9. Preliminary assessment of the specimens*

The preliminary assessment of the specimens is realized to evaluate the acceleration leading to the collapse of the structure. The first step of the assessment is to make some assumptions about the way of collapse. First of all, we have to know the mechanicals and geometrical properties, like the strength of the units, the wall inertia, etc. Then, we have to identify the phenomena which could appear during the tests. Finally, the specimens will be designed to be sur of the strength.

### 4.9.1. Mechanical characteristics

The units used to realize the walls are "*Zonnebeke POROTHERM"*. The walls are built in thin bed masonry with "*PORO+mortar*". Vertical joints are empty and horizontal ones are glued. The block size is :

$$(Length\ x\ Width\ x\ Height) = (300.0\ mm\ x\ 138.0\ mm\ x\ 188.0\ mm)$$

Mechanical characteristics of the units and masonry are the following ones :

- Normalised compressive strength of units (EN 772-1 Annex A)

$$f_b = 13.0\ N/mm^2$$

- Measured characteristic masonry compressive strength (EN 1052-1)

$$f_k = 5.6 N/mm^2$$

- Characteristic compressive strength (EN 1996-1-1)

$$f_k = 4.2 N/mm^2$$

- Characteristic compressive strength (NBN-EN 1996-1-1)

$$f_k = 3.9 N/mm^2$$

No specific characterization has been carried out for shear behaviour. Usual standard values are considered for further assessment :

- Initial shear strength (NBN-EN 1996-1-1)

$$f_{vk0} = 0.3 N/mm^2$$

- Characteristic shear strength (NBN-EN 1996-1-1)

$$f_{vk} = 0.5 f_{vk0} + 0.4\sigma_d \leq 0.045 f_b\ (= 0.585 N/mm^2)$$

### 4.9.2. Geometrical characteristics

The frame is composed of two walls and one lintel. The walls properties are developed here under and the lintel ones are calculated later.

Unlike the walls of the first test series, the geometrical characteristics of the specimens are not so easy to find. First of all, we have to find the centre of gravity of each wall. Here, the walls are the "columns" of our frame. To be sure that no mistake is made about the vocabulary, we will follow the naming and the axis convention given in Figure 117 and Figure 118. The origin of axis is marked with a green point.

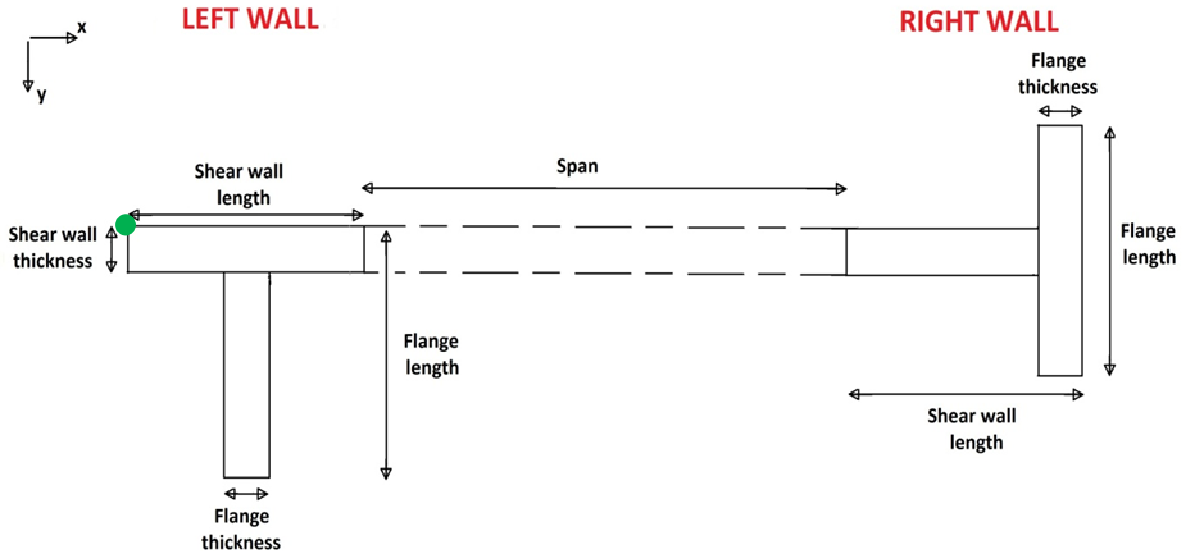


Figure 117 – Sketch of the specimen with T-shaped walls

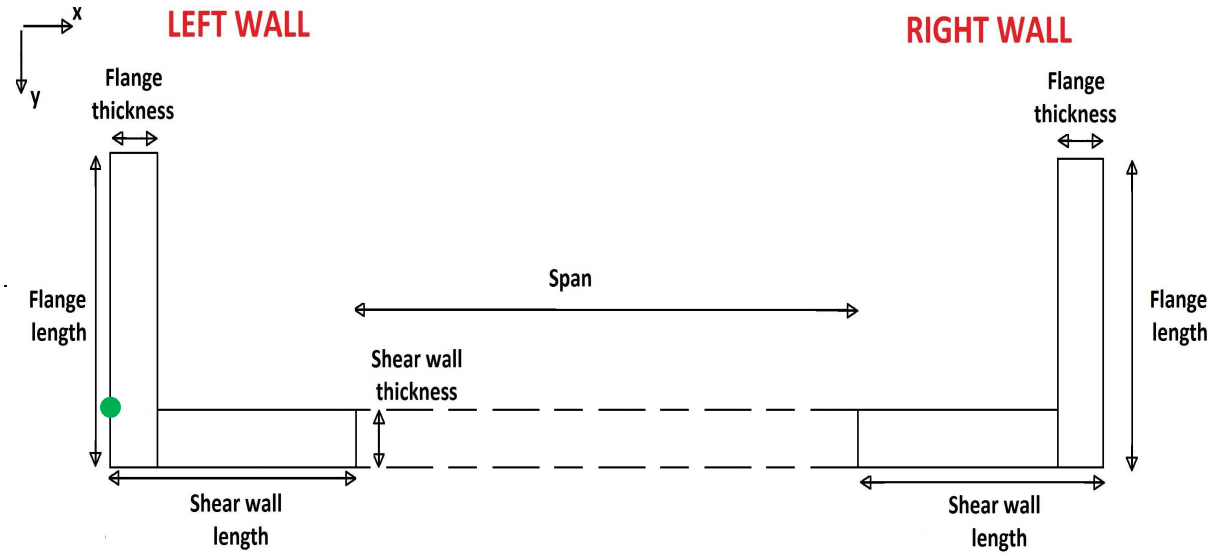


Figure 118– Sketch of the specimen with L-shaped walls

Table 31 and Table 32 detail the geometrical characteristics in X and Y directions. The effective length of the wall perpendicular to the stress direction is calculated according to the Eurocode 6.

Table 31 – Mechanical characteristics of the specimen – X direction

| Specimen | With T-shaped walls | | With L-shaped walls | |
|---|---|---|---|---|
| Wall | Left | Right | Left | Right |
| Effective length of the flange | $0.498\ m$ | $0.74\ m$ | $0.498\ m$ | $0.498\ m$ |
| Gravity centre of shear wall : | $0.37\ m$ | $1.941\ m$ | $0.37\ m$ | $1.941\ m$ |
| flange : | $0.37\ m$ | $2.311\ m$ | $0.069\ m$ | $2.311\ m$ |
| all : | $0.37\ m$ | $2.145\ m$ | $0.2715\ m$ | $2.109\ m$ |
| Area of shear wall : | $0.10212\ m^2$ | $0.08308\ m^2$ | $0.10212\ m^2$ | $0.04968\ m^2$ |
| flange : | $0.04968\ m^2$ | $0.10212\ m^2$ | $0.04968\ m^2$ | $0.10212\ m^2$ |
| all : | $0.1518\ m^2$ | $0.1852\ m^2$ | $0.1518\ m^2$ | $0.1518\ m^2$ |
| Inertia $I$ | $0.004739\ m^4$ | $0.008943\ m^4$ | $0.007767\ m^4$ | $0.007767\ m^4$ |
| Shear area $A_{eff}$ | $0.10212\ m^2$ | $0.10212\ m^2$ | $0.10212\ m^2$ | $0.10212\ m^2$ |

Table 32 – Mechanical characteristics of the specimen – Y direction

| Specimen | With T-shaped walls | | With L-shaped walls | |
|---|---|---|---|---|
| Wall | Left | Right | Left | Right |
| Effective length of the shear wall | $0.74\ m$ | $0.498\ m$ | $0.498\ m$ | $0.498\ m$ |
| Gravity centre of shear wall : | $0.069\ m$ | $0.069\ m$ | $0.069\ m$ | $0.069\ m$ |
| flange : | $0.439\ m$ | $0.069\ m$ | $-0.301\ m$ | $0.0497\ m$ |
| all : | $0.235\ m$ | $0.069\ m$ | $-0.134\ m$ | $-0.134\ m$ |
| Area of shear wall : | $0.10212\ m^2$ | $0.04968\ m^2$ | $0.06872\ m^2$ | $0.04968\ m^2$ |
| flange : | $0.0.8308\ m^2$ | $0.10212\ m^2$ | $0.08308\ m^2$ | $0.10212\ m^2$ |
| all : | $0.1852\ m^2$ | $0.1518\ m^2$ | $0.1518\ m^2$ | $0.1518\ m^2$ |
| Inertia $I$ | $0.008943\ m^4$ | $0.004739\ m^4$ | $0.007767\ m^4$ | $0.007767\ m^4$ |
| Shear area $A_{eff}$ | $0.10212\ m^2$ | $0.10212\ m^2$ | $0.10212\ m^2$ | $0.10212\ m^2$ |

In theses tables, the value of inertia is the local one and it is assumed that the shear area is the one of the wall in the same direction than the stress.

Another characteristic which could be interesting to know is the stiffness of the walls. To determinate it, three assumptions have to be made : one for the value of the Young modulus $E$, another for the value of the shear modulus $G$. For theses, we follow the Eurocode 6 and 8 :

- To take into account the effect of cracking, the Eurocode 8 says : "Unless a more accurate analysis of the cracked elements is performed, the elastic flexural and shear stiffness properties of masonry may be taken to be equal to one-half of the corresponding stiffness of uncracked elements". So, we must take $E/2$.
- $G = 0.4\ E$ according to the Eurocode 6.

The last one is about the supports of the walls. If we can say without any problems that the wall is built in at the bottom, the support of the top is unknown : it can be built-in, simply supported or free. In masonry, the stiffness of a wall is calculated thanks to the formula (Tomazevic, 1999) :

$$k = \frac{1}{\frac{h^3}{\alpha EI} + \frac{h}{GA'}}$$

where $\alpha$ is a parameter depending of the support conditions ;

$h$ is the height of the level.

The different values of stiffness are given in Table 33.

Table 33 – Stiffness of the walls [N/m]

| Specimen Wall | With T-shaped walls Left | With T-shaped walls Right | With L-shaped walls Left | With L-shaped walls Right |
|---|---|---|---|---|
| X-direction Built-in $\alpha = 12$ | 13270855.98 | 19771365.56 | 18246458.1 | 18246458.1 |
| Simply supported $\alpha = 6$ | 7808878.006 | 12737298.62 | 11499076.55 | 11499076.55 |
| Free $\alpha = 3$ | 4283170.115 | 7442006.868 | 6610250.348 | 6610250.348 |
| Y-direction Built-in $\alpha = 12$ | 19771365.56 | 13270855.98 | 18246458.1 | 18246458.1 |
| Simply supported $\alpha = 6$ | 12737298.62 | 7808878.006 | 11499076.55 | 11499076.55 |
| Free $\alpha = 3$ | 7442006.868 | 4283170.115 | 6610250.348 | 6610250.348 |

A last characteristic of the walls is the position of the rigidity centre or shear centre. This one are useful to know if the wall is subject to torsion. The torsional stress is actually directly proportional to the distance between the gravity centre and the rigidity centre.

In (Serge Cescotto & Charles Massonet, 2001), it can be read that “In the case of section without any symmetrical axis, but with parts which axis converge on a same point, the rigidity centre is necessarily that point.” Therefore, the shear centre of a L-shaped or T-shaped wall is located as shown in Figure 119.

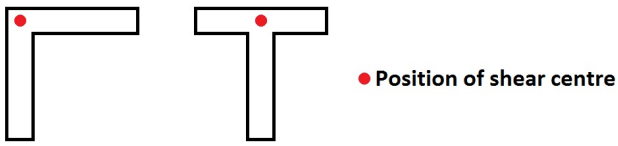


Figure 119 – Position of shear centre

With the convention axis and the position of the origin, the values of the rigidity centre are given in Table 34.

Table 34 – Position of the rigidity centre

| Specimen | With T-shaped walls X-direction | With T-shaped walls Y-direction | With L-shaped walls X-direction | With L-shaped walls Y-direction |
|---|---|---|---|---|
| Rigidity centre | | | | |
| Left wall : | $0.37\ m$ | $0.069\ m$ | $0.069\ m$ | $0.069\ m$ |
| Right wall : | $2.311\ m$ | $0.069\ m$ | $2.311\ m$ | $0.069\ m$ |
| Frame : | $1.042\ m$ | $0.069\ m$ | $1.19\ m$ | $0.069\ m$ |

The last element of the frame to characterize is the lintel. Its mechanical characteristics are only useful for the numerical model used to determinate the internal forces of the frame. Indeed, the lintel is overdesigned such as its collapse never happens.

### 4.9.3. Assessment of the acceleration

Once the mechanical and geometrical properties of the elements of the our frame are determined, the assessment of the maximum acceleration can be made. A specific method is followed in order to calculate it. The method used is called “static equivalent” (push-over) because the seismic action is represented with a horizontal shear. This shear can have two orientations (X or Y-axis) and two directions (positive or negative according to the axis convention). In the method, the specimen studied is modelled thanks to a frame-model where the walls are the columns and the lintel, the beam.

Hereafter, the method is described in one particular case and, after each step, some numerical values are given. For example, the calculation until the collapse of the T-shaped walls specimen is considered with a horizontal shear coming from the right side and oriented in the X-axis. Two other assumptions are made :

- the lintel is built-in at its two extremities
- the load is on the both part of the wall

The other cases have been developed in a separated document and implemented in “Excel”. Numerical values of the final results are given in Table 49 to Table 52

The first step consists in doing a first guess of the horizontal shear $V$.

The second step is the determination of the internal forces in each element of the frame. These values are performed thanks to OSSA2D, a software developed by the University of Liege to realize an elastic analysis of a structure.

A first frame-model with a load increment is used until the ultimate load of the weakest wall is reached. (Figure 120, left side).

Then , another load increment is applied on a second frame-model where the horizontal stiffness of the weakest wall is neglected (Figure 120, right side). Practically, the wall which has reached its ultimate load is replaced with a support. This support only prevents the vertical displacement.

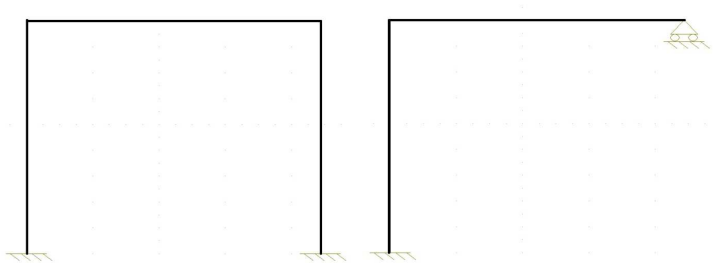

Figure 120 - Types of modelling

As said, using this software requires to make an assumption about the support conditions of the lintel. This one can be simply supported on each walls or it can be built-in. In fact, the reality is between these two possibilities, but there is no methods to estimate the value of the restraint.

Table 35 – Example of the assessment method (first iteration)

| | External forces | Internal forces | | |
|---|---|---|---|---|
| | | Bottom wall to the left | Lintel | Bottom wall to the right |
| $N\ [N]$ | 50000 | 26216.77 | 2010.98 | 23783.23 |
| $V\ [N]$ | 5000 | -2010.98 | 1216.77 | -2989.02 |
| $M\ [Nm]$ | / | 2610 | -833.34 | -4230.22 |

NB : N positive if compression

Table 36 – Example of the assessment method ( Xth iteration)

| | External forces | Internal forces | | |
|---|---|---|---|---|
| | | Bottom wall to the left | Lintel | Bottom wall to the right |
| $N\ [N]$ | 50000 | 26985.59 | 3223.01 | 23014.41 |
| $V\ [N]$ | 8000 | -3223.01 | 1985.59 | -4776.99 |
| $M\ [Nm]$ | / | 4254.27 | -1359.23 | -6721.31 |

Table 37 – Example of the assessment method (Last iteration)

| | External forces | Internal forces | | |
|---|---|---|---|---|
| | | Bottom wall to the left | Lintel | Bottom wall to the right |
| $N\ [N]$ | 50000 | 28043.99 | 4891.56 | 21956.01 |
| $V\ [N]$ | 12130 | -4891.56 | 3043.99 | -7238.44 |
| $M\ [Nm]$ | / | 6280.22 | -2083.21 | -10150.71 |

In Table 35, the normal stress $N$ of the external forces is the dead load. The shear stress $V$ of these ones represents the seismic action and the bending moment is calculated from the normal and shear stresses. All these values are applied at the gravity centre of the wall.
In order to take into account the loading case (dead load placed on the shear wall, the flange or both of them), the bending moment must be corrected. Indeed, in some cases, the loading case can have positive or negative effects depending on whether the bending moment is increasing or decreasing. It is summarized in Table 38 for the specimen with T-shaped walls.

Table 38 – Loading case influence

| Wall / Loading case | X-axis | | Y-axis | |
|---|---|---|---|---|
| | Direction (+) | Direction (-) | Direction (+) | Direction (-) |
| Shear wall | No influence $x_g = x_V$ | No influence $x_g = x_V$ | Favourable Influence $y_g > y_V$ | Unfavourable Influence $y_g > y_V$ |
| Left wall Flange | No influence $x_g = x_V$ | No influence $x_g = x_V$ | Unfavourable Influence $y_g < y_V$ | Favourable Influence $y_g < y_V$ |
| Both | No influence $x_g = x_V$ | No influence $x_g = x_V$ | No influence $y_g = y_V$ | No influence $y_g = y_V$ |
| Shear wall | Favourable Influence $x_g > x_V$ | Unfavourable Influence $x_g > x_V$ | No influence $y_g = y_V$ | No influence $y_g = y_V$ |
| Right wall Flange | Unfavourable Influence $x_g < x_V$ | Favourable Influence $x_g < x_V$ | No influence $y_g = y_V$ | No influence $y_g = y_V$ |
| Both | No influence $x_g = x_V$ | No influence $x_g = x_V$ | No influence $y_g = y_V$ | No influence $y_g = y_V$ |

As it can be seen, the positive or negative effects depend on the horizontal shear direction and on the position of the gravity centre of the wall ($x_g$ or $y_g$) relative to the position of the application point of the dead load ($x_V$ or $y_V$). Their values are calculated according to the convention of Figure 117 and are given by the formulas :

$$M_{loading\ case,\ x} = N.(x_g - x_V)$$
$$M_{loading\ case,\ y} = N.(y_g - y_V)$$

Where $N\ [N]$ is positive if it goes in the positive X- or Y-direction.

The third step is an iterative one and comes to an end when the value of the horizontal shear $V$ is equal to the maximum shear which fulfils the strength criteria. These criteria are stemmed from, among others, the mechanical characteristics. For example, the position of the shear centre compared with the gravity centre one regulate the presence of torsion. The different kinds of stresses are the followings :

- Bending stress, directly characterized by the compressive length ;
- Shear stress, defined by the design value of shear resistance depending on the compressive length ;
- Torsion stress, function of the distance between the gravity centre and the shear centre ;
- Crushing of the units, depending on the compressive stress of the wall.

All these stresses are directly or indirectly linked to the compressive length, except for the torsion one. Therefore, the first part of the iterative step is devoted to the understanding of the calculus of the compressive length. Then, the rules to verify the criteria are developed. Finally, a table will summarized the results of the assessment.
Obviously, the internal forces must be reassessed thanks to OSSA2D as soon as the horizontal shear $V$ changes.

#### *4.9.3.1. Compressive length*

This part is the continuation of the Annex 3 of the Master's Thesis of Benjamin Cerfontaine (Cerfontaine, 2010). The method described below is based on his reasoning, but the configurations are different and the formulas are explicitly developed.
The calculus of the compressive length is based on the equilibrium equations for materials without tensile strength, where Navier's equations are not valid. The present difficulty is due to the shape of the walls because the thickness is not constant all along the wall.
The principle of calculation is based on some assumptions. The first one is the uniform distribution of compressive stress on the section. The second supposes that the horizontal shear at the shear wall – flange interface is inferior to the shear strength. The third and last one is the linear distribution of the stresses on the section.
This principle is the same than the one for a wall with a rectangular section. The equilibrium equations are written in a section stressed by a moment and a normal stress. The unknowns of these equations are the compressive length $L_c$ and the maximum stress $\sigma_1$. The detail of a T-shaped wall is the presence of different cases. These ones are illustrated in Figure 121 and correspond to the next situations :

- At the left, all the section is compressed (No one-side-uplift) ;
- At the middle left, there is one-side-uplift in one part of the shear wall;
- At the middle right, the one-side-uplift goes until a part of the flange
- At the right, the flange is totally uplifted and only a part of the shear wall is still compressed.

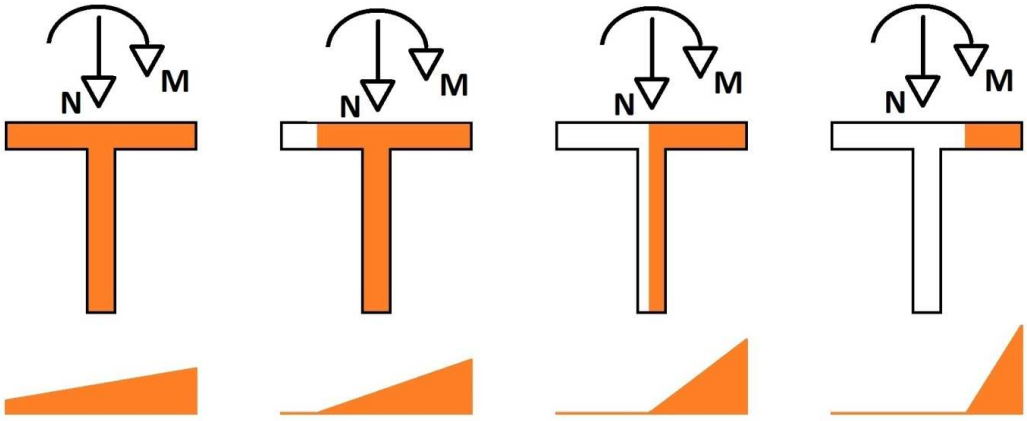


Figure 121 – cases of taking off

Considering that the position of gravity centre of the global section and its inertia is known, the four possible cases can be developed.

- First case : no one-side-uplift

When the whole section is all in compression, the Navier's equations are still available. Any uplift will happen until the stress is positive everywhere in the section (convention : stress is positive if there is compression). The stress is calculated with the next formula :

$$\sigma_1 = \frac{N}{A} - \frac{M}{I}.l_1 \geq 0$$

Where $N\ [N]$ is the normal stress ;
$M\ [Nm]$ is the bending moment due to the horizontal shear ;
$A\ [m^2]$ is the considered section ;
$I\ [m^4]$ is the inertia of the all section ;
$l_1[m]$ is the distance between the gravity centre and the furthest point.

In this case, the compressive length is equal to the length of the T-shaped wall.

Table 39 – Example of the assessment method

| *First case* | *Compressive length* $[m]$ | *Maximal stress* $[MPa]$ |
|---|---|---|
| *First iteration* | / | 0.0128 |
| *Xth iteration* | / | 0.1361 |
| *Last iteration* | / | 0.2873 |

NB : stress positive if traction

- Second case : one-side-uplift of the left part of the shear wall

If a part of the section is uplifted and if there is only one-side-uplift in the shear wall, the global section is divided into three areas (shear wall to the left of the flange, the flange and the shear wall on the right of the flange). The stress at the areas interface are function of the maximal stress $\sigma_1$.

$$\begin{cases} \sigma_2 = \dfrac{L_c - \dfrac{\left(L_{shear\ wall} - t_{flange}\right)}{2}}{L_c}\sigma_1 \\ \sigma_3 = \dfrac{L_c - \dfrac{\left(L_{shear\ wall} + t_{flange}\right)}{2}}{L_c}\sigma_1 \end{cases}$$

Where $\sigma_2\ [MPa]$ is the stress at the interface between the part of the shear wall to the right of the flange and the flange and $\sigma_3\ [MPa]$ is the stress at the interface between the flange and the part of the shear wall on the left of the flange. The naming comes from Figure 117.

A normal stress and an eccentricity (distance between the gravity centre and the position where the stress is applied) are then assigned to each area and the equilibrium equations are written :

$$N = N_1 + N_2 + N_3 \qquad M = N_1.e_1 + N_2.e_2 + N_3.e_3$$

Where $N_1\ [N]$ is the normal stress of the part of the shear wall to the right of the flange ;
$e_1\ [m]$ is the eccentricity of $N_1$ ;
$N_2[N]$ is the normal stress of the flange ;
$e_2\ [m]$ is the eccentricity of $N_2$ ;
$N_3[N]$ is the normal stress of the part of the shear wall to the left of the flange
$e_3\ [m]$ is the eccentricity of $N_3$ ;

In the case studied, the stresses and their eccentricity have the following expressions :

- For the part of the shear wall to the right of the flange

$$N_1 = \frac{\sigma_1 + \sigma_2}{2}.\frac{\left(L_{shear\ wall} - t_{flange}\right)}{2}.t_{shear\ wall}$$
$$= \frac{1}{8L_c}\left[4L_c - \left(L_{shear\ wall} - t_{flange}\right)\right].\left(L_{shear\ wall} - t_{flange}\right).t_{shear\ wall}.\sigma_1$$

$$e_1 = L_{shear\ wall} - \frac{\left(L_{shear\ wall} - t_{flange}\right)}{2}.\frac{1}{3}.\frac{\sigma_1 + 2\sigma_2}{\sigma_1 + \sigma_2} - x_g$$
$$= L_{shear\ wall} - \frac{\left(L_{shear\ wall} - t_{flange}\right)}{2}.\frac{1}{3}.\frac{6L_c - 2L_{shear\ wall} + 2t_{flange}}{4L_c - L_{shear\ wall} + t_{flange}} - x_g$$

- For the part of the flange

$$N_2 = \frac{\sigma_2 + \sigma_3}{2}.L_{flange}.t_{flange} = \frac{1}{4L_c}[4L_c - 2L_{shear\ wall}].L_{flange}.t_{flange}.\sigma_1$$

$$e_2 = L_{shear\ wall} - \frac{(L_{shear\ wall} - t_{flange})}{2} - \frac{t_{flange}}{3}.\frac{\sigma_2 + 2\sigma_3}{\sigma_2 + \sigma_3} - x_g$$
$$= \frac{(L_{shear\ wall} + t_{flange})}{2} - \frac{t_{flange}}{3}.\frac{6L_c - 3L_{shear\ wall} - t_{flange}}{4L_c - 2L_{shear\ wall}} - x_g$$

- For the part of the shear wall to the left of the flange

$$N_3 = \frac{\sigma_3}{2}.\left[L_c - \frac{(L_{shear\ wall} + t_{flange})}{2}\right].t_{shear\ wall}$$
$$= \frac{1}{8L_c}\left[2L_c - (L_{shear\ wall} + t_{flange})\right]^2.t_{shear\ wall}.\sigma_1$$

$$e_3 = L_{shear\ wall} - \frac{(L_{shear\ wall} + t_{flange})}{2} - \frac{1}{3}.\left[L_c - \frac{(L_{shear\ wall} + t_{flange})}{2}\right] - x_g$$
$$= L_{shear\ wall} - \frac{1}{3}.\left[L_c + L_{shear\ wall} + t_{flange}\right] - x_g$$

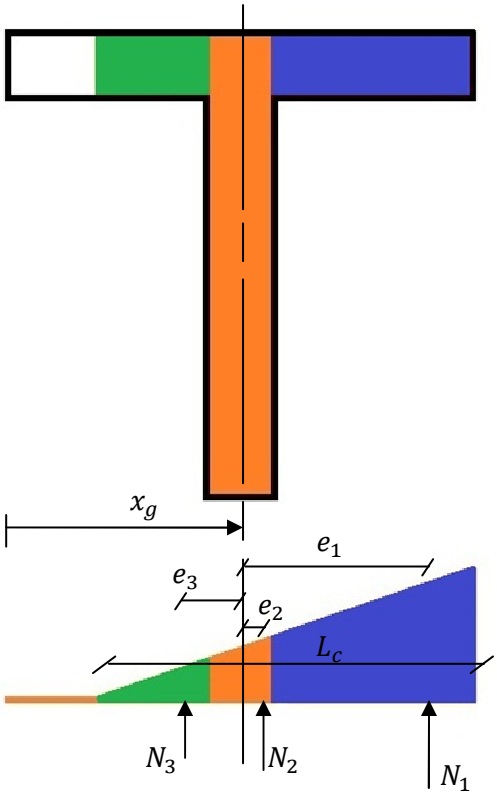


Figure 122 – Sketch of the second case

Putting these expressions in the equilibrium equations allows the calculus of the maximal stress thanks to the first equation. The second one gives a non-linear relation from which the compressive length $L_c$ can be determined.

$$\sigma_1 = \frac{4L_c.N}{Num}$$

Where $$Num = 0.5.(4L_c - L_{shear\ wall} + t_{flange}).(L_{shear\ wall} - t_{flange}).t_{shear\ wall}.\sigma_1$$
$$+ [4L_c - 2L_{shear\ wall}].L_{flange}.t_{flange}.\sigma_1 + 0.5.\left[2L_c - (L_{shear\ wall} + t_{flange})\right]^2.t_{shear\ wall}.\sigma_1$$

$$M = N.\frac{Num}{Denom}$$

Where $Num = 0.5.\left(4L_c - L_{shear\ wall} + t_{flange}\right).\left(L_{shear\ wall} - t_{flange}\right).t_{shear\ wall}.\sigma_1 + [4L_c - 2L_{shear\ wall}].L_{flange}.t_{flange}.\sigma_1 + 0.5.\left[2L_c - \left(L_{shear\ wall} + t_{flange}\right)\right]^2.t_{shear\ wall}.\sigma_1$

$$Denom = \left[0.5.\left(4L_c - L_{shear\ wall} + t_{flange}\right).\left(L_{shear\ wall} - t_{flange}\right).t_{shear\ wall}.\sigma_1\right].e_1 + \left[(4L_c - 2L_{shear\ wall}).L_{flange}.t_{flange}.\sigma_1\right].e_2 + \left[0.5.\left(2L_c - \left(L_{shear\ wall} + t_{flange}\right)\right)^2.t_{shear\ wall}.\sigma_1\right].e_3$$

These equations are available if the compressive length found is between $L_{shear\ wall}$ and $\frac{L_{shear\ wall}+t_{flange}}{2}$.

Table 40 – Example of the assessment method

| Second case | Num | Denom | Compressive length [m] | Maximal stress [MPa] |
|---|---|---|---|---|
| First iteration | 0.0189 | 0.2099 | 0.7155 | 0.3574 |
| Xth iteration | 0.0151 | 0.1053 | 0.5217 | 0.5349 |
| Last iteration | 0.0112 | 0.0549 | 0.4114 | 0.8401 |

- Third case : one-side-uplift of the flange

In the third case, the null stress is located somewhere in the flange. The shear wall to the left of the flange is completely uplifted and there is one-side-uplift of the flange. As in the second case, the global section is divided into several areas, namely two areas (the part of the flange in contact with the basis and the shear wall to the right of the flange). The stress at the flange – shear wall on the right of the flange interface are function of the maximal stress $\sigma_1$.

$$\sigma_2 = \frac{L_c - \frac{\left(L_{shear\ wall} - t_{flange}\right)}{2}}{L_c}\sigma_1$$

Where $\sigma_2\ [MPa]$ is the stress at the interface between the part of the shear wall to the right of the flange and the flange. The naming comes from Figure 117.

To write the equilibrium equations, a normal stress and an eccentricity (distance between the gravity centre and the position where the stress is applied) are assigned to each area :

$$N = N_1 + N_2 + N_3 \qquad M = N_1.e_1 + N_2.e_2 + N_3.e_3$$

Where $N_1\ [N]$ is the normal stress of the part of the shear wall to the right of the flange ;
$e_1\ [m]$ is the eccentricity of $N_1$ ;
$N_2[N]$ is the normal stress of the flange part ;
$e_2\ [m]$ is the eccentricity of $N_2$ ;
The expression of the stress and their eccentricity are the following :

- For the part of the shear wall to the right of the flange

$$N_1 = \frac{\sigma_1 + \sigma_2}{2} . \frac{\left(L_{shear\ wall} - t_{flange}\right)}{2} . t_{shear\ wall}$$
$$= \frac{1}{8L_c} \left[ 4L_c - \left(L_{shear\ wall} - t_{flange}\right)\right] . \left(L_{shear\ wall} - t_{flange}\right) . t_{shear\ wall} . \sigma_1$$

$$e_1 = L_{shear\ wall} - \frac{\left(L_{shear\ wall} - t_{flange}\right)}{2} . \frac{1}{3} . \frac{\sigma_1 + 2\sigma_2}{\sigma_1 + \sigma_2} - x_g$$
$$= L_{shear\ wall} - \frac{\left(L_{shear\ wall} - t_{flange}\right)}{2} . \frac{1}{3} . \frac{6L_c - 2L_{shear\ wall} + 2t_{flange}}{4L_c - L_{shear\ wall} + t_{flange}} - x_g$$

- For the part of the flange

$$N_2 = \frac{\sigma_2}{2} . \left[ L_c - \frac{\left(L_{shear\ wall} - t_{flange}\right)}{2} \right] . L_{flange} = \frac{1}{8c} \left[ 2L_c - \left(L_{shear\ wall} - t_{flange}\right)\right]^2 . L_{flange} . \sigma_1$$

$$e_2 = \frac{\left(L_{shear\ wall} + t_{flange}\right)}{2} - \frac{1}{3} \left[ L_c - \frac{\left(L_{shear\ wall} - t_{flange}\right)}{2} \right] - x_g$$
$$= \frac{1}{3} \left[ -L_c c + 2 . L_{shear\ wall} + t_{flange} \right] - x_g$$

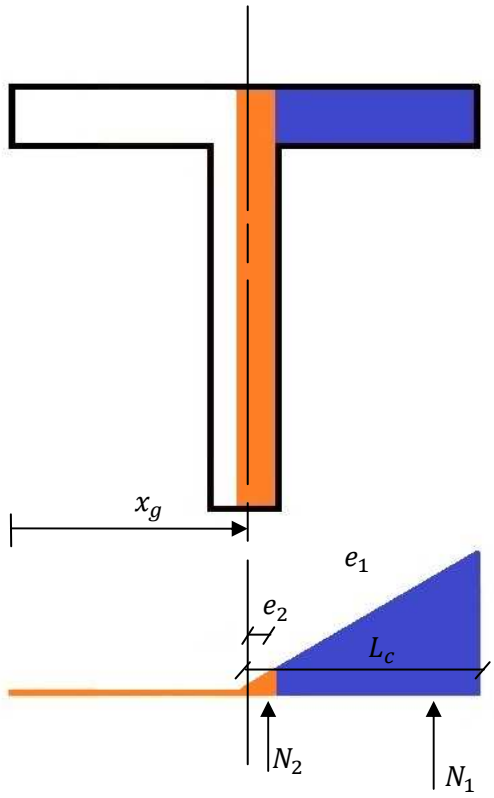


Figure 123 – Sketch of the third case

Putting these expressions in the equilibrium equations allows the calculus of the maximal stress thanks to the first equation. The second one gives a non-linear relation from which the compressive length $L_c$ can be determined.

$$\sigma_1 = \frac{8L_c.N}{Num}$$

Where $$Num = \left[4L_c - \left(L_{shear\ wall} - t_{flange}\right)\right].\left(L_{shear\ wall} - t_{flange}\right).t_{shear\ wall} + \left[2L_c - \left(L_{shear\ wall} - t_{flange}\right)\right]^2.L_{flange}$$

$$M = N.\frac{Num}{Denom}$$

Where $$Num = \left[4L_c - \left(L_{shear\ wall} - t_{flange}\right)\right].\left(L_{shear\ wall} - t_{flange}\right).t_{shear\ wall} + \left[2L_c - \left(L_{shear\ wall} - t_{flange}\right)\right]^2.L_{flange}$$

$$Denom = \left[\left(4L_c - \left(L_{shear\ wall} - t_{flange}\right)\right).\left(L_{shear\ wall} - t_{flange}\right).t_{shear\ wall}\right].e_1 + \left[\left(2L_c - \left(L_{shear\ wall} - t_{flange}\right)\right)^2.L_{flange}\right].e_2$$

These equations are available if the compressive length found is between $\frac{L_{shear\ wall}+t_{flange}}{2}$.and $\frac{L_{shear\ wall}- t_{flange}}{2}$.

Table 41 – Example of the assessment method

| Third case | Num | Denom | Compressive length [m] | Maximal stress [MPa] |
|---|---|---|---|---|
| First iteration | 0.02978 | 0.3309 | 0.6022 | 0.38176 |
| Xth iteration | 0.02835 | 0.1984 | 0.5030 | 0.54734 |
| Last iteration | 0.02202 | 0.1081 | 0.4076 | 0.84614 |

- Fourth case : taking off in the right part of the shear wall

In the fourth and last case, the null stress is located somewhere at the right of the flange. The shear wall to the left of the flange and the flange are completely uplifted. Once again, the global section is divided into several areas, but only one leaves (the part of the shear wall to the right of the flange). Considering the configuration, the maximal stress $\sigma_1$ can be directly found thanks to the equilibrium equations. The naming comes from Figure 117. To write the equilibrium equations, a normal stress and an eccentricity (distance between the gravity centre and the position where the stress is applied) are assigned to the area :

$$N = N_1 \qquad M = N_1.e_1$$

Where $N_1\ [N]$ is the normal stress of the part of the shear wall to the right of the flange ;
$e_1\ [m]$ is the eccentricity of $N_1$ ;

These equations give :

$$\sigma_1 = \frac{2N}{L_c t_{shear\ wall}} \qquad L_c = 3\left(-\frac{M}{N} + L_{shear\ wall} - x_g\right)$$

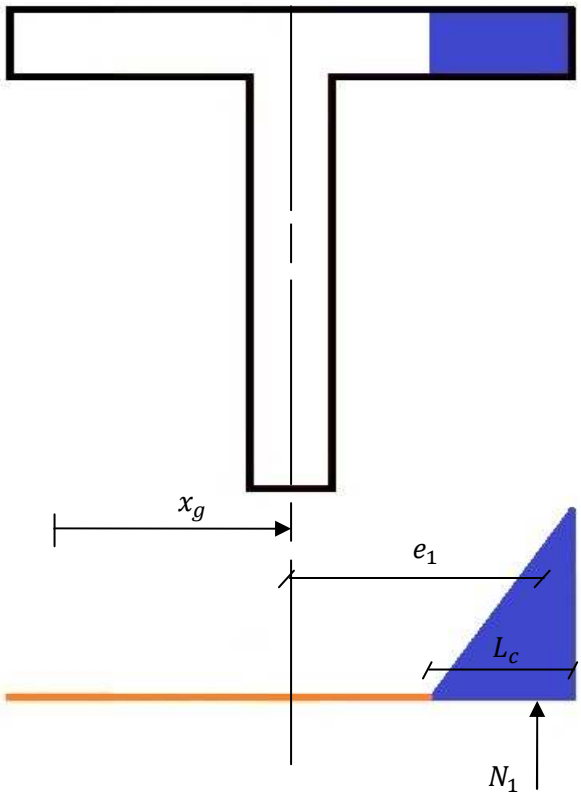


Figure 124 –Sketch of the fourth case

These equations are available if the compressive length found is between 0 and $\frac{L_{shear\ wall} - t_{flange}}{2}$.

Table 42 – Example of the assessment method

| *Fourth case* | *Num* | *Denom* | *Compressive length [m]* | *Maximal stress [MPa]* |
|---|---|---|---|---|
| *First iteration* | 0.09001 | 1 | 0.83997 | 0.4523 |
| *Xth iteration* | 0.14293 | 1 | 0.68122 | 0.5741 |
| *Last iteration* | 0.20375 | 1 | 0.49876 | 0.8149 |

Once the compressive length is known, the strength criteria have to be verified. The overturning is borne out as long as the compressive length is positive.

Table 43– Example of the assessment method

| *Conclusion* | *Compressive length* [m] | *Maximal stress [MPa]* |
|---|---|---|
| *First iteration* | 0.7155 | 0.3574 |
| *Xth iteration* | 0.5217 | 0.5349 |
| *Last iteration* | 0.4076 | 0.8461 |

#### *4.9.3.2. Shear strength*

As the compressive length $c$ and the maximum stress $\sigma_1$ are assessed, the shear strength is checked according to Eurocode 6 methods.
Taking into account the characteristics of the masonry unit, the mean compressive stress in masonry $\sigma$ and characteristic shear strength of masonry, $f_{vk}$, are calculated :

$$\sigma = \frac{N}{A_c}$$

$$f_{vk} = \min\left(\frac{f_{vk0}}{2} + 0.4\sigma; 0.045 f_b\right)$$

From the value of the characteristic shear strength of masonry, the design value of shear resistance is determined :

$$V_{Rd} = A_c . f_{vk}$$

Where $A_c$ $[m^2]$ is the compressive area and depends on the compressive length. The Table 44 gives the formula used to obtain the compressive area in function of the compression length.

Table 44 – Formulas for the compressive area

| Case | Compressive Area $A_c$ |
|---|---|
| $L_c > 0$<br>$L_c < \frac{L_{s\ ear\ wall} - t_{flange}}{2}$ | $L_c . t_{shear\ wall}$ |
| $L_c > \frac{L_{shear\ wall} - t_{flange}}{2}$<br>$L_c < \frac{L_{shear\ wall} + t_{flange}}{2}$ | $\left(\frac{L_{shear\ wall} - t_{flange}}{2}\right) . t_{shear\ wall} + \left[L_c - \left(\frac{L_{shear\ wall} - t_{flange}}{2}\right)\right] . L_{flange}$ |
| $L_c > \frac{L_{shear\ wall} + t_{flange}}{2}$<br>$L_c < L_{shear\ wall}$ | $L_c . t_{shear\ wall} + \left(L_{flange} - t_{shear\ wall}\right) . t_{flange}$ |
| $L_c > L_{shear\ wall}$ | $L_{shear\ wall} . t_{shear\ wall} + \left(L_{flange} - t_{shear\ wall}\right) . t_{flange}$ |

Finally, the shear strength of the wall criterion is checked if the design value of shear resistance is greater than the horizontal shear, in other words, if the following relation is verified :

$$\frac{V - V_{Rd}}{V_{Rd}} < 0$$

Table 45 – Example of the assessment method

| *Results* | $\sigma$ $[MPa]$ | $f_{vk}$ $[MPa]$ | $A_c$ $[mm^2]$ | *Criterion* |
|---|---|---|---|---|
| *First iteration* | 0.1766 | 0.2207 | 148412.21 | -93.86 % |
| *Xth iteration* | 0.2218 | 0.2387 | 121678.17 | -88.91 % |
| *Last iteration* | 0.2964 | 0.2685 | 94626.85 | -80.75 % |

#### 4.9.3.3. Crushing of the units

Checking the criterion of the crushing of the units is done with the calculation of the mean compressive stress in masonry $\sigma$. This stress is compared to the characteristic compressive strength of masonry, $f_k$and must be lower than this one:

$$f_k = 0.5\, f_b^{0.8} \qquad \sigma = \frac{N}{t.Lc}$$

$$f_k \geq \sigma$$

Table 46 – Example of the assessment method

| Results | $\sigma$ [MPa] | $f_k$ [MPa] | Criterion |
|---|---|---|---|
| First iteration | 0.1766 | 3.892 | Ok |
| Xth iteration | 0.2218 | 3.892 | Ok |
| Last iteration | 0.2964 | 3.892 | Ok |

#### 4.9.3.4. Torsion strength

If the distance, perpendicular to the horizontal shear direction, between the application point of the horizontal shear and the shear centre is not null, a torsion moment exists. According to the axis convention and the origin taken in Figure 117 and Figure 118, the value of the torsion moment is first calculated by the next formula :

- if the horizontal shear direction is the X-axis

$$M_T = (y_r - y_V).V$$

Where $y_r\ [m]$ is the Y-coordinate of the shear centre ;
$y_v\ [m]$ is the Y-coordinate of the application point of the horizontal shear ;
$V\ [N]$ is the horizontal shear.

- if the horizontal shear direction is the Y-axis

$$M_T = (x_r - x_V).V$$

Where $x_r\ [m]$ is the X-coordinate of the shear centre ;
$x_v\ [m]$ is the X-coordinate of the application point of the horizontal shear ;
$V\ [N]$ is the horizontal shear.

Next, the shear stress $\tau$ is given by (Serge Cescotto & Charles Massonet, 2001). Above all, we must keep in mind that the following formulae have been developed in the case of opened elastic sections with thin walls, not for masonry walls. Nevertheless, it's the only way to consider the torsion effects.

$$\tau_{torsion} = G\frac{M_T.t}{C}$$

Where $t\ [m]$ is the thickness ;
$G\ [N/m^2]$ is the shear modulus ;
$C\ [Nm^2]$ is the torsional stiffness.

The calculation of the coefficient $C$ is done with the formula :

$$C = k.\frac{G}{3}.\sum hb^3$$

In this relation, the sum is enlarged on all rectangles making up the T-shaped wall. The parameters $h$ and $b$ are the length and the thickness of each rectangles. Therefore, $h$ must always be superior to $b$. Obviously, all the taken off wall parts are not considered. The coefficient $k$ is taken to 1.1 according to *Föppl*.

After all, the criterion for the torsion strength can be verified. As this one is based on the comparison between the shear stress and the shear strength, the shear contribution must be added to the torsion one :

$$\tau_{shear} = \frac{V}{A_c}$$

Where $A_c\ [m^2]$ is the compressive area.

It follows,

$$\tau_{total} = \tau_{torsion} + \tau_{shear} \leq f_{vk}$$

Where $\tau\ [N/m^2]$ is the shear stress ;
$f_{vk}\ [N/m^2]$ is characteristic shear strength of masonry.

Table 47 – Example of the assessment method

| *Results* | C $[mm^4]$ | $\tau_{total}[MPa]$ | $f_{vk}[MPa]$ | Criterion |
|---|---|---|---|---|
| *First iteration* | 1036332778 | 0.058 | 0.2207 | -73.72 % |
| *Xth iteration* | 849654319 | 0.1134 | 0.2387 | -52.51 % |
| *Last iteration* | 511270744 | 0.2708 | 0.2685 | 0.85 % |

Remark : for the verification of the torsion strength, there are no models. Thus, the verification is based on the comparison of the shear stresses.

To summarize, the last iteration gives us a value of the horizontal shear which leads to the collapse of the structure. For one orientation of the horizontal shear, there are two possible values (one by direction) as the design done is a “static equivalent”. Obviously, the lowest value is kept.

#### *4.9.3.5. Designed acceleration*

As soon as the value of horizontal shear leading to the collapse of the all structure is assessed, the corresponding acceleration can be determined. Nevertheless, this step is a little bit harder than in the case of the first test series because the specimens of the second test series can't be considered like a single-degree freedom structure.

The used method of assessment comes from the (Eurocode8*, 2004) . The difference is that we don't want to determinate a target displacement, but the acceleration involving this displacement.
Therefore, the "target displacement" must be calculated before. Actually this "target displacement" is the ultimate displacement of the specimen. Its calculation is possible thanks to the PhD of Marcelo Rafael Oropeza Ancieta (Oropeza Ancieta, 2011). He gives a formulation to estimate the ultimate drift, called $\delta_u$, and the ultimate top displacement $\Delta_u$. According to him, the ultimate drift depends on two dimensionless parameters, namely the aspect ratio $\frac{h_p}{l_w}$ and the normal stress over the wall strength $\frac{\sigma_n}{f_{xd}}$. To assess the ultimate drift, two other parameters are defined :

$$a = 0.6\frac{\min(h_0, h_p)}{l_w} + 0.3 \qquad b = 0.9\frac{\min(h_0, h_p)}{l_w} + 0.3\frac{h_p}{l_w}$$

Where $h_0\ [m]$ is the height of the level
$h_p\ [m]$ is the height of the building
$l_w [m]$ is the length of the specimen

These two parameters are function of the boundary conditions and the geometry of the specimen. It follows :

$$\delta_u = \begin{cases} a & \frac{h_p}{l_w} \geq 1\ \&\ \frac{\sigma_n}{f_{xd}} \leq 0.05 \\ b & \frac{h_p}{l_w} < 1\ \&\ \frac{\sigma_n}{f_{xd}} > 0.05 \\ \frac{2a}{1.85 + 3\frac{\sigma_n}{f_{xd}}} & \frac{h_p}{l_w} \geq 1\ \&\ \frac{\sigma_n}{f_{xd}} \leq 0.05 \\ \frac{2b}{1.85 + 3\frac{\sigma_n}{f_{xd}}} & \frac{h_p}{l_w} < 1\ \&\ \frac{\sigma_n}{f_{xd}} > 0.05 \end{cases}$$

Table 48 - Values of the parameters and the ultimate drift

| $h_p/l_w$ | $\sigma_n/f_{xd}$ | $a$ | $b$ | $\delta_u$ [%] |
|---|---|---|---|---|
| 0.75 | 0.0647 | 0.75 | 0.9 | 0.881 |

Finally, the ultimate top displacement $\Delta_u$ is :

$$\Delta_u = d_m^* = \delta_u . h_p = 15.85\ mm$$

Once the ultimate top displacement is known, and so the target displacement, the curve of the horizontal shear can be drawn in function of the top displacement. Figure 125 shows it in the case of the specimen with T-shaped walls all loaded, with the assumption of a left and right built-in lintel.

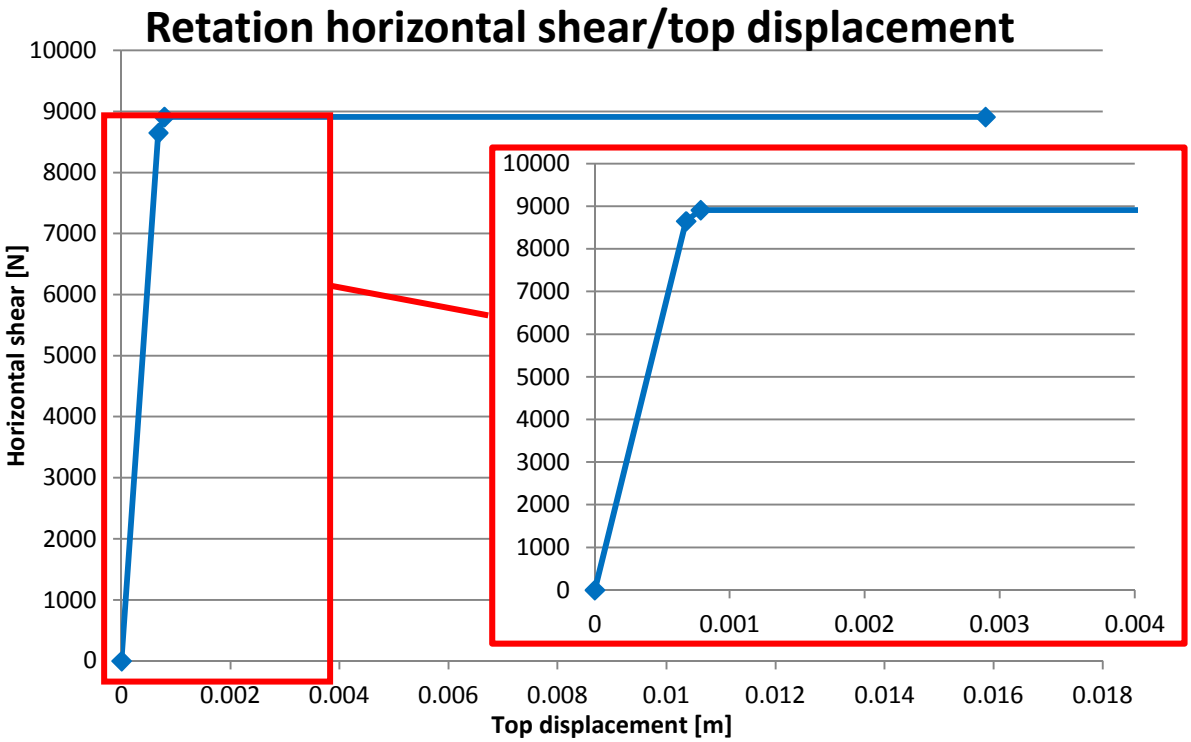


Figure 125 – Horizontal shear/top displacement relation

In Figure 125, three points are marked. The first one is the moment when the first wall reaches its shear strength, the second one corresponds to the moment when the second wall shear strength is reached. The last one represents the target displacement.

Thanks to the curve of the horizontal shear in function of the top displacement, the actual deformation energy up to the formation of the plastic mechanism $E_m^*$ can be determined :

$$E_m^* = \frac{d_{1^e\ point}.shear_{1^e\ point}}{2} + \frac{(shear_{1^e\ point} + shear_{2^e\ point}).(d_{2^e\ point} - d_{1^e\ point})}{2}$$

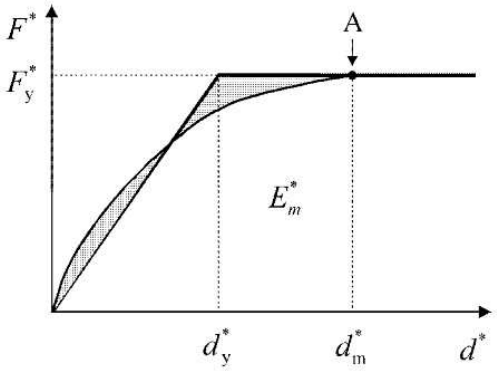


Figure 126 – Graph from the EC 8, Annex B

It follows the calculation of the yield displacement of the idealised SDOF system, $d_y^*$ :

$$d_y^* = 2\left(d_m^* - \frac{E_m^*}{F_y^*}\right)$$

The last formulae used before the one giving the value of the acceleration are necessary to assess the period of the idealised equivalent SDOF system $T^*$ and the target displacement of the structure with this period $T^*$ and unlimited elastic behaviour are given by :

$$T^* = 2.\pi \sqrt{\frac{m^*.d_y^*}{F_y^*}} \qquad\qquad d_{et}^* = S_e(T^*).\left[\frac{T^*}{2\pi}\right]^2$$

Where $m^* = 5000\ kg$ (dead load)

$S_e(T^*)$ is determined thanks to the equations of EurocCode 8, for a type II of elastic response spectrum and a ground type A.

However, the structure doesn't have an unlimited elastic behaviour. In our case, the period is in the short period range and the next criterion is respected :

$$\frac{F_y^*}{m^*} \geq S_e(T^*)$$

It follows

$$d_t^* = \frac{d_{et}^*}{q_u}\left(1 + \frac{(q_u - 1)T_C}{T^*}\right) \geq d_{et}^*$$

Where $q_u = \frac{S_e(T^*)m^*}{F_y^*}$ and $T_C = 0.25s$ (type II of elastic response spectrum)

Finally, the value of the design acceleration is found by changing it until the value of $d_t^*$ calculated with the formula is equal to the ultimate top displacement $d_m^*$. The results for the case of a horizontal shear in the x-direction are given in Table 49 and Table 50.

Table 49 – Results of the preliminary assessment (T-shaped walls, x-axis horizontal shear)

| Supported conditions of the lintel | Loading case | Horizontal shear [N] | Acceleration [g] |
|---|---|---|---|
| Left and right built-in | Shear wall | 13745 | 0.93925 |
| | Flange | 4148 | 0.79500 |
| | Both | 8912 | 0.85675 |
| Left and right simply supported | Shear wall | 10808 | 0.78001 |
| | Flange | 3527 | 0.64014 |
| | Both | 6797 | 0.76345 |

Table 50 – Results of the preliminary assessment (L-shaped walls, x-axis horizontal shear)

| Supported conditions of the lintel | Loading case | Horizontal shear [N] | Acceleration [g] |
|---|---|---|---|
| Left and right built-in | Shear wall | 13795 | 1.19992 |
| | Flange | 8220 | 0.75234 |
| | Both | 9610 | 0.99707 |
| Left and right simply supported | Shear wall | 10850 | 0.85351 |
| | Flange | 7120 | 0.65358 |
| | Both | 8430 | 0.82919 |

### 4.9.4. Specificities of the Y-direction

If an earthquake occurs in the Y-direction, our frame-model is no more valid. The collapse happens as soon as one of the wall has reached its strength because the structure is statically determinate in this plan.

The horizontal shear will split between the two walls according to their bending stiffness, the position of the specimen shear centre and the position of the gravity centre of each wall (Figure 127 and Figure 128).

$$x_{Shear\ centre,frame} = \frac{x_{Shear\ centre,left\ wall} \cdot I_{y,left\ wall} + x_{Shear\ centre,right\ wall} \cdot I_{y,right\ wall}}{I_{y,left\ wall} + I_{y,right\ wall}}$$

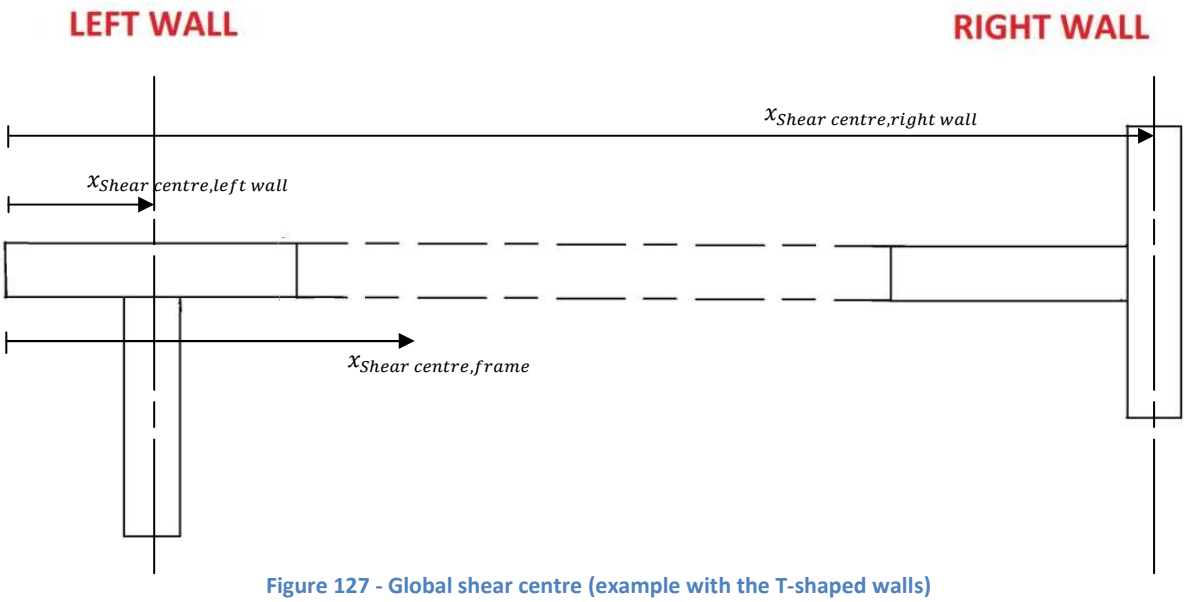


Figure 127 - Global shear centre (example with the T-shaped walls)

$$V_{left} = -V.\frac{x_{Shear\ centre,frame} - x_{right\ wall}}{x_{left\ wall} + x_{right\ wall}}$$

$$V_{right} = V.\frac{x_{Shear\ centre,frame} + x_{left\ wall}}{x_{left\ wall} + x_{right\ wall}}$$

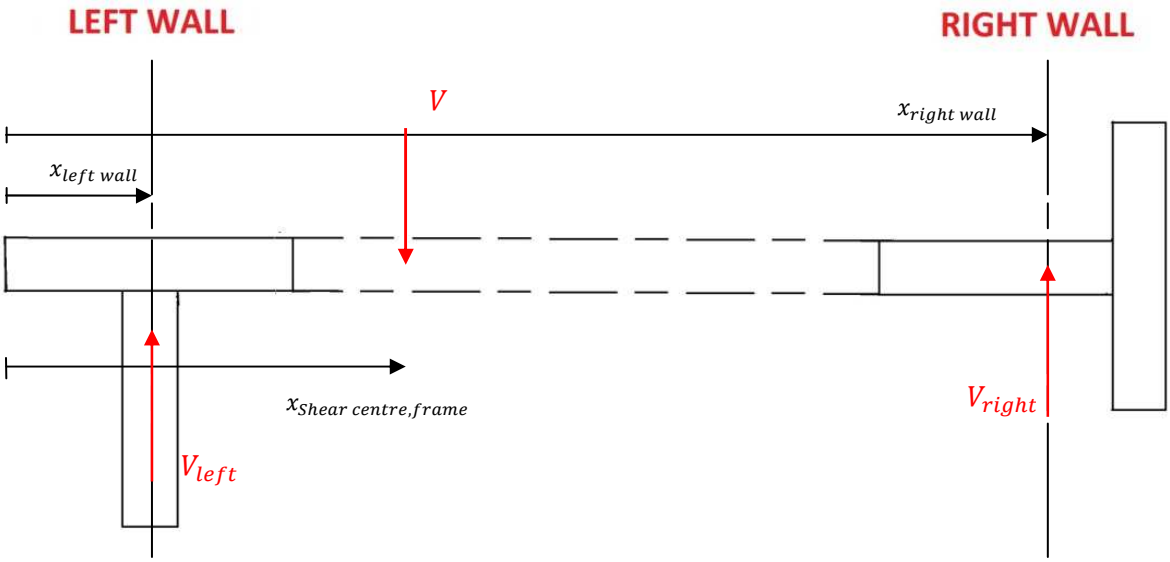


Figure 128 - Calculation of the shear stress (example with the T-shaped walls)

The method used to assess the value of the acceleration leading to the collapse is the same than the one used for the first test series. Different loading cases also exist, but this method makes an assumption about the supported conditions of the walls. They can be :

- built-in at the bottom and free at the top (only considered);
- built-in at the bottom and simply supported at the top ;
- built-in at the bottom and at the top.

As it was made for the x-direction analysis, the specimens are verified for the rocking, the shear, the torsion and the crushing of the units. The final results are given in Table 51 and Table 52.

Table 51 – Results of the preliminary assessment (T-shaped walls, y-axis horizontal shear)

| Supported conditions of the walls | Loading case | Horizontal shear [N] | Acceleration [g] |
|---|---|---|---|
| Top wall free | Shear wall | 1548 | 0.013 |
| | Flange | 6800 | 0.055 |
| | Both | 5652 | 0.046 |

Table 52 – Results of the preliminary assessment (L-shaped walls, y-axis horizontal shear)

| Supported conditions of the walls | Loading case | Horizontal shear [N] | Acceleration [g] |
|---|---|---|---|
| Top wall free | Shear wall | 7632 | 0.0567 |
| | Flange | 10960 | 0.0814 |
| | Both | 8516 | 0.0633 |

### 4.9.5. Comparison with a specimen without flanges

This part is performed to give an idea on the influence of the flanges. Therefore, the configuration studied is a specimen with two 0.74m long walls separated by an opening. The frame behaviour is also still valid. Obviously, the comparison is only made for an earthquake direction in the plan of the frame. The results are given in Table 53.

Table 53 - Results for a simple frame

| Wall Shape | Compressive load [kg] | Compression Level [MPa] | $V_{Sd}$ [N] | $a_g$ [g] | $a_{g,T-shaped}$ [g] | $a_{g,L-shaped}$ [g] |
|---|---|---|---|---|---|---|
| T-shape | 5000 | 0.245 | 11450 | 0.884 | 0.939 | 1.199 |

The comparison shows a gain of 6% to 26% according to the cases.

### 4.9.6. Comparison with a simple wall

In order to be able to compare the influence of an opening and of the perpendicular walls, the analysis is also made for a simple wall of the same length. Therefore, the preliminary assessment must be applied to a 1.5m long wall.

The method is the same as the one used for the first test series. That kind of wall can collapse due to the crushing of the units or because the shear or the bending strength is reached. The rocking is the last possibility if the compressive length becomes zero. The results give the following values :

Table 54 - Results for a simple wall

| Length [m] | Compressive load [kg] | Compression Level [MPa] | $V_{Sd}$ [N] | $a_g$ [g] | Stiffness $K$ [N/m] | Period $T$ [s] |
|---|---|---|---|---|---|---|
| 1.5 | 5000 | 0.242 | 20350 | 0.148 | $77.003.10^6$ | 0.089 |

## 4.10. Building aspects (beams of support)

As it was made for the first test series, the specimens are built on steel beams. Here again, it's essential to let the shaking table free before the tests because the laboratory has other activities.
Considering the time required for the setting and hardening of the mortar, the specimen must be put on the table as a whole. Indeed, a period of 28 days is necessary to erect the walls and also to fix the lintel. So, it is not possible to transport the walls one after another. This requirement has an influence on the design of the support beams.

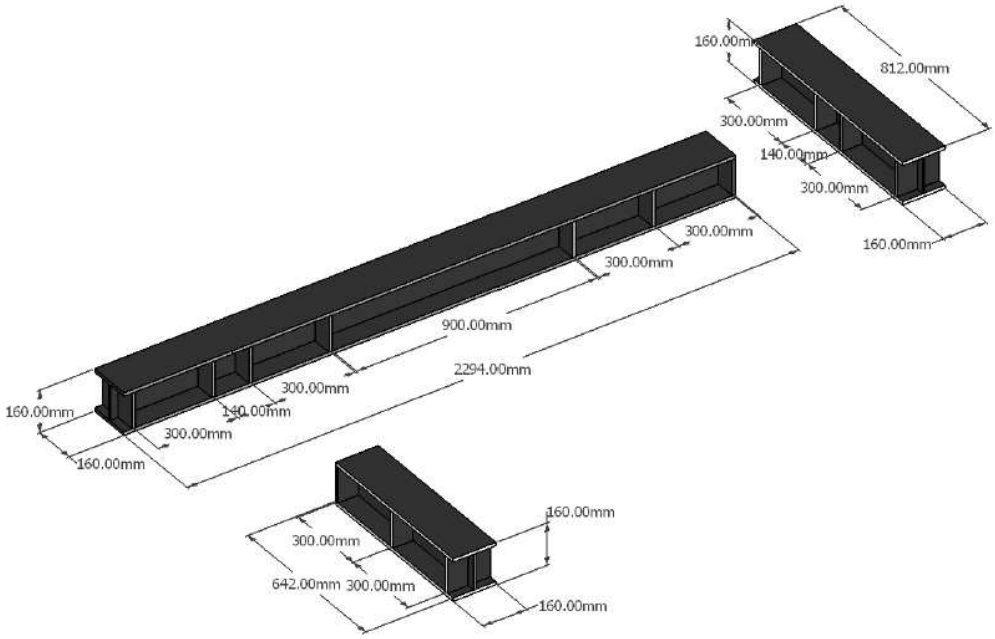


Figure 129 – 3D view of the support beams (T-shaped walls)

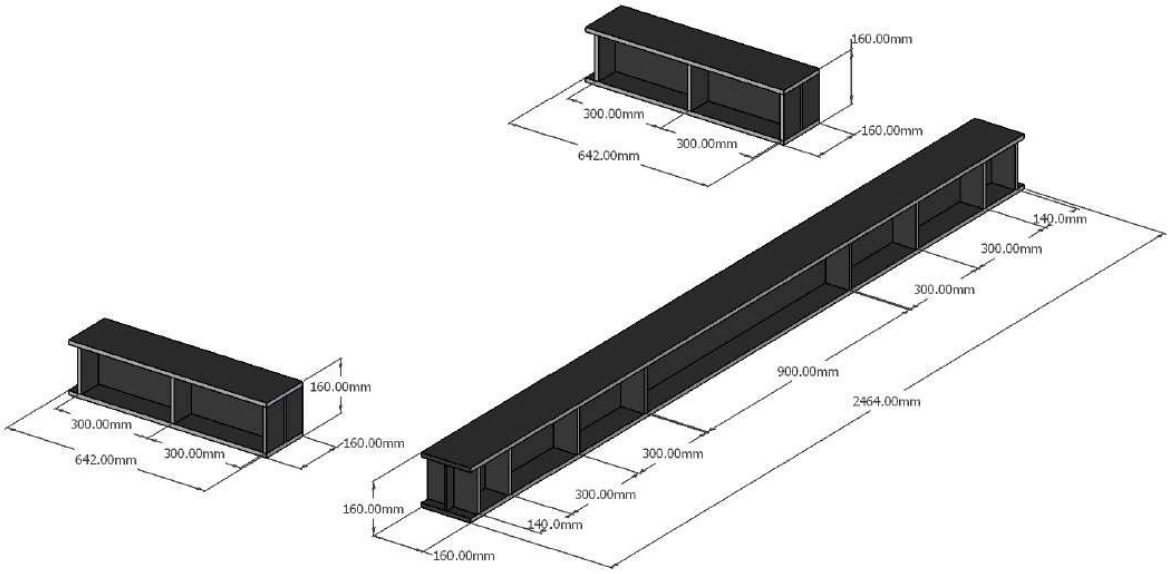


Figure 130 – 3D view of the support beams (L-shaped walls)

As it can be seen in Figure 129 and Figure 130, the support is composed of three steel beams. All the parts must be bolted together in order to form the shape of the specimen cross section.
To set up the specimen on the shaking table, the method is the same than the one used for the first test series is used again.

## 4.11. Origin of axis and axis convention

The origin of the axis and the axis convention in the laboratory are the same than these described in the Chapter 2 : "Summary of the design of the first test series".

## 4.12. Instrumentation of the specimens

In this paragraph, the instrumentation of the specimens is given. The needed instrumentation devices measure the acceleration or the displacement. Their characteristics and the definitive positions are described below.

### 4.12.1. Characteristics of instrumental devices[8]

- Acceleration measurement

SETRA type 141A accelerometers will be used. The accelerometers generally have a calibrated range of +/-8g that is traceable to national standards.

- Displacement measurement

Displacements of the test specimen relative to the ES will be monitored using either Celesco draw wire displacement transducers or Linear Variable Differential Transformers (LVDT), whichever is most convenient. These will be deployed within specified chains of electronic equipment that comprise also of an amplifier and a filter. Each displacement transducer chain that will be used during testing is recorded (as a row) within the Test Instrumentation Record.

### 4.12.2. Positions of instrumental devices

The following instrumentation layouts have been suggested and put in place for the two specimens of the second test series. The plans of the instrumentation layouts are given in Annex E.
All the information about the devices are given in Annex F. Besides the devices placed on the specimen, four accelerometers are fixed on the slab in order to measure the acceleration in X- and Y-direction.
All the devices were calibrated before the tests.

The instrumentation layouts also include a vision data system. It consists of a Imetrum Video-Gauge Vision System (VS) which processes the data. Fourteen targets are placed on the specimen and the slab (Figure 131 and Figure 132) and their horizontal and vertical displacements are recorded.

[8] Description from the report "*Test Method Statement – TA5/TMS – Seismic Behaviour of L- and T-shaped Unreinforced Masonry Shear Walls Including Acoustic Insulation Devices*".

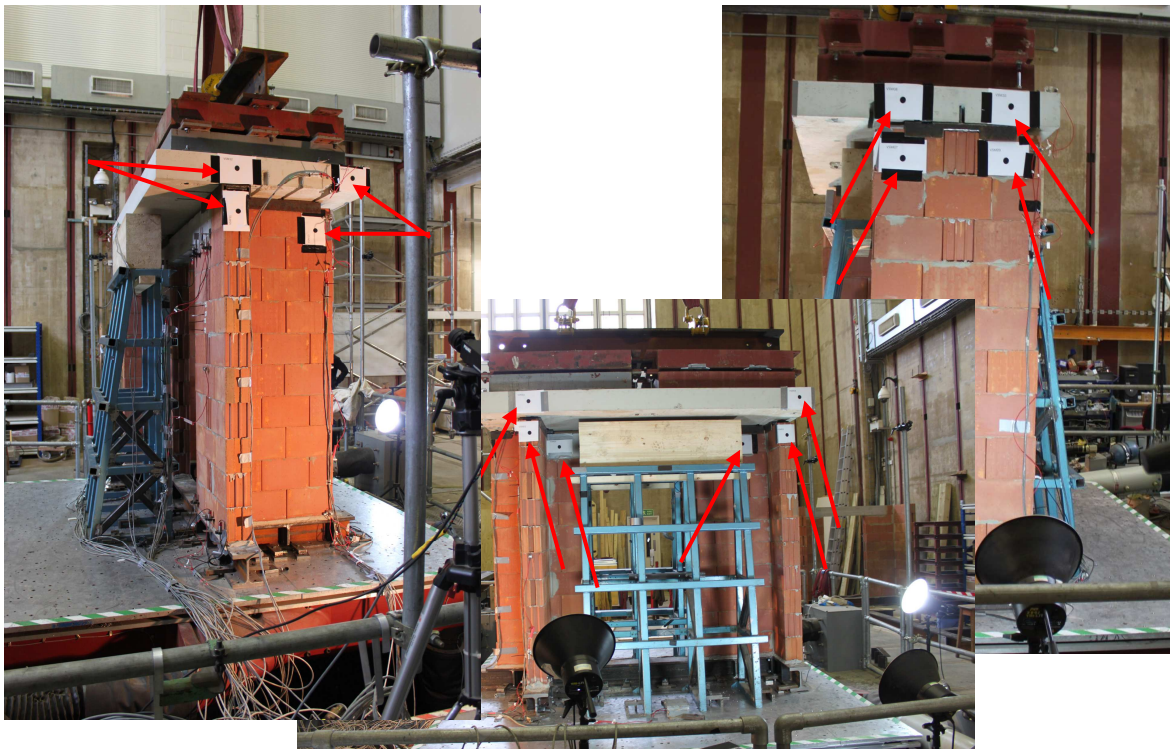

Figure 131 - View of the targets (T-shaped walls) for the Imetrum Video-Gauge Vision System (VS).

Figure 132 - View of the targets (L-shaped walls) for the Imetrum Video-Gauge Vision System (VS).

# Chapter 5 :
# Results of the second test series

## 5.6. Introduction

The second test series took place during the two last weeks of May. Considering that this Master's Thesis ends the week after, there is not enough time to interpret and analyze all the results. Nevertheless, the course of the tests and the phenomena that were visible to the naked eye are developed below.
The use of the data given by the instrumentation devices should confirm these observations.

## 5.7. Set up of the specimens

Like the walls of the first test series, the specimens of the second test series are built next to the table.
As the specimens are also built on a steel beam with reinforcements, their set up is done thanks to the method used for the first phase. Let's start by recalling that some steel bars are used to connect the bottom beam and the top one. The crane of the laboratory takes the wall at the top beam of the specimen and places it on the table. Figure 133 illustrates the equipment used for the setting up.

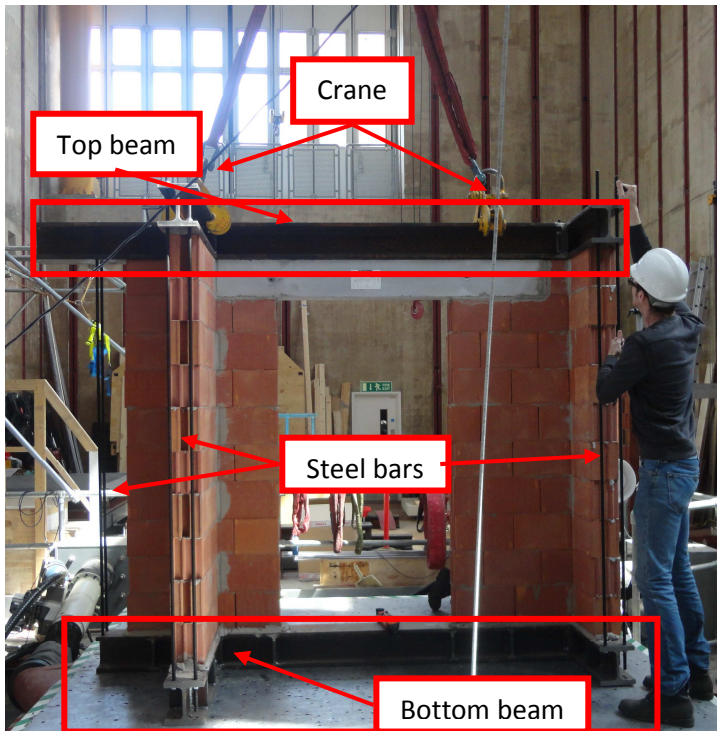

Figure 133 – Set up of the T-shaped walls

Finally, the specimen is placed such as the frame plan is along the Y-direction of the axis convention of the laboratory and the mass (slab) is put on the specimen (Figure 134 and Figure 135).

Figure 134 – View from the mezzanine (T-shaped walls)

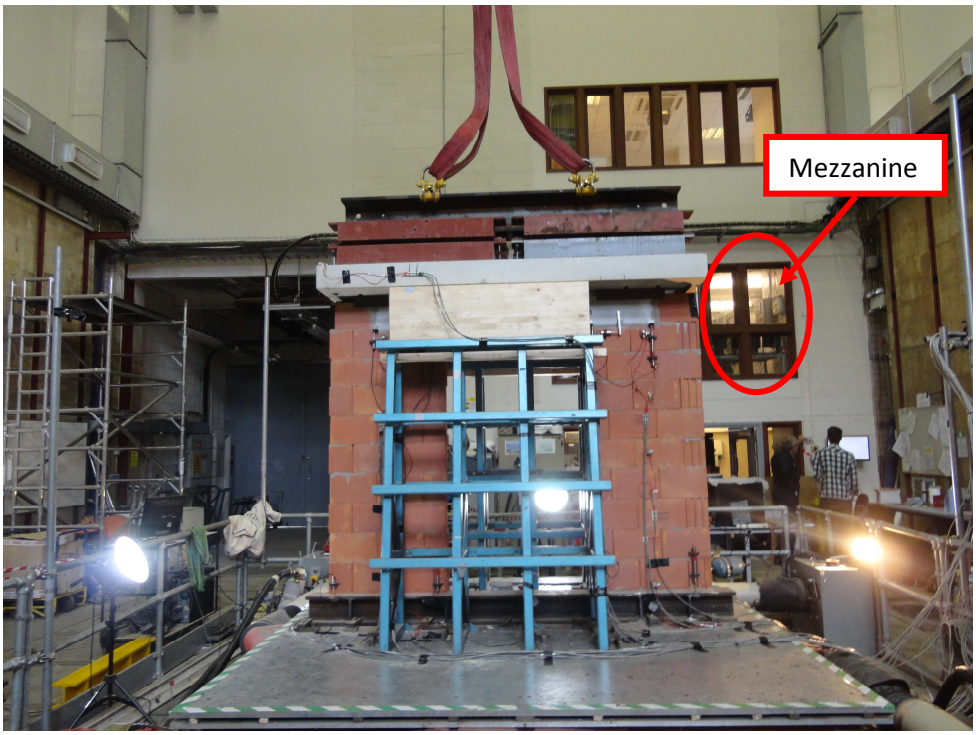


Figure 135 – View of the L-shaped walls specimen

## 5.8. Sequences of the tests

The sequence of the tests aims to describe the course of the tests. Two tables remind the different tests realized. Like the first test series, the second one includes white noise test at the beginning to characterize the specimen and after each seismic test to study the effects of these ones. In this test series, the white noise tests are performed in the X and Y directions because of the wish to see the influence of an earthquake in one direction on the behaviour of the specimen according to the two directions.

Table 55 and Table 56 give the sequence of the tests for the T-shaped walls and the L-shaped walls respectively.

All the tests given below have a clear and precise naming :

- TA5_120522 is the folder with the results of the T-shaped walls;
- TA5_120528 is the folder with the results of the L-shaped walls ;

Each folder contains files with the Noise tests (N"X") and the Seismic tests (S"X") where "X" is a number in accordance with Table 55 and Table 56.

Table 55 – Sequence of tests for the T-shaped walls

| Test No. | Type of test | Direction | %[9] | PGA [g] | Level [mm/V] | Acq rate [Hz] |
|---|---|---|---|---|---|---|
| Loading on shear walls and flanges | | | | | | |
| 1 | Noise (N1) | X | / | / | 1.5 | 512 |
| 2 | Noise (N2) | Y | / | / | 1.5 | 512 |
| 3 | Seismic (S1) | Y | 16 | ~0.08 | / | 512 |
| 4 | Noise (N3) | X | / | / | 1.5 | 512 |
| 5 | Noise (N4) | Y | / | / | 1.5 | 512 |
| 6 | Seismic (S2) | Y | 32 | ~0.16 | / | 512 |
| 7 | Noise (N5) | X | / | / | 1.5 | 512 |
| 8 | Noise (N6) | Y | / | / | 1.5 | 512 |
| 9 | Seismic (S3) | Y | 64 | ~0.32 | / | 512 |
| 10 | Noise (N7) | X | / | / | 1.5 | 512 |
| 11 | Noise (N8) | Y | / | / | 1.5 | 512 |
| 12 | Seismic (S4) | X | 10 | ~0.05 | / | 512 |
| 13 | Noise (N9) | X | / | / | 1.5 | 512 |
| 14 | Noise (N10) | Y | / | / | 1.5 | 512 |
| 15 | Seismic (S5) | X | 20 | ~0.1 | / | 512 |
| 16 | Noise (N11) | X | / | / | 1.5 | 512 |
| 17 | Noise (N12) | Y | / | / | 1.5 | 512 |
| 18 | Seismic (S6) | X | 40 | ~0.2 | / | 512 |
| 19 | Noise (N13) | X | / | / | 1.5 | 512 |
| 20 | Noise (N14) | Y | / | / | 1.5 | 512 |
| 21 | Seismic (S7) | X | 60 | ~0.4 | / | 512 |
| 22 | Noise (N15) | X | / | / | 1.5 | 512 |
| 23 | Noise (N16) | Y | / | / | 1.5 | 512 |
| 24 | Seismic (S8) | Y | 96 | ~0.45 | / | 512 |
| 25 | Noise (N17) | X | / | / | 1.5 | 512 |
| 26 | Noise (N18) | Y | / | / | 1.5 | 512 |

[9] The 100% corresponds to the PGA of the waveform sent to the table (0.485g)

Table 56 – Sequence of tests for the L-shaped walls

| Test No. | Type of test | Direction | %[10] | PGA [g] | Level [mm/V] | Acq rate [Hz] |
|---|---|---|---|---|---|---|
| | | | Loading on shear walls and flanges | | | |
| 1 | Noise (N1) | X | / | / | 1.5 | 512 |
| 2 | Noise (N2) | Y | / | / | 1.5 | 512 |
| 3 | Seismic (S1) | Y | 16 | ~0.08 | / | 512 |
| 4 | Noise (N3) | X | / | / | 1.5 | 512 |
| 5 | Noise (N4) | Y | / | / | 1.5 | 512 |
| 6 | Seismic (S2) | X | 10 | ~0.05 | / | 512 |
| 7 | Noise (N5) | X | / | / | 1.5 | 512 |
| 8 | Noise (N6) | Y | / | / | 1.5 | 512 |
| 9 | Seismic (S3) | Y | 32 | ~0.16 | / | 512 |
| 10 | Noise (N7) | X | / | / | 1.5 | 512 |
| 11 | Noise (N8) | Y | / | / | 1.5 | 512 |
| 12 | Seismic (S4) | X | 20 | ~0.1 | / | 512 |
| 13 | Noise (N9) | X | / | / | 1.5 | 512 |
| 14 | Noise (N10) | Y | / | / | 1.5 | 512 |
| 15 | Seismic (S5) | Y | 48 | ~0.24 | / | 512 |
| 16 | Noise (N11) | X | / | / | 1.5 | 512 |
| 17 | Noise (N12) | Y | / | / | 1.5 | 512 |
| 18 | Seismic (S6) | X | 30 | ~0.15 | / | 512 |
| 19 | Noise (N13) | X | / | / | 1.5 | 512 |
| 20 | Noise (N14) | Y | / | / | 1.5 | 512 |
| 21 | Seismic (S7) | Y | 64 | ~0.32 | / | 512 |
| 22 | Noise (N15) | X | / | / | 1.5 | 512 |
| 23 | Noise (N16) | Y | / | / | 1.5 | 512 |
| 24 | Seismic (S8) | X | 40 | ~0.2 | / | 512 |
| 25 | Noise (N17) | X | / | / | 1.5 | 512 |
| 26 | Noise (N18) | Y | / | / | 1.5 | 512 |
| | | | Loading on flanges only | | | |
| 27 | Noise (N19) | X | / | / | 1.5 | 512 |
| 28 | Noise (N20) | Y | / | / | 1.5 | 512 |
| 29 | Seismic (S9) | Y | 16 | ~0.08 | / | 512 |
| 30 | Noise (N21) | X | / | / | 1.5 | 512 |
| 31 | Noise (N22) | Y | / | / | 1.5 | 512 |
| 32 | Seismic (S10) | X | 10 | ~0.05 | / | 512 |
| 33 | Noise (N23) | X | / | / | 1.5 | 512 |
| 34 | Noise (N24) | Y | / | / | 1.5 | 512 |
| 35 | Seismic (S11) | Y | 20 | ~0.1 | / | 512 |
| 36 | Noise (N25) | X | / | / | 1.5 | 512 |
| 37 | Noise (N26) | Y | / | / | 1.5 | 512 |
| 38 | Seismic (S12) | X | 20 | ~0.1 | / | 512 |
| 39 | Noise (N27) | X | / | / | 1.5 | 512 |
| 40 | Noise (N28) | Y | / | / | 1.5 | 512 |
| 41 | Seismic (S13) | Y | 30 | ~0.15 | / | 512 |
| 42 | Noise (N29) | X | / | / | 1.5 | 512 |
| 43 | Noise (N30) | Y | / | / | 1.5 | 512 |
| 44 | Seismic (S14) | X | 30 | ~0.15 | / | 512 |
| 45 | Noise (N31) | X | / | / | 1.5 | 512 |
| 46 | Noise (N32) | Y | / | / | 1.5 | 512 |
| 47 | Seismic (S15) | Y | 40 | ~0.2 | / | 512 |
| 48 | Noise (N33) | X | / | / | 1.5 | 512 |
| 49 | Noise (N34) | Y | / | / | 1.5 | 512 |
| 50 | Seismic (S16) | X | 40 | ~0.2 | / | 512 |
| 51 | Noise (N35) | X | / | / | 1.5 | 512 |
| 52 | Noise (N36) | Y | / | / | 1.5 | 512 |
| 53 | Seismic (S17) | Y | 50 | ~0.25 | / | 512 |

[10] The 100% corresponds to the PGA of the waveform sent to the table (0.485g)

## 5.9. Acceleration really experimented on the table

In Table 55 and Table 56, the values of the PGA are theoretical ones. Like the simple walls of the first test series, the weight of the specimens has an influence on the PGA. Two sensors are directly placed on the shaking table in order to measure the real acceleration sent. These sensors are connected to the channels 42 (X-direction) and 43 (Y-direction) for the specimen with T-shaped walls and to the channels 44 (X-direction) and 45 (Y-direction) for the specimen with L-shaped walls .
These values are thus given in Table 57. They are obtained thanks to the maximum values of channel 42(44) and 43 (45).

Table 57 – Acceleration experimented on the table

| Test | T-shaped walls | | | | L-shaped walls | | | |
|---|---|---|---|---|---|---|---|---|
| | Theoretical PGA [g] | | Real PGA [g] | | Theoretical PGA [g] | | Real PGA [g] | |
| | X-direct. | Y-direct. | X-direct. | Y-direct. | X-direct. | Y-direct. | X-direct. | Y-direct. |
| **S1** | 0 | 0.0776 | 0,0069 | 0.0690 | 0 | 0.0776 | 0,0059 | 0,0618 |
| **S2** | 0 | 0.1552 | 0,0182 | 0.1459 | 0.0485 | 0 | 0,0375 | 0,0006 |
| **S3** | 0 | 0.3104 | 0,0007 | 0.2791 | 0 | 0.1552 | 0,0146 | 0,0044 |
| **S4** | 0.0485 | 0 | 0,0379 | 0.0049 | 0.097 | 0 | 0,0871 | 0,0006 |
| **S5** | 0.097 | 0 | 0,0831 | 0.0079 | 0 | 0.2328 | 0,0364 | 0,0060 |
| **S6** | 0.194 | 0 | 0,1759 | 0.0245 | 0.1455 | 0 | 0,1347 | 0,0008 |
| **S7** | 0.291 | 0 | 0,2763 | 0.0565 | 0 | 0.3104 | 0,0771 | 0,0068 |
| **S8** | 0 | 0.4656 | 0,1074 | 0.4652 | 0.194 | 0 | 0,1798 | 0,0014 |
| **S9** | / | / | / | / | 0 | 0.0776 | 0,0110 | 0,0611 |
| **S10** | / | / | / | / | 0.0485 | 0 | 0,0394 | 0,0067 |
| **S11** | / | / | / | / | 0 | 0.097 | 0,0144 | 0,0771 |
| **S12** | / | / | / | / | 0.097 | 0 | 0,0797 | 0,0179 |
| **S13** | / | / | / | / | 0 | 0.1455 | 0,0259 | 0,1334 |
| **S14** | / | / | / | / | 0.1455 | 0 | 0,1246 | 0,0352 |
| **S15** | / | / | / | / | 0 | 0.194 | 0,0390 | 0,1946 |
| **S16** | / | / | / | / | 0.194 | 0 | 0,1697 | 0,0365 |
| **S17** | / | / | / | / | 0 | 0.2425 | 0,0577 | 0,1974 |

Table 57 shows that there is always a motion in both direction, even if the seismic action should theoretically be in a single direction. The acceleration perpendicular to the seismic action is between 10% and 30% of the value of the acceleration in the seismic direction

The relative difference between the theoretical acceleration sent to the table and the experimented one varies between 5% and 23% in the X-direction and between 0% to 21% in the Y-direction. These values are based on the comparison of all tests, save for the tests S3, S5 and S7 of the specimen with L-shaped walls. For these three tests, it clearly seems that the measurement is wrong or that a problem happened during the acquisition of data because the relative difference is about 97%.

# 5.10. Observations and comments of the tests

## 5.10.1. Specimen with T-shaped walls

The specimen with T-shaped walls was tested under one loading case only. In this loading case, the shear walls and the flanges were both loaded. As said in the part “Set up of the specimens”, the specimen is such as the frame plan is in the Y-direction (axis convention of the laboratory).

### 5.10.1.1. *Position of the slab*

For different reasons, there was an eccentricity of the centre of mass of the slab in comparison to the position of the gravity centre of the walls (Figure 136). This eccentricity had a huge influence on the wall behaviour because the eccentricity led to a torsion stress of the wall.

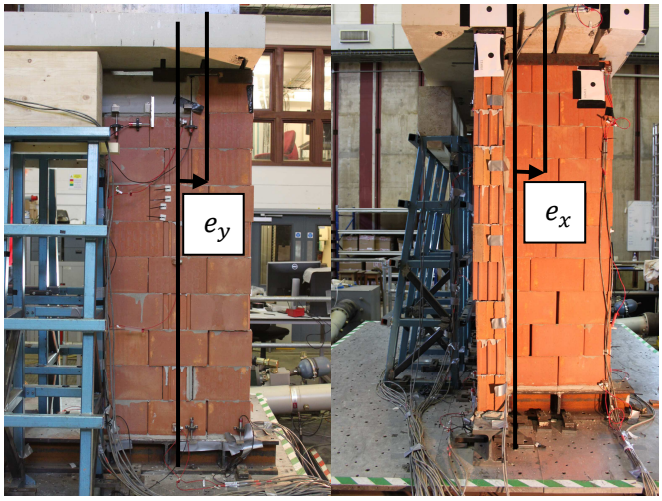


Figure 136 – Eccentricity of the load (Left wall)

The measured eccentricities were for the “left wall”:

$$e_x \approx 0.15m \qquad e_y \approx 0.10m$$

As said previously, the eccentricity led to a torsion stress. This stress was under-evaluated at the preliminary assessment because the assumption of a perfect loading was made.
Furthermore, the position of the steel plate on the shear wall (left) had another effect. As it was not centred, the part which should be on the lintel was less important. Therefore, the assumption of a built-in lintel should be wrong.

For the “right” wall, the eccentricity was lower in the x-direction and equal to zero in the y-direction, as shown in Figure 137.

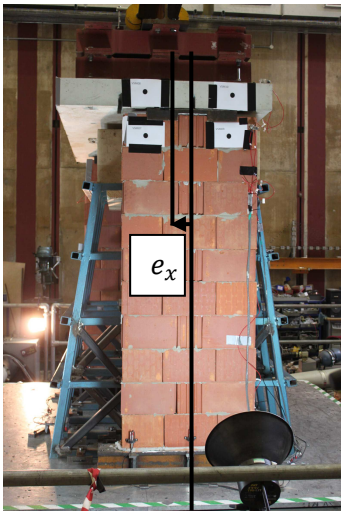


Figure 137 – Eccentricity of the load (Right wall)

The measured eccentricities were for the "right wall":

$$e_x \approx 0.03m \qquad e_y \approx 0.00m$$

In this case, the value of the eccentricity is not significant.

#### 5.10.1.2. *Phenomena observed*

Due to a lack of time, the data recorded during the second test series are not used in this work. Nevertheless, some phenomena were observed and they are described below. Obviously, it's expected that the data processing will confirm what was observed.

The first phenomenon concerns the lintel and its behaviour. During the second seismic test, some cracks appeared at the interface of the lintel and the wall. The observed cracks were not only vertical ones, but also horizontal ones. It means that the lintel was totally free. The cracks were located on both sides of the lintel.
During the last seismic test, the lintel lifted up from the wall and stayed in the air a short moment.

Figure 138 –Cracks at the interface between lintel and the walls

The second phenomenon is the rocking of the specimen. There are no movies or pictures of this phenomenon because it happened during the seismic tests, but everybody in the laboratory saw it.

The third and last phenomenon is the torsion of the wall. The torsion stress was due to two main origins. The first one was the non-symmetrical configuration. Indeed, the two walls had not the same bending stiffness. Therefore, a global torsion stress existed. The “left” wall was overstressed in comparison to the “right” wall.
The second one was due to the eccentricity of the loading and to the distance between the gravity centre and the shear centre. For example, the crank was equals to  0.32m (0.17 (distance) + 0.15 (eccentricity)).if the seismic action was in the Y-direction.
It was the reason of the premature collapse of the specimen. As illustrated in Figure 139, several units of the “left” wall switched and some joints opened. There were also many cracks on the wall.

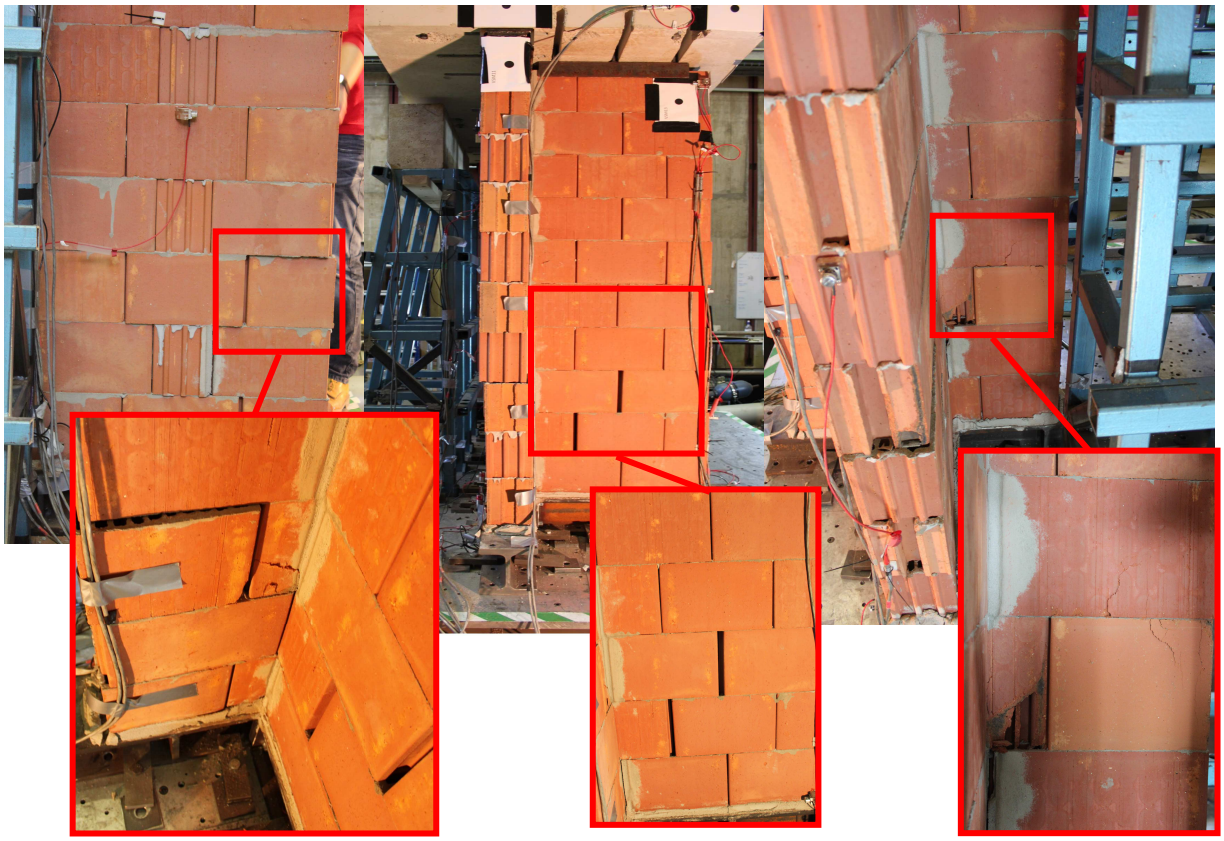

Figure 139 –Collapse of the “left” wall

For the “right” wall, there are only cracks at the bottom of the wall.

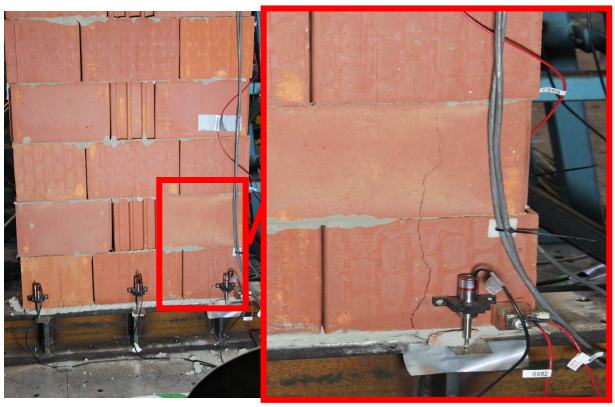

Figure 140 –Cracks in the right” wall

To summarized, a rocking behaviour can be observed during the seismic tests. This kind of behaviour is the same than the one of a single wall. Nevertheless, a torsion stress appears because of the geometry of the specimen and the eccentricity of the loading. The torsion stress is more important in the left side of the specimen and leads to the collapse of the wall.
Concerning the lintel, this one can't be considered as built-in because there is already cracking when the acceleration level is low. This assumption is not the good one because the load is directly put on the wall and, so, the lintel is not loaded. If the lintel is loaded, this assumption could be more relevant. The coupling of the walls and the frame behaviour is also very weak and limited.
Only one loading case was tested because of the collapse of the specimen.

### 5.10.2. Specimen with L-shaped walls

The specimen with L-shaped walls was tested under two loading case . Firstly, the shear walls and the flanges were both loaded. Secondly, the mass was only supported by the flanges.
As said in the part "Set up of the specimens", the specimen is such as the frame plan is in the Y-direction (axis convention of the laboratory).

#### 5.10.2.1. *Position of the slab*

Even if the slab used to load the specimen with L-shaped walls was the same than the one used for the specimen with T-shaped walls, the centre of mass of the slab and the gravity centre of the specimen were nearly the same (Figure 141).
Because of the symmetry of the specimen, the only origin of torsion is the distance between the gravity centre and the shear centre of the wall. Therefore, the crank was equal to 0.3m.

Figure 141 - Position of the slab (L-shaped walls)

#### 5.10.2.2. *Phenomena observed*

##### 5.10.2.2.1. First loading case

Under the first loading case, two phenomena were observed.
On one hand, the specimen behaviour was also in rocking. As the acceleration level increased, the one-side-uplift at the bottom of the wall increased too. Once again, this phenomenon is very fast and there are no pictures of it, but the movies clearly illustrated it.
On the other hand, there was progressively the appearance of vertical and horizontal cracks. The cracks are shown in  after the seismic test S6 (Figure 142).

Figure 142 - Cracks near the lintel (after S6)

After the seismic test S6, there were only cracks at the interface of the lintel and the “right” wall. On the left side of the specimen, nothing was observed.

##### 5.1.1.1.1. Second loading case

The configuration at the beginning of the tests under the second loading case was a specimen with some deteriorations. The main ones was the cracks at the interface of the lintel and the “right” wall. Under this loading case, the phenomena observed were :

- The rocking behaviour
- The appearance of cracks at the interface of the lintel and the “left” wall
- The collapse of the “left” wall.

In Figure 143, the cracks at the interface of the lintel and the “left” wall are illustrated. The cracking means that the assumption of a built-in lintel is not available.

Figure 143 - Cracks near the lintel (after S17)

The Figure 143 shows the collapse o the specimen with L-shaped walls. To remind, the testing of this specimen aimed to study the connection between the flange and the shear wall. The collapse happened in the wall which the flange and the shear wall were built-in.

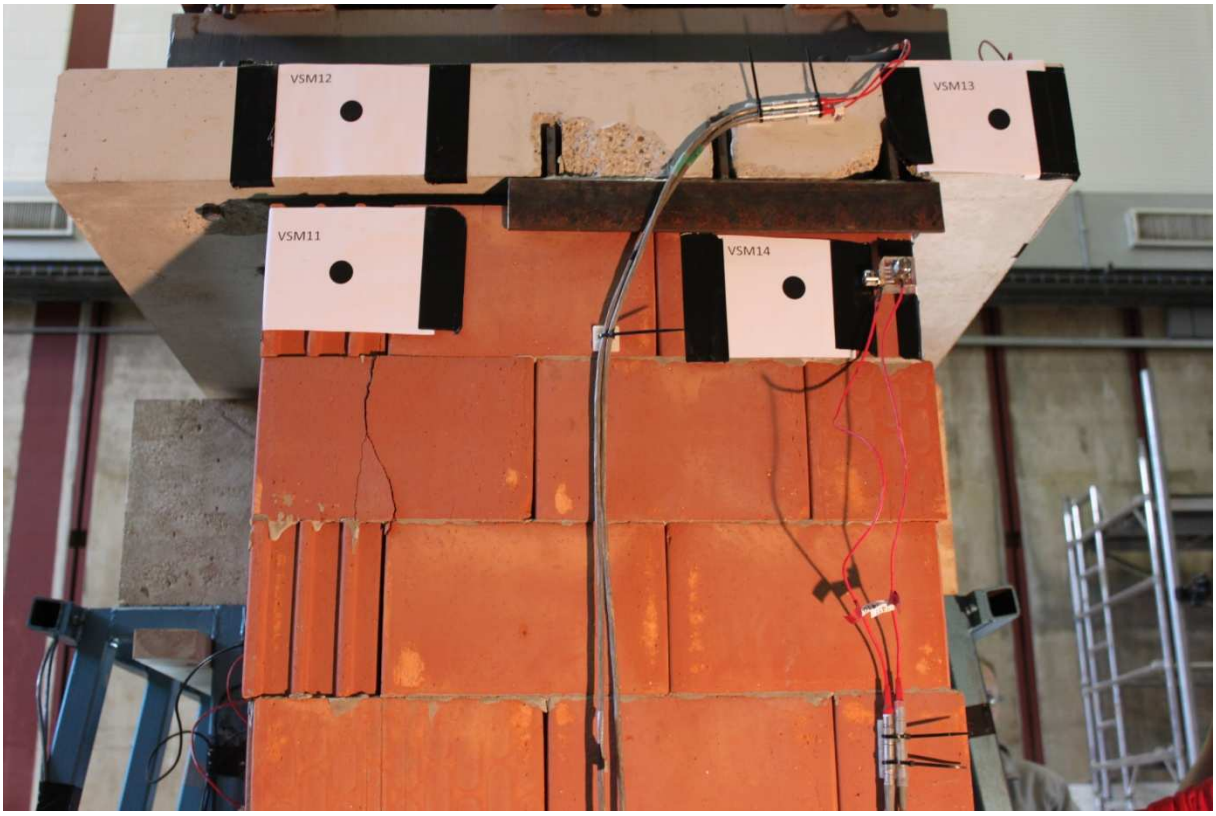


**Figure 144 – Collapse of the « left » wall**

Thanks to the type of collapse happened, it seems than the connection with a mortar joint (flange and shear wall glued together) is better than the one where the flange and the shear wall are built-in. This conclusion is only valid in the configuration tested. Indeed, the collapse happened under a seismic action in the Y-direction. At that moment, the mortar joint of the right wall was stressed by a shear stress along all the height of the wall. For its part, the stress of the "left" wall was only transmitted from the shear wall to the flange thanks to the horizontal joints because the specimen had opened vertical joints.
It can explained why the strength of the connection of the "right" wall was better because the shear area was higher and the strength of mortar is good.
If the glued interface of the "right" wall was perpendicular to the seismic action, the strength would depend on the shear strength of the units.

To summarized, the specimen with L-shaped walls has also a rocking behaviour. The collapse is not happened when the shear walls and the flanges were both loaded, but when only flanges are loaded. The seismic direction was in the frame plan. The reason of the collapse is a weakness of the connection between the flange and the shear wall.
Like the lintel of specimen with T-shaped walls, the lintel of this specimen can't be considered as built-in because of the cracking. This assumption is not the good one because the load is directly put on the wall and, so, the lintel is not loaded. If the lintel is loaded, this assumption could be more relevant.

# Chapter 6 :
# Conclusions & prospects

The conclusions of this Master's Thesis are numerous and varied. Before approaching the learning from the results of the test series, one word about the contribution and the experience taken from the carrying out the tests seems to be appropriate.
Although the tested specimens have been designed and a preliminary assessment have been done, some technical aspects had an influence on the performing of the tests. For example, we learned that the safety of the people and the facilities led to the necessity to set up many devices such as steel frames, timber beam or to hang the mass from the crane during the tests.

Concerning the learning coming from of the results of the two test series, they are first developed for the first test series and, then, for the second one.

The results of the first test series teach us that the behaviour of simple masonry walls in dynamic conditions is a rocking behaviour. Indeed, the rocking behaviour was observed during the seismic tests of every wall, regardless of the length of the wall or the presence of acoustic insulation devices.
The processing of the results provided several learning.
Firstly, the characterization of the walls thanks to white noise tests gave some results which have been compared to those obtained with the method of the preliminary assessment. The comparison was made for the walls without acoustic insulating devices and taught us that the values and formulae recommended by the Eurocode 6 don't seem to be valid in the case of walls built in thin bed masonry with empty vertical joints and glued horizontal ones. The value of the shear modulus (recommended value : 0.4*E) is actually overestimated because of the type of vertical joints. It can be concluded that the shear modulus value cannot be simply taken as a percentage of the elastic modulus. Concerning the walls with acoustic insulating devices, the comparison was not possible with the model used for the walls without these devices because the presence of the rubber changes to behaviour of the wall. According to us, another model must be developed. This one could represent the wall and the two layers of rubber with a system composed of three springs in series. The one in the middle would have the characteristics of the masonry wall and the others, the characteristics of the rubber. This model would be an iterative one because the behaviour of the rubber is a function of the compression level and of the Poisson coefficient.
In terms of frequencies, the acoustic insulation devices decrease the stiffness of the structure and, so, its natural frequencies are lower.
Secondly, the seismic tests showed that the static equivalent model (Push-over) used for the preliminary assessment are valid if the acceleration level is low or moderate. In that case, the measured values of the compressive length are between the values given by the approach based on the resolution of the equilibrium equations for materials without tensile strength. Actually, the results of this approach depend of the assumption made. The lower bound is obtained when a constant distribution of the stress along the wall is supposed and the upper bound is deduced if the assumption is a linear distribution of the stress along the wall. Once the acceleration level becomes high, the results of this model are no more relevant and a dynamic approach must be used to investigate the behaviour of the wall. The remarks comes from the evaluation of the compressive length and of the measurement of the slope of the wall bottom when the wall is considered like a rigid body.
In terms of compressive length, the acoustic insulation devices allow higher displacement, but the value of the compressive length is higher.

Thirdly, the calculation of the shear stress in the wall and in the SonicStrip devices was quite difficult and gives not relevant results. As already said, two main modifications must be applied to the calculation model. The first one is to include the two types of transfer mechanisms (classic one and the strut and tie model) in order to take into account the fact that the shear is not only a horizontal one, but a vertical component exists. The second modification concerns the distribution of the shear along the acoustic insulation devices and their behaviour. It was said that the rocking leads to a non homogeneous distribution of the shear and the behaviour of the rubber depends on the compression level and the thickness of the devices.
Fourthly and finally, the data given by the Imetrum Video-Gauge Vision System can be used for others things than the comparison with the results obtained thanks to the devices placed on the walls. For example, the relation between the horizontal displacement of the mass and the force of inertia of the mass (F=m*a) can be drawn and its envelope would the “Push” curve. This system could be also used in the calculation of the shear strength. Indeed, the walls behaviour owns two part. The first one, under a low or moderate seismic action, looks like a bracket wall? The second one, under a high acceleration level, is the rocking. For the different seismic tests, the comparison between the rotation at the top and the bottom of the wall should show these two behaviour.

Concerning the second test series, all the processing of the results must be carried out. The learning coming from the phenomena observed are interesting, but it’s not enough to conclude some relevant ideas. The only things that can be said concern the torsion, the frame behaviour and the consideration of intersecting wall (perpendicular wall) acting as a flange.
For the torsion, it seems to be clear that this stress is the one which led to the collapse of the specimen with T-shaped walls. As no model is proposed in the standards, its development should be of the first importance.
For the frame behaviour, it seems that this one is limited and depends on the loading case. If the loading is not applied on the lintel, the frame behaviour is weak because of the connection between the lintel and the wall. Furthermore, the support conditions of the lintel can’t be considered as built-in.
For the contribution to the strength of the wall perpendicular to the seismic action, the main conclusion is about the strength of the connection between the flange and the shear wall. If this connection is not strength enough, it leads to the collapse of the structure.

As an end of the conclusion of this work, I would like to say that the behaviour of load-bearing masonry subjected to earthquake action is a interesting and captivating field. The experimental part of the work was a complete discovery for me and I liked to be careful to all the details of the set up and of the testing. For example, I was involved in the second test series from the beginning to the end and I have the possibility to see my work come true and real. An amazing experience !
Moreover, the two stays in Bristol allow me to improve my English, at least the understanding and the speaking, to meet great people and to discover the operating of a team of another university.

# Chapter 7 : Bibliography

# Bibliography


Cerfontaine, B. (2010). *Development of a software for automatical application of masonry part Eurocode 8 in Belgium.* Liège.

Dietz, M. (2012). *TEST METHOD STATEMENT - TA5/TMS - Seismic behaviour of L- and T-shaped unreinforced masonry shear xalls indluding acoustic insulation devices.* Bristol: University of Bristol - Departement of Civil Engineering - Earthquake Engineering Research Centre.

Eurocode6. (2004). *Eurocode 6 : Design of the masonry structures - Part 1-1 : Common rules for reinforced and unreinforce masonry structures.*

Eurocode8. (2004). *Eurocode 8 : Design of structures for earthquake resistance - Part 1 : General rules, seismic actions and rules for buildings.*

Eurocode8*. (2004). *EurcoCode8 : Annex B(Informative) : "Determination of the target displacement for nonlinear static (pushover) analysis.*

Grigoletto, S. (2006). *Etude du comportement sismique de structures à comportement non continu.* Liège.

Hervé Degee & Laurentiu Lascar. (2011). *Cyclic shear behaviour of clay masonry walls – Part 1 : walls including acoustic devices or with a door opening.* Liege.

Hervé Degee & Larentiu Lascar. (2011). *Cyclic shear behaviour of clay masonry walls – Part 2 : Cyclic shear test on prefabricated clay masonry walls with T-shaped.* Liege.

Jaspart, J.-P. (2010). *Constructions métalliques et en béton II - Partim constructions métalliques - "Chapitre 9 : Elements d'assemblage".* Liege.

K.Beyer, A.Abo-El-Ezz & A.Dazio. (2010). *Quasi-static cyclic trsts on different types of masonry spandrels.* Zürich.

Oropeza Ancieta, M. (2011). *Fragility Functions for Seismic Risk in Regions with Moderate Seismicity.* Lausanne.

Serge Cescotto & Charles Massonet. (2001). *Mécanique des matériaux.* Bruxelles: De Boeck.

Stuerz. (2009, 02 10). *ESECMaSE - Enhanced Safety and Efficient Construction of Masonry Structures in Europe*. Retrieved May 2012, from ESECMaSE: http://www.esecmase.org

Tomazevic, M. (1999). *Earthquake-Resistant Design of Masonry Buildings.* London: Imperial College Press.

# Annexes